ON THE EVOLUTION OF YOUNG NEUTRON STARS WITH FALLBACK DISKS

by

ŞİRİN ÇALIŞKAN

Submitted to the Graduate School of Engineering and Natural Sciences
in partial fulfillment of
the requirements for the degree of
Doctor of Philosophy

Sabancı University
January 2013

ON THE EVOLUTION OF YOUNG NEUTRON STARS WITH FALLBACK DISKS

APPROVED BY:

Assoc. Prof. Ünal Ertan .....

(Dissertation Supervisor)

Prof. M. Ali Alpar .....

Assoc. Prof. M. Hakan Erkut .....

Prof. Ersin Göğüş .....

Assoc. Prof. Mehmet Keskinöz .....

DATE OF APPROVAL: 18.02.2013

© ŞİRİN ÇALIŞKAN 2013
All Rights Reserved

To my mom, dad,

Seylan and Sevinç

TABLE OF CONTENTS

1 Introduction **1**

1.1 Optical and Infrared Emission from the AXPs and SGRs 10

1.2 X-ray Outbursts of Transient AXPs and SGRs 10

1.3 The Evolution of SGR 0418+5729 with a fallback disk 12

1.4 The Peculiar Braking Index and Evolution of PSR J1734−3333 . . . 13

2 Optical and Infrared Emission from the AXPs and SGRs **15**

2.1 Introduction 16

2.2 Optical/IR Emission from the Irradiated Disk 19

2.3 Results and Discussion 21

2.4 Conclusion 24

3 On the X-ray Outbursts of Transient Anomalous X-ray Pulsars and Soft Gamma-ray Repeaters **28**

3.1 Introduction 29

3.2 The Numerical Model 33

3.2.1 Description of the Model Parameters 33

3.2.2 Parameter Study 36

3.2.2.1 Different burst energies 36

3.2.2.2 Quiescent X-ray luminosity and critical temperature 39

3.2.2.3 X-Ray irradiation 41

3.2.2.4 Viscosity parameter 44

3.2.2.5 Outer disk radius 47

3.3 Application of the Model to the X-ray Enhancement Light Curves of Transient AXPs 48

3.4 Results and Discussion 53

3.5 Conclusions 59

4 SGR 0418+5729 - How Does a Young Neutron Star Spin Down to a 9 s Period With a Dipole Field Less Than 10^{13} G ? **62**

4.1 Introduction 63

4.2 Evolution With a Fallback Disk 65

4.3 Spin and Luminosity Evolution of SGR 0418+5729 68

4.4 Discussion and Conclusions 72

5 On The Evolution of The Radio Pulsar PSR J1734-3333 **73**
5.1 Introduction 74
5.2 The Model 76
5.3 Results and Discussion 80
5.4 Conclusions 88

6 Summary and Outlook **91**

Bibliography **97**

LIST OF TABLES

1.1 The period, period derivative, estimated distance and X-ray luminosity of known AXPs and SGRs. The references are as follows: 1. McGarry et al. (2005), 2. Tiengo et al. (2008), 3. Dib et al. (2007), 4. Durant & van Kerkwijk (2006a), 5. Dib et al. (2009), 6. Gaensler et al. (2005), 7. Dib et al. (2012), 8. Tiengo et al. (2010), 9. Levin et al. (2010), 10. Woods et al. (2011), 11. Kothes & Dougherty (2007), 12. Dib et al. (2008), 13. Sato et al. (2010), 14. Tian & Leahy (2012), 15. Camilo et al. (2007a), 16. Minter et al. (2008), 17. Tian & Leahy (2008), 18. Kothes & Foster (2012), 19. Gavriil & Kaspi (2002), 20. Rea et al. (2010), 21. van der Horst et al. (2010), 22. Göğüş et al. (2010), 23. Leahy & Tian (2007), 24. Tiengo et al. (2009), 25. Klose et al. (2004), 26. Esposito et al. (2009b), 27. Esposito et al. (2009a), 28. Corbel et al. (1999), 29. Nakagawa et al. (2009), 30. Bibby et al. (2008), 31. Rea et al. (2012), 32. Scholz et al. (2012), 33. Esposito et al. (2011), 34. Kargaltsev et al. (2012), 35. Leahy & Tian (2008), 36. Mereghetti et al. (2006a), 37. Davies et al. (2009). 5

1.2 The observed optical and near-infrared magnitudes and upper limits of known AXPs and SGRs. In cases of multiple observations, the range of magnitudes are given. In case of multiple upper limits, the lowest upper limit is given. The data were taken from the McGill Online Catalog (http://www.physics.mcgill.ca/∼pulsar/magnetar/main.html). 11

2.1 The Irradiated Disk Model and the Observational Flux Values Note: The data flux values were calculated by using the magnitudes and A_V values given in the following references. For the AXP 4U 0142+61, a plausible range for reddening is $2.6 < A_V < 5.1$ (Hulleman et al., 2004); the data for this source here correspond to $A_V = 3.5$. The A_V values for the other sources are: $A_V = 7.8$ (J1708-40), $A_V = 6.1$ (1E 2259+58), $A_V = 8.4$ (1E 1841-045), $A_V = 5.6$ (1E 1048-59). REFERENCES: (J1708-40) Durant & van Kerkwijk 2006b, Rea et al. 2003; (1E 2259+586) Hulleman et al. 2001, Woods et al. 2004; (4U 0142+61) Hulleman et al. 2000, Hulleman et al. 2004, Patel et al. 2003, Morii et al. 2005; (1E 1841-45) Wachter et al. 2004, Morii et al. 2003; (1E 1048-59) Wang & Chakrabarty 2002, Mereghetti et al. 2004 22

2.2 The Parameters of the Irradiated Disk Model Note: This model gives the optical/IR flux values seen in Table 2.1. For all the sources, we set $\cos i = 1$, where i is the inclination angle between the disk normal and the line of sight of the observer, and we take the outer disk radius to be $r_{\rm out} = 5 \times 10^{12}$ cm (see Section 2.3 for details). 27

3.1 The parameters for the model curves presented in Figures 3.6–3.9. Note that the parameters $\alpha_{\rm hot}$, $\alpha_{\rm cold}$, p and $T_{\rm crit}$ are expected to be similar for all AXPs and SGRs. Irradiation efficiency, C, which could change with accretion rate is also likely to be similar for the sources in the same accretion regimes. In quiescence, Σ_0 scales with accretion rate. The width of the Gaussian pile-up is represented by Δr. The parameters Δr, r_0, and $\Sigma_{\rm max}$ could vary from source to source, depending on the burst energy and geometry. The values of inner disk radius $r_{\rm in}$ are close to the Alfvén radii of the sources with $B_0 \simeq 10^{12}$ G. We set $r_{\rm out} = 10^{13}$ cm and $f = \dot{M}/\dot{M}_{\rm in} = 1$ for all our models. 60

LIST OF FIGURES

1.1 The period and period derivatives of pulsars. The plus signs show radio pulsars. AXP/SGRs are denoted with red triangles at the top right corner. XDINS are immediately below them, shown with green squares. RRATs with measured period derivatives are shown with red dots. The interesting SGR 0418+5729 is shown with a filled black triangle, with its currently known $\dot{P}$ upper limit ($\dot{P} < 6 \times 10^{-15}$ s s^{-1}). The radio pulsar PSR J1734–3333 is shown with a black filled circle. The data were taken from the online ATFN pulsar catalog (http://www.atnf.csiro.au/research/pulsar/psrcat/) 6

3.1 Model light curves produced by pure viscous evolution of disks for three different δE values. The short-term light curve, in the inset, shows peak luminosities of 10^{37} erg s^{-1}, 3×10^{36} erg s^{-1}, and 10^{36} erg s^{-1}, which all decay to the same quiescent luminosity in the long term. The δM values are 4.9×10^{22} g, 2.1×10^{21} g, and 8.9×10^{20} g and the estimated δE values are 9.2×10^{39} erg, 3.8×10^{39} erg, and 1.7×10^{39} erg respectively. The model light curves can be fitted with power laws in the early decay phase ($\sim$ a few weeks). The values of power indices (n) are given in the inset. 38

3.2 Short-term and long-term model light curves of a typical transient source for three different δE values. For these models, δM values are 2.4×10^{21} g, 1.2×10^{21} g, and 6.4×10^{20} g and estimated δE values are 4.5×10^{38} erg, 2.3×10^{38} erg, and 1.2×10^{38} erg respectively. The decay phases of the light curves can be fitted with power laws for the first $\sim$ 100 days (inset). The values of power indices (n) are given in the inset. 40

3.3 Model light curves for persistent (a) and transient (b) sources, for $T_{\rm crit}$= 1500 K, 1750 K, and 2000 K. Solid curves illustrate the pure viscous decay with the same initial conditions for comparison. For a given $T_{\rm crit}$, comparing (a) and (b), the difference between the model curves of the transient and persistent sources is clearly seen. 42

3.4 Top panel shows the model light curves of a persistent source for different C values, and the bottom panel shows the light curves for a transient source, for the dame parameter values. The model curves representing pure viscous decay are given with solid lines and $T_{\rm crit}$ = 1750 K for the other models. It is seen that the evolution of persistent sources diverges from the pure viscous decay curve much later than transients. 45

3.5 Top panel shows the light curve of a persistent source for different $\alpha_{\rm cold}$ values, and the bottom panel shows the light curves for a transient source, for the same parameter values. The pure viscous decay curves are also presented (solid lines) for comparison. For the other models, we take $T_{\rm crit}$ = 1750 K and $C = 1 \times 10^{-4}$. 46

3.6 0.1 – 10 keV unabsorbed X-ray flux and luminosity data of XTE J1810–197. The absorbed 0.6 – 10 keV XMM data (Bernardini et al., 2009) were converted to unabsorbed 0.1 – 10 keV flux using the 3BB model described in their paper. The XTE data were given in counts s^{-1} cpu^{-1} with a conversion factor for 2 – 10 keV absorbed flux (Ibrahim et al., 2004), with no spectral fits. The XTE data were rescaled by a factor of 2.3 to match the first XMM data, taken in 2003 September (see the text for details). The luminosity is calculated assuming d = 3.5 kpc. For this model, $\delta M \sim 1 \times 10^{23}$ g and the estimated $\delta E \sim 1 \times 10^{40}$ erg. 49

3.7 Unabsorbed 2 – 10 keV flux and luminosity data of SGR 1627–41 (Mereghetti et al., 2006b). The parameters of the model curve, given by the dashed line, are listed in Table 3.1. The solid curve represents pure viscous decay with the same initial conditions. These model curves are obtained with $\delta M \sim 4 \times 10^{22}$ g, which gives $\delta E \sim 4 \times 10^{39}$ erg with the chosen $r_{\rm in}$ (see the text for details). The luminosity is calculated assuming $d = 11$ kpc. 51

3.8 Unabsorbed 2 – 10 keV flux data of CXOU J164710.2–455216 (Israel et al., 2007; Woods et al., 2011). The long term model light curves are obtained with $T_{\rm crit} = 1750$ K, and $T_{\rm crit} = 2000$ K. For these models, $\delta M \sim 2 \times 10^{21}$ g and the estimated $\delta E \sim 2 \times 10^{38}$ erg. The luminosity is calculated assuming $d = 5$ kpc. 52

3.9 Absorbed 1–10 keV flux and luminosity data of SGR 0501+4516 (Rea et al., 2009). The model light curves are obtained with $T_{\rm crit}$= 1750 K, and $T_{\rm crit}$= 2000 K. The horizontal line shows the estimated quiescent flux of the source (1.3×10^{-12} erg cm^{-2} s^{-1}), obtained from *ROSAT* observations in 1992, extrapolated to the 1–10 keV band assuming a blackbody emission Rea et al. (2009). The luminosity is calculated assuming $d = 5$ kpc. These model curves are obtained with $\delta M \sim 3 \times 10^{21}$ g. We estimate $\delta E \sim 2 \times 10^{38}$ erg. It is seen that the source is about to diverge from the pure viscous decay curve (solid curve). . 54

4.1 Luminosity, period and period-derivative evolution of model sources for an initial period $P_0 = 150$ ms. Values of the initial disk mass (in units of 10^{-6} $M_\odot$) and the magnetic field (in 10^{12} Gauss) at the poles of the neutron star are given in the figure. The horizontal lines correspond to the period (9.1 s) and the present upper limit on the period-derivative of SGR 0418+5729 (6×10^{-15} s s^{-1}). We also present the minimal torque case (dotted curve) where the disk torque is assumed to vanish when $r_A \geq r_{LC}$. 69

4.2 Luminosity, period and period-derivative evolution of model sources for a polar magnetic field of $B_0 = 1.2 \times 10^{12}$ G on the surface of the neutron star. Values of the initial disk mass (in units of 10^{-6} $M_\odot$) and initial period are given in the figure. The horizontal lines show the present period and upper-limit on $\dot{P}$. The period derivative curves converge to a final value of $\sim 4 \times 10^{-17}$ s s^{-1}, a lower limit given by the dipole spin-down torque when the disk becomes inactive. The dipole spin-down case is given by the dotted-dashed curve. 71

5.1 Evolution of the luminosity, period, first and second period derivatives of the model sources. Horizontal lines show the properties of PSR J1734−3333, with the observational uncertainties in $L_{\rm X}$ and $\ddot{P}$. The vertical lines are to show the time period over which the solid (red) model curve traces the uncertainty range of $\ddot{P}$. Values of B_0 are given in the second panel. For these calculations, we have taken $\rm M_d = 3 \times 10^{-7}$ $M_\odot$ and $P_0 = 300$ ms. In the accretion phase, sources enter the constant $\dot{P}$ phase and $\ddot{P}$ becomes 0 (see text for details). 81

5.2 Evolution of the luminosity, period, first and second period derivatives of model sources. Horizontal dotted lines represent the properties of PSR J1734−3333 with the range of uncertainties in $L_{\rm X}$ and $\ddot{P}$. These illustrative model curves are obtained for $B_0 = 2 \times 10^{12}$ G. The values of initial period and disk mass are given in the second panel. The cooling luminosity is shown with the dot-dot-dashed (black) curve. It is seen that the source properties could be well reproduced with different initial periods. Between the vertical lines given with the same color, the model sources trace the uncertainty range of $\ddot{P}$ (see text for details). 83

5.3 Evolution of the luminosity, period, first and second period derivatives, for models that do not work for PSR J1734–3333. Horizontal dotted lines show the properties of PSR J1734−3333, with the uncertainties in $L_{\rm X}$ and $\ddot{P}$. These model curves are obtained with $B_0 = 2 \times 10^{12}$ G and $P_0 = 300$ ms. The solid lines are the same as the solid lines in Figures 5.1 and 5.2, for the model that works. We also present two illustrative model curves for smaller and greater $\mathrm{M_d}$ that cannot represent the evolution of PSR J1734−3333 (see text for details). 85

5.4 Evolution of the luminosity, period, first and second period derivatives, for model sources with the lowest and highest allowed B_0 values. The magnetic field is given in units of 10^{11} G, the initial period is in seconds and the disk mass is given in units of 10^{-8} $M_\odot$. The cooling luminosity is shown with the dot-dot-dashed (black) curve. 87

5.5 The evolution of the three model sources of Figure 5.3 on the P - $\dot{P}$ diagram. The values of initial disk mass $\mathrm{M_d}$ are shown in the Figure. All sources start with $\mathrm{P_0}$ = 300 ms. The model source with the lowest $\mathrm{M_d}$ (blue) never enters the accretion regime and its period converges to ~ 0.5 s. The model source with the highest $\mathrm{M_d}$ (green) enters the accretion regime early on and after 10^5 years it has P > 30 s. The model represented by the solid curve can reproduce the properties of PSR J1734−3333 (see Figure 5.3). The rectangle shows the current position of the source on the P - $\dot{P}$ diagram. The size of the rectangle represents the uncertainty in the measured $\ddot{P}$ value. . . 89

LIST OF SYMBOLS AND ABBREVIATIONS

r_{in}	Inner radius of the disk
r_{out}	Outer radius of the disk
r_0	The center of the Gaussian pile-up
Δr	The width of the Gaussian pile-up
Σ	The surface density of the disk
Σ_{max}	The maximum surface density of the Gaussian pile-up
Σ_0	The maximum surface density of the extended disk
P_0	The initial spin period of the neutron star
P	The spin period of the neutron star
$\dot{P}$	The time derivative of the spin period
$\ddot{P}$	The second time derivative of the spin period
$M_\odot$	The mass of the Sun
r_{LC}	The light cylinder radius
r_{p}	The passive disk radius
r_{A}	The Alfvén radius
$\mathrm{r_{co}}$	The corotation radius
r_{h}	The hot/cold disk transition radius
$\mathrm{M_d}$	The mass of the disk
$\dot{M}$	The mass-flow rate to the inner disk radius
$\dot{M}_{\mathrm{in}}$	The mass-flow rate to the inner disk radius
$\dot{M}_{\mathrm{acc}}$	The accreted mass-flow rate
δM	The total amount of mass inside the Gaussian pile-up
$R_\odot$	The radius of the Sun
$\dot{E}$	The energy loss rate
E_{tot}	The total energy

δE	The total energy imparted on the disk during burst
$\dot{\Omega}$	The time derivative of the spin frequency
$\dot{\Omega}_*$	The time derivative of the spin frequency
$L_{\rm disk}$	The luminosity of the disk
$L_{\rm X}$	The X-ray luminosity
$F_{\rm X}$	The X-ray flux
$F_{\rm irr}$	The irradiation flux
$T_{\rm eff}$	The effective temperature
$T_{\rm irr}$	The irradiation temperature
$T_{\rm p}$	The passive disk temperature
$T_{\rm crit}$	The critical temperature
n	The braking index
p	The power-law index of the surface density of the disk
μ	The dipole magnetic moment
C	The irradiation parameter
D	The intrinsic dissipation of the disk
$R_{\rm c}$	The critical radius where $F_{\rm irr} = D$
M	The mass of the neutron star
M_*	The mass of the neutron star
τ	The characteristic age of the neutron star
$A_{\rm V}$	The reddening parameter
$\alpha_{\rm hot}$	The viscosity parameter of the hot disk
$\alpha_{\rm cold}$	The viscosity parameter of the cold disk
B_0	The dipole magnetic field at the poles
B	The dipole magnetic field on the equator
B_*	The magnetic field of the star
σ	The Stefan-Boltzmann constant
η	The conversion efficiency of rest mass energy into X-rays
ϵ	The albedo of the disk face
c	The speed of light
c_s	The speed of sound
i	The angle between disk normal and line of sight

v_K	The Keplerian velocity
Ω_K	The Keplerian angular velocity
h	The thickness of the disk
H	The thickness of the disk
H_{in}	The half-thickness of the disk at $r_{\rm in}$
n_H	The Hydrogen column density

AXP	Anomalous X-Ray Pulsar
CCO	Central Compact Object
FDM	Fallback Disk Model
IR	Infrared
PSR	Pulsar
RRAT	Rotating Radio Transient
SGR	Soft Gamma-Ray Repeater
SNR	Supernova Remnant
XDINS	Dim Thermal Isolated Neutron Star

ABSTRACT

ON THE EVOLUTION OF YOUNG NEUTRON STARS WITH FALLBACK DISKS

Şirin Çalışkan

Physics, Ph.D. Thesis, 2013

Supervisor: Ünal Ertan

Keywords: *neutron stars, pulsars, disks, bursts*

In the last decades, developments in observational techniques led to the discovery of new young isolated neutron star populations. Despite distinguishing differences, these young systems also have striking similarities, which suggest possible evolutionary links between them. The emergence of these different populations is likely to be due to their different initial conditions. Understanding the nature of these neutron stars in a single coherent picture requires a detailed investigation of individual properties of the sources that belong to different classes. The properties and emergence of these young neutron stars as distinct populations could be explained if absence, presence and properties of fallback disks are included in the initial conditions in addition to magnetic moment and initial period (Alpar 2001). Pursuing this idea, we investigate the properties of AXP/SGRs and the radio pulsar PSR J1734−3333. We show that: (i) persistent optical/infrared emission of AXP/SGRs can be fit by the emission from the disk surface, (ii) X-ray enhancement light curves of AXP/SGRs can be produced by the relaxation of the disk that has been pushed back by a soft gamma- ray burst, (iii) Luminosity and rotational properties of SGR 0418+5729 can be achieved simultaneously by a neutron star evolving with a fallback disk, and (iv) rotational properties, including the anomalous breaking index and X-ray luminosity of PSR J1734−3333 can be produced simultaneously in the fallback disk model. The model we use is self-consistent in that we use the same basic disk parameters and do not require special assumptions in any of these explanations.

ÖZET

GENÇ NÖTRON YILDIZLARININ YAYILMA DİSKLERİ İLE EVRİMİ ÜZERİNE

Şirin Çalışkan

Fizik, Doktora Tezi, 2013

Danışman: Ünal Ertan

Anahtar kelimeler: *nötron yıldızı, pulsar, disk, patlama*

Son yıllarda, gelişen gözlemsel teknikler yeni genç izole nötron yıldızı sınıflarının keşfine yol açmıştır. Ayırdedici farklılıklarının yanısıra, bu genç nötron yıldızı sistemleri çarpıcı benzerlikler de göstermektedir. Bu benzerlikler, farklı sınıflar arasında evrimsel bağlantılar olabileceğine işaret etmektedir. Bu yıldızların farklı sistemler olarak ortaya çıkmasının nedeni ilk koşullarindaki farklılıklar olmalıdır. Bu nötron yıldızlarının doğasının ve olası evrim ilişkilerinin tutarlı tek bir resim içinde anlaşılabilmesi, değişik sınıflardaki kaynakların kendine has özelliklerinin detaylı olarak incelenmesini gerektirir. Bu genç sistemlerin özellikleri ve farklı sınıflar olarak ortaya çıkmaları, etraflarında bir yayılım diskinin varlığının (veya yokluğunun) ve özelliklerinin manyetik moment ve ilk periyotla birlikte ilk koşullara eklenmesi ile açıklanabilir (Alpar 2001). Bu fikri takip ederek, Anormal X-ışını Pulsarlarının (AXP), Gama-ışını Tekrarlayıcılarının (SGR) ve radyo pulsarı PSR J1734−3333'ün özelliklerini inceleyerek şu sonuçlara varmaktayız: (i) AXP/SGR'lerdeki sürekli optik/kızılötesi ışıması disk ışımasıyla açıklanabilir, (ii) AXP/SGR'lerin X-ışını parlama ışık eğrileri, bir gama-ışını patlaması sonrası geriye itilen iç diskin bundan sonraki yayılması ve kütle aktarımı ile üretilmesi mümkündür, (iii) SGR 0418+5729'un ışıma ve dönme özelliklerine, yayılma diskiyle evrimleşen bir nötron yıldızı eş zamanlı olarak ulaşılabilir, ve (iv) yayılma diski modelinde, bir nötron yıldızı PSR J1734−3333'ün X-ışını ışıma ve dönme özelliklerine, anormal frenleme indeksi de dahil olmak üzere, eş zamanlı olarak ulaşabilir. Bu farklı kaynak özelliklerini, tutarlı bir şekilde, benzer temel disk parametreleriyle ve özel varsayımlara gerek kalmadan açıklayabilmekteyiz.

ACKNOWLEDGEMENTS

First and foremost, I would like to thank my advisor Ünal Ertan for his guidance, good humor, unending enthusiasm and incredible patience. I am lucky to have been his student. I would also like to thank Ali Alpar for his continuous support and encouragement. I'd like to thank Ersin Göğüş, Emrah Kalemci and all members of the High Energy Astrophysics group at Sabancı University. I have always cherished the welcoming and motivating atmosphere here. I would like to thank Graham Wynn for the opportunity to work together. I'd also like to thank Atakan Gürkan for the encouraging chats and extensive help with LaTeX.

I acknowledge support from TÜBİTAK through grants 110T243 and 107T013. I also acknowledge support from FP6 Marie Curie Actions Transfer of Knowledge (ASTRONS, MTKD-CT-2006-042703).

I would like to thank Sinem, Aslıhan and Yıldız for the lively chats during much-needed coffee breaks. I'd like to thank Erkan, Genco, Özgün and Caner for their moral support. I am deeply grateful for Defne, Anastassia and Aslı for their company during both joyous times and difficult times.

Lastly, I would like to thank my mom, who has always looked after me, even when I took her for granted.

Şirin Çalışkan January 2013

Chapter 1

INTRODUCTION

Neutron stars are a subset of compact stars, formed through supernova explosions or through the gravitational collapse of a white dwarf. With radii of $\sim$ 10 km and masses of $\sim$ 1 - 2 $M_\odot$, neutron stars are the objects with the highest densities and the strongest magnetic fields known in our universe. These objects provide excellent opportunity to study the properties of matter under extreme conditions.

Most neutron stars were detected as radio pulsars which emit regular radio pulsations. In the standard model of pulsars, radio beams are produced at the magnetic polar cap regions of the star by the charges accelerated along the open field lines. In the model, magnetic and rotational axes of the pulsar are not aligned. As the star spins around the rotational axis, if the beam of radiation emitted from the magnetic poles sweeps the Earth's position, the observer receives periodic pulses, like those produced by a lighthouse.

Several months before the neutron was discovered by J. Chadwick in 1932, in a paper about the dense stars with mass greater than 1.5 $M_\odot$, L. D. Landau stated: *"The density of matter becomes so great that atomic nuclei come in close contact, forming one gigantic nucleus."* (Landau, 1932). The following year, W. Baade and F. Zwicky summarized the results of their study on supernova explosions with a very compact and modest statement: *"With all reserve we advance the view that supernovae represent the transitions from ordinary stars to neutron stars, which in their final stages consist of extremely closely packed neutrons."* (Baade & Zwicky, 1934).

The first pulsar was discovered in 1967 by J. Bell and A. Hewish and this discovery was awarded the Nobel Prize in 1974, underlining their importance in astrophysics. Russell A. Hulse and Joseph H. Taylor Jr. discovered a double pulsar system in 1974 (Hulse & Taylor, 1975), observed the system for several years and showed that the variations in orbital period of these pulsars is consistent with the expected energy loss through gravitational waves. This verified the predictions of Einstein's general theory of relativity and was the first indirect proof of the existence of gravitational waves, one of the most influential topics of 21st century physics. For this work, Hulse and Taylor were awarded the Nobel Prize in 1993. There are more than 2000 known pulsars at present.

The first X-ray pulsar discovered, Cen X-3, was detected by the X-ray satellite *UHURU* in 1971 (Giacconi et al., 1971). This pulsar is in a binary orbit with a supergiant and the viewing angle allowed astronomers to see eclipses, periodic variations in X-rays as the companion star passes in front of the pulsar. The orbital period and the spin period were easily measured from the X-ray pulses and the periodicity of the eclipse. *UHURU* scanned the entire sky in X-rays and detected a total of 339 X-ray sources, including binaries, SNRs and galaxies (Forman et al., 1978). Since *UHURU*, many other X-ray satellites have been sent to orbit in order to observe X-ray sources. Chief among them are *Chandra*, *XMM Newton*, *Beppo SAX*, *RXTE* and most recently *Suzaku*. X-ray observations are made by detectors onboard high altitude satellites, because the Earth's atmosphere is opaque to X-rays.

Many neutron stars were also discovered as members of binary star systems. These systems are classified into two groups according to the mass of the companion star: High Mass X-ray Binaries (HMXBs) or Low Mass X-ray Binaries (LMXBs). Most of the neutron stars in HMXBs are thought to accrete matter from the stellar wind of their high-mass companions, while some HMXBs also show signs of accretion disks.

Young neutron stars are expected to have short periods as a result of angular momentum conservation during their formation. The discovery of many radio pulsars with very short periods, so-called millisecond pulsars, in globular clusters, was surprising and unexpected, due to the very old ages of these clusters. The neutron

stars in LMXBs have old-type low-mass companions. When the companion of the neutron star fills its Roche lobe, matter falls into the Roche lobe of the neutron star. Conservation of angular momentum prevents this mass to fall directly onto the neutron star and an accretion disk is formed around the neutron star.

It was proposed that millisecond pulsars were spun up by disk torques in binary systems (Alpar et al., 1982). The increasing number of millisecond pulsars recently discovered in LMXBs shows that these systems were indeed recycled by the spin-up torques of accretion disks.

Single neutron stars that have no companions are called *isolated* neutron stars. In the last decades, several young isolated neutron star populations have been identified through broad-band observations from radio to gamma-rays. These isolated neutron star populations are: Anomalous X-ray Pulsars (AXPs), Soft Gamma-ray Repeaters (SGRs), Dim Thermal Isolated Neutron Stars (XDINs), Rotating Radio Transients (RRATs), Compact Central Objects (CCOs) and isolated radio pulsars. These systems show both similarities and striking differences in their observed properties. The physical conditions that lead to the emergence of these neutron stars as different populations, possible connections and differences in the evolutionary paths of these systems are not yet very clear.

Among these systems, Anomalous X-ray Pulsars (AXPs) and Soft Gamma-ray Repeaters (SGRs), are characterized by X-ray luminosities much higher than their rotational powers, a narrow period range and sporadic super-Eddington soft gamma-ray bursts. All of the currently known AXPs and SGRs have periods in the range $2 - 12$ seconds and period derivatives $\dot{P} = 10^{-13} - 10^{-9}$ s s^{-1} (see, e.g. Mereghetti, 2008, for a review of AXPs and SGRs), placing them in the upper right corner of the P-$\dot{P}$ diagram (see Figure 1.1). The period, period derivative, estimated distance and X-ray luminosity of currently known AXPs and SGRs are given in Table 1.1. There are 11 (plus 1 candidate) AXPs and 9 (plus 2 candidate) SGRs known at present. The number of AXPs and SGRs are continually increasing with new discoveries: The newest members of the group, namely SGR 0501+4516, SGR 0418+5729, SGR 1833-0832 and Swift J1822.3-1606, were discovered between 2008 and 2011. Each new source provides new information and helps us better understand the physics behind these neutron stars. Initially, super-Eddington bursts were thought to be

distinguishing properties of SGRs. Later, detection of similar bursts also from six previously known AXPs, namely 4U 0142+61, 1E 1048.1-5937, 1E 1547.0-5408, CXO J164710.2-455216, XTE J1810-197, and 1E 1841-045 (Gavriil et al., 2002, 2007; Kaspi et al., 2003; Mereghetti et al., 2009a; Woods et al., 2005; Krimm et al., 2006; Kumar & Safi-Harb, 2010), implied that AXPs and SGRs actually constitute a single class of neutron stars. The nomenclature has, however, not changed, and their names remained as originally identified. (We use the word "AXPs" to denote both "AXPs and SGRs".)

Dim Thermal Isolated Neutron Stars (XDINs) also lie near the upper right corner of the P-$\dot{P}$ diagram (see Figure 1.1), with periods in the same range (3 – 12 seconds) as that of AXPs. Their period derivatives ($\sim 10^{-14} - 10^{-13}$ s s^{-1}) are close to the lower end of the period derivative range of AXPs. All known XDINs are within a distance of 500 pc, indicating that they are more abundant than the other neutron star populations. Nevertheless, so far only seven of these sources have been detected, despite extensive searches.

Rotating Radio Transients (RRATs) are transient neutron stars that emit short sporadic radio bursts (see McLaughlin, 2009, for a recent review of RRATs). These bursts last a few to tens of milliseconds, much shorter than their spin periods ($\sim$ 0.1 – 10 s). Their period derivatives are in $\sim 10^{-15} - 10^{-12}$ s s^{-1} range (see Figure 1.1). The first 11 RRATs were discovered in 2006 during a pulsar survey (McLaughlin et al., 2006) and today there are more than 60 confirmed RRATs (Keane et al., 2011).

Neutron stars are born with small periods (on the order of a fraction of a second), due to the conservation of angular momentum. Work by Faucher-Giguère & Kaspi (2006) indicates that the statistical distribution of their initial periods can be represented by a Gaussian profile with a mean of $\sim$ 300 ms and a standard deviation of $\sim$ 150 ms. AXPs are spinning down much faster than all the other pulsars; their $\dot{P}$ values are several orders of magnitude greater than other radio pulsars. The efficient torque mechanism acting on AXPs needs to be explained self-consistently with the observed period, period derivative, X-ray luminosity and statistical properties.

What is the mechanism that powers and slows down these young neutron stars to such long periods on short timescales ($\sim 10^3 - 10^5$ years)? Brief super-Eddington soft

Table 1.1: The period, period derivative, estimated distance and X-ray luminosity of known AXPs and SGRs. The references are as follows: 1. McGarry et al. (2005), 2. Tiengo et al. (2008), 3. Dib et al. (2007), 4. Durant & van Kerkwijk (2006a), 5. Dib et al. (2009), 6. Gaensler et al. (2005), 7. Dib et al. (2012), 8. Tiengo et al. (2010), 9. Levin et al. (2010), 10. Woods et al. (2011), 11. Kothes & Dougherty (2007), 12. Dib et al. (2008), 13. Sato et al. (2010), 14. Tian & Leahy (2012), 15. Camilo et al. (2007a), 16. Minter et al. (2008), 17. Tian & Leahy (2008), 18. Kothes & Foster (2012), 19. Gavriil & Kaspi (2002), 20. Rea et al. (2010), 21. van der Horst et al. (2010), 22. Göğüş et al. (2010), 23. Leahy & Tian (2007), 24. Tiengo et al. (2009), 25. Klose et al. (2004), 26. Esposito et al. (2009b), 27. Esposito et al. (2009a), 28. Corbel et al. (1999), 29. Nakagawa et al. (2009), 30. Bibby et al. (2008), 31. Rea et al. (2012), 32. Scholz et al. (2012), 33. Esposito et al. (2011), 34. Kargaltsev et al. (2012), 35. Leahy & Tian (2008), 36. Mereghetti et al. (2006a), 37. Davies et al. (2009).

Name	P (s)	$\dot{P}$ (10^{-11} s/s)	d (kpc)	$L_{\rm X}$ (10^{35} erg/s)	References
CXOU J010043.1-721134	8.02	1.89	60	∼0.61	1, 2
4U 0142+61	8.69	0.2	3.6(4)	1.1	3, 4
1E 1048.1-5937	6.46	∼2.25	2.7(1)	0.059	5, 6
1E 1547.0-5408	2.07	∼4.7	4.5(5)	∼0.0078	7, 8
PSR J1622-4950	4.33	1.7	∼9	∼0.0063	9
CXO J164710.2-455216	10.61	∼0.073	3.9(7)	∼0.0027	10, 11
1RXS J170849.0-400910	11.00	1.91	3.8(5)	0.59	4, 12
CXOU J171405.7-381031	3.83	6.40	∼13.2	∼0.60	13, 14
XTE J1810-197	5.54	0.78	3.5(5)	∼0.00031	15, 16
1E 1841-045	11.78	3.93	∼8.5	∼1.9	12, 17
1E 2259+586	6.98	0.05	3.2(2)	0.22	18, 19
SGR 0418+5729	9.08	<0.0006	∼2		20, 21
SGR 0501+4516	5.76	0.582	0.8±0.4		22, 23
SGR 0526-66	8.05	3.8	50	1.4	24, 25
SGR 1627-41	2.59	1.9	11.0±0.3	∼0.025	26, 27, 28
SGR 1806-20	7.60	75	$8.7^{+1.8}_{-1.5}$	1.6	29, 30
Swift J1822.3-1606	8.44	0.0254	1.6±0.3		31, 32
SGR 1833-0832	7.57	0.35			33
Swift J1834.9-0846	2.48	0.796	4.2±0.3		34, 35
SGR 1900+14	5.20	9.2	12.5±1.7	0.90	36, 37

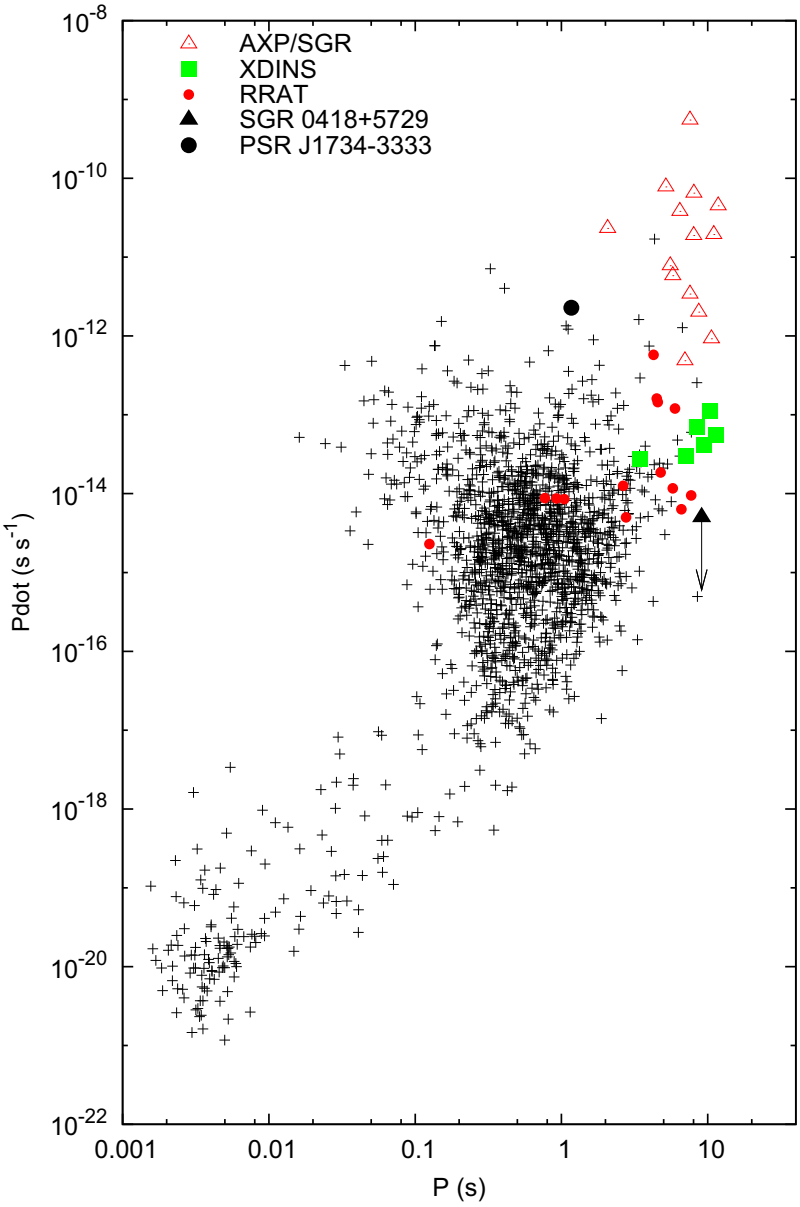

Figure 1.1: The period and period derivatives of pulsars. The plus signs show radio pulsars. AXP/SGRs are denoted with red triangles at the top right corner. XDINS are immediately below them, shown with green squares. RRATs with measured period derivatives are shown with red dots. The interesting SGR 0418+5729 is shown with a filled black triangle, with its currently known $\dot{P}$ upper limit ($\dot{P} < 6 \times 10^{-15}$ s s^{-1}). The radio pulsar PSR J1734–3333 is shown with a black filled circle. The data were taken from the online ATFN pulsar catalog (http://www.atnf.csiro.au/research/pulsar/psrcat/)

gamma-ray bursts require presence of strong fields on the surface of the neutron star. Whether these strong magnetic fields are stored in the dipole or higher multipole components is quite important and distinguishing between theoretical models.

In the magnetar model (Duncan & Thompson, 1992; Thompson & Duncan, 1995, 1996), it is assumed that AXPs and SGRs are neutron stars with extremely strong dipole magnetic fields ($B_0 > 10^{14}$ G), rotating in vacuum. In this model, strong torques acting on AXPs are provided by magnetar dipole radiation, while the field decay produces the X-ray luminosity of these sources.

The magnetar model cannot explain the statistical properties and the period clustering of these sources. Furthermore, recent observations of bursts from SGR 0418+5729 showed that it has an unusually low period derivative ($\dot{P} < 6 \times 10^{-15}$ s s^{-1}). If the spindown is caused by the magnetic dipole torques in vacuum, as proposed by the magnetar model, the upper limit on the strength of the dipole magnetic field perpendicular to the rotational axis can be evaluated as $B = 3.2 \times 10^{19}\sqrt{P\dot{P}} < 7.5 \times 10^{12}$ G, on the equator of the star. This shows that magnetar dipole fields are not required in order to produce bursts (Rea et al., 2010). The strength of the total magnetic field on the surface of the star was estimated to be 1.1×10^{14} G (Güver et al., 2011).

In the fallback disk model (Chatterjee et al., 2000; Alpar, 2001), AXPs are young neutron stars with conventional dipole fields ($10^{12} - 10^{13}$ G) and evolving with fallback disks, left over from supernova explosions. The subsequent evolution of the neutron star depends on the properties of the fallback disk, among other initial parameters (magnetic dipole moment and initial period of the neutron star). The properties of the fallback disk as an additional initial parameter was proposed to be responsible for the emergence of different young neutron star populations, including AXPs and SGRs (Alpar, 2001). In this model, some of the supernova matter that remains bound to the system forms a disk around the star. Accretion of disk matter onto the star produces the X-ray luminosity. The rotational evolution of the neutron star is determined by the interaction between the disk and the magnetic dipole field of the source. The efficient torque applied on the star by the disk could lead to the observed long periods within $\sim 10^3 - 10^5$ years. Dipole fields of magnetar strength are not required in the fallback disk model – the model sources that can explain the

basic properties of AXP/SGRs typically have $B_0 \sim 10^{12} - 10^{13}$ G. The burst energies can be stored in the higher multipoles of the magnetic field. The field strength of these higher multipoles decreases rapidly with increasing radial distance and thus do not interact with the disk.

Fallback disks around AXP/SGRs differ from the accretion disk found in LMXBs in several aspects. The outer radius of an accretion disk of a binary is truncated at a radius determined by tidal forces. In a fallback disk, the lack of a companion star removes this constraint on the outer radius. The outer boundary of an active fallback disk is likely to be determined by a critical temperature below which the turbulent viscosity mechanism cannot operate. The inner radius of a fallback disk around AXPs is also larger compared to that of the accretion disk in an LMXB, since much stronger magnetic dipole fields of AXPs increase the Alfvén radius. While the inner disk radius is close to the surface of the neutron star in most of LMXBs, it is about 10^9 cm for AXPs with conventional dipole fields. For accretion disks in LMXBs, there is a continuous mass supply from the companion star, while AXPs have no companions and the disk is free to expand without any additional mass source. This makes the lifetime of a fallback disk shorter compared to a disk in a binary system.

The ratio of the disk luminosity to the X-ray luminosity, like in LMXBs, could vary depending on the inclination angle of the disk with respect to the observer. Nevertheless, the relative fluxes at different infrared/optical bands are expected to be the same for the fallback disks in the same evolutionary phase (in the same accretion regime with the same disk size). In all our calculations we take $\cos i = 1$ (face-on disk), that is, in the calculation of infrared/optical fluxes the uncertainty in the inclination angle of the disk is absorbed into the irradiation parameter (see Chapter 2 for description). The irradiation of LMXB disks is believed to be indirect (see e.g. Dubus et al., 1999) probably from a hot scattering corona continuously fed by the thermally unstable matter from the optically thin surface layers of the inner disk. In the AXP and SGR disks, such thermally unstable inner disk regions close to the neutron star do not exist, since the disk is cut by dipole magnetic fields of AXPs, much stronger than those of LMXBs. Nevertheless, the heating resulting from the disk-magnetosphere interaction might provide hot scattering matter around

the inner rim of the disk. In our calculations, we find that the irradiation efficiencies of fallback disks to be roughly in the same range as those estimated for LMXB disks.

The chemical composition of a fallback disk is not well known. It is likely to have a much higher metallicity than in the accretion disks of LMXBs. This is because a fallback disk is formed during a core collapse supernova, while the LMXB disks are fed by mass-flow from the outer, mainly hydrogen, envelope of a low-mass star.

AXPs occasionally show outbursts/enhancements. An abrupt increase in soft X-ray luminosity is followed by a gradual decline, converging to the pre-outburst level. In most cases, these X-ray enhancements are observed to be preceded by soft gamma-ray bursts. In the fallback disk model, it is assumed that the bursts push the inner disk matter out to larger radii, causing a pile-up at the inner disk. Subsequent relaxation of this pile-up produces the X-ray enhancement light curves of AXPs. This model can account for the enhancement of the SGR 1900+14 following its giant flare (Ertan & Alpar, 2003) and the correlated contemporaneous X-ray and IR enhancement light curves of AXP 2259+58 (Ertan et al., 2006b).

An irradiated, active fallback disk model can also account for the optical/IR emission observed from AXPs (Ertan & Çalışkan, 2006; Ertan et al., 2007). The detection of AXP 4U 0142+61 in mid-IR bands was a clear indication of the presence of a disk around this source (Wang et al., 2006). This mid-IR data, together with earlier detections in optical and near-IR bands, can be fit by an irradiated active disk model, provided that the dipole field strength is less than 10^{13} G on the surface of the neutron star (Ertan et al., 2007). A few years later, another AXP, 1E 2259+586, was also detected in the mid-IR bands (Kaplan et al., 2009), providing yet another supporting evidence for the presence of fallback disks around these sources.

In this thesis, we have investigated the following basic properties of young neutron star systems in the frame of the fallback disk model:

- Persistent optical/infrared emission from the fallback disks of AXP/SGRs,
- X-ray enhancements (outbursts) of persistent and transient AXP/SGRs after a soft gamma-ray burst,
- The long term evolution of SGR 0418+5729 with a fallback disk,
- The peculiar braking index and the long term evolution of PSR J1734-3333.

In Sections 1.1 - 1.4, we summarize the observations and the model calculations related to these topics. Detailed explanations are given in Chapters 2 - 5.

1.1 Optical and Infrared Emission from the AXPs and SGRs

The suggestion of fallback disks around AXPs motivated observational searches for disk emission in the optical and IR bands, and resulted in various constraints on the models. Most of the AXPs have been detected in the near-IR bands (Hulleman et al., 2001; Israel et al., 2002; Wang & Chakrabarty, 2002; Kaspi et al., 2003; Israel et al., 2003; Hulleman et al., 2004; Israel et al., 2004; Tam et al., 2004; Morii et al., 2005; Durant & van Kerkwijk, 2006b; Camilo et al., 2007b; Tam et al., 2008; Wang et al., 2008; Testa et al., 2008; Morii et al., 2009; Dhillon et al., 2011). AXP 4U 0142+61 was also detected in the optical R and V bands (Hulleman et al., 2000, 2004; Dhillon et al., 2005), as well as in near-IR and mid-IR bands which provided strong evidence of a disk (Wang et al., 2006). SGR 0501+4516 and AXP 1E 1048.1-5937 were detected in the I band (Dhillon et al., 2009, 2011; Durant & van Kerkwijk, 2005), while upper limits were obtained on the R band luminosity (Halpern, 2008; Wang et al., 2008). The optical and near-infrared detections/upper limits of AXP/SGRs are listed in Table 1.2.

In Chapter 2, we study the unpulsed optical/IR emission from the AXPs and SGRs in their persistent states, and test the expectations of the irradiated accretion disk model through the observations in different optical/IR energy bands. The accretion of matter from the inner disk onto the neutron star produces the X-ray luminosity. The X-ray irradiation flux dominates the heating by viscous dissipation, except for the innermost disk region. The blackbody temperature profile of the disk is calculated taking into account both the irradiation flux and the viscous dissipation (Shakura & Sunyaev, 1973; Dubus et al., 1999; King, 1999). In Chapter 2, we show that the optical/IR data of the AXPs can be explained by the irradiated active disk model with reasonable disk parameters.

1.2 X-ray Outbursts of Transient AXPs and SGRs

Both AXPs and SGRs undergo occasional soft gamma-ray bursts. After a burst episode, these sources enter an X-ray outburst phase, characterized by a sharp

Table 1.2: The observed optical and near-infrared magnitudes and upper limits of known AXPs and SGRs. In cases of multiple observations, the range of magnitudes are given. In case of multiple upper limits, the lowest upper limit is given. The data were taken from the McGill Online Catalog (http://www.physics.mcgill.ca/∼pulsar/magnetar/main.html).

Name	K/K_S	H	J	I	R	V
CXOU J010043.1-721134				>25.9		>26.2
4U 0142+61	19.7-20.8	20.5-20.9	21.2-22.0	23.4-24.0	24.9-25.6	25.3-26.1
1E 1048.1-5937	19.4-21.5	20.8-22.7	21.7-23.4	24.9-26.2	>24.8	
1E 1547.0-5408	18.5					
PSR J1622-4950	>18.1	>18.8	>20.4			
CXO J164710.2-455216	>18.5					
1RXS J170849.0-400910	18.9-19.3	20.0-20.3	21.9		>26.5	
CXOU J171405.7-381031						
XTE J1810-197	20.8-21.9	21.5-22.6	22.9-23.9	>24.3		
1E 1841-045	19.6-20.5	20.8	>22.1			
1E 2259+586	20.4-21.7		>23.8	>24.2	>25.6	
SGR 0418+5729	>19.6		>27.4	>25.1	>24	>28.6
SGR 0501+4516	18.6-19.7			23.3-24.4	>23.0	
SGR 0526-66				>24.3		>23.7
SGR 1627-41	>18.1	>18.8	>20.4			
SGR 1806-20	19.3-21.9	>19.5	>21.2			
Swift J1822.3-1606	>17.3	>18.3	>19.3	>22.2		
SGR 1833-0832	>22.4			>24.9		
Swift J1834.9-0846	>19.5			>21.6		
SGR 1900+14	19.2-19.7			>21		

increase and eventual decay in X-ray luminosity. Some AXPs, called *transient* AXPs, have very low X-ray luminosities ($\sim 10^{33}$ erg s^{-1}) in the quiescent phase. These sources were detected during their X-ray enhancement phases. In an outburst, the X-ray luminosity, $L_{\rm X}$, of the transient sources increases from $\sim 10^{33}$ erg s^{-1} to a maximum that remains in the $L_{\rm X}$ range of *persistent* AXPs (10^{34} – 10^{36} erg s^{-1}).

The optical, infrared and X-ray observations of persistent AXPs and SGRs in both quiescent and enhancement phases can be explained consistently by the presence of active, accreting fallback disks around these systems (Ertan & Alpar, 2003; Ertan & Cheng, 2004; Ertan et al., 2006b; Ertan & Çalışkan, 2006). In Chapter 3, we investigate the X-ray enhancement light curves of both persistent and transient AXPs. We pursue the results of the work by Ertan & Erkut (2008) on the transient AXP XTE J1810–197, whose light curve showed a different decay morphology than those of persistent sources (Ibrahim et al., 2004; Bernardini et al., 2009). By means of model fits to the X-ray enhancement data, Ertan & Erkut (2008) concluded that this difference could be due to a viscous disk instability in the fallback disk. The fallback disks around AXPs are expected to have similar chemical compositions. If one of the AXP disks undergoes a thermal-viscous disk instability at a particular critical temperature, then the others are also expected to show the same instability at the same temperature. Furthermore, other basic disk parameters, namely kinematic viscosity, irradiation strength and the radius dependence of the surface density of the extended disk, are expected to be similar in all fallback disks around AXPs. This led to a difficult task of producing the X-ray outburst light curves of AXPs with a single set of these basic disk parameters. Together with a detailed parameter study, the model calculations and results are given in Chapter 3.

1.3 The Evolution of SGR 0418+5729 with a fallback disk

SGR 0418+5729 has a period $P = 9.1$ s (Göğüş et al., 2009). The period derivative has not been measured yet (Kuiper & Hermsen, 2009; Woods et al., 2009; Esposito et al., 2010; Rea et al., 2010). Recently Rea et al. (2010) reported that $\dot{P} < 6 \times 10^{-15}$ s s^{-1}[1]. If this is the dipole spin-down of an isolated star in vacuum,

[1]A more recent measurement of $\dot{P} = 5 \times 10^{-15}$ s s^{-1} was reported by Rea (2012), but it has not been confirmed yet.

the surface dipole magnetic field $B < 7.5 \times 10^{12}$ G on the equator, which is much lower than fields previously inferred from spin-down rates of magnetars. The characteristic age $P/(2\dot{P})$ of this source is greater than 2.5 $\times 10^7$ years, although AXPs and SGRs, some of which are associated with supernova remnants, are thought to be young neutron stars with ages $\sim 10^3 - 10^5$ years. If SGR 0418+5729 is a standard magnetar, it provides a clear counterexample to the proposition that the magnetic dipole component of AXPs should have magnetar strength.

If the spin-down of the source was achieved by magnetic dipole radiation, it would make SGR 0418+5729 an unusual neutron star that mimicks all SGR and AXP properties, but does not belong to the class. Furthermore, if the true age of SGR 0418+5729 is its characteristic age, greater than 2.5×10^7 years, then its quiescent X-ray luminosity cannot be explained by cooling, reheating or magnetic field decay. The soft gamma-ray outbursts occurring at such an old age cannot be explained either. If this SGR is much younger than its characteristic age, but spun-down with dipole radiation, then its initial spin period would have to be close to the present 9.1 second period, which makes this source stand far out from the initial period distribution inferred from population synthesis (Faucher-Giguère & Kaspi, 2006). A rapid decay of the dipole field was proposed to explain the evolution of this source, which also requires an exceptional evolution with extremely strong initial toroidal fields (Turolla et al., 2011).

In Chapter 4, we investigate evolutionary scenarios for SGR 0418+5729 employing a fallback disk. Our results imply that SGR 0418+5729 does not have exceptional properties. With a dipole magnetic field similar to the other AXP/SGRs ($B_0 < 10^{13}$ G), the properties of the source can be reached by the model sources in the frame of the fallback disk model.

1.4 The Peculiar Braking Index and Evolution of PSR J1734−3333

Newly discovered radio pulsars with strong inferred dipole magnetic fields ($\gtrsim 10^{14}$ G) and the radio pulses observed from some AXPs and SGRs hint at the possibility of links between these sources (Kaspi & McLaughlin, 2005; Espinoza et al., 2011). The locations and evolutionary tracks of pulsars in the $P - \dot{P}$ diagram may decipher these links. PSR J1734−3333 has a spin period $P = 1.17$ s, period derivative $\dot{P} =$

2.28×10^{-12} s s^{-1} and period second derivative $\ddot{P} = 5.3 \times 10^{-24}$ s s^{-2} (Espinoza et al., 2011). Its braking index can be calculated as $n \equiv 2 - (P\dot{P}/\ddot{P}^2) = 0.9 \pm 0.2$. With this unusually low braking index, the lowest among young pulsars, PSR J1734−3333 provides a tight constraint to test the models.

If the spindown of PSR J1734−3333 is due to the magnetic dipole radiation in vacuum, as proposed by the magnetar model, and the magnetic dipole moment remains constant, then the braking index should be $n = 3$. In this case, the period derivative should steadily decrease throughout the life of the source. The positive period second derivative and low n value of PSR J1734−3333 therefore challenges the magnetar model. Within the magnetar model, explaining the behavior of AXPs and the so-called "high B" pulsars evolving towards the AXP region in the $P - \dot{P}$ diagram requires field growth for some sources, while the field should decay for some others in the long term evolution.

For neutron stars evolving with fallback disks, the low braking index (and growing $\dot{P}$) can be explained naturally in certain phases of the long term evolution. In Chapter 5, we study the evolution of PSR J1734−3333 in the frame of the fallback disk model. Tracing possible initial conditions, we try to constrain the allowed values of disk mass and dipole field strength that can simultaneously produce the properties ($P, \dot{P}, \ddot{P}$ and $L_{\rm X}$) of PSR J1734−3333.

We investigate the persistent optical and infrared emission properties of AXPs with a fallback disk in Chapter 2. A detailed analysis of the X-ray enhancement light curves of transient and persistent AXPs is given in Chapter 3. In Chapters 4 and 5, we test whether the fallback disk model can self-consistently explain the properties of both SGR 0418+5729 and PSR J1734−3333, a soft gamma-ray repeater and a radio pulsar. We summarize and discuss our results in Chapter 6. Our conclusions and future plans are also summarized in Chapter 6.

Chapter 2

OPTICAL AND INFRARED EMISSION FROM THE AXPS AND SGRS

This chapter of the thesis was published in
The Astrophysical Journal Letters, 2006, Volume 649, pp. 87 - 90
Ünal Ertan & Şirin Çalışkan

Abstract

We show that the irradiated accretion disk model can account for all the optical and infrared observations of the anomalous X-ray pulsars in the persistent state. While placing an upper limit on the inner disk radii, and thus on the strength of the dipole component of the stellar magnetic field, the model fits do not constrain the outer disk radii. And while magnetar fields ($B_* > 10^{14}$ G) in higher multipoles are compatible with the irradiated disk model, magnetic dipole components of magnetar strength are not consistent with optical data.

2.1 Introduction

Anomalous X-ray pulsars (AXPs) and soft gamma-ray repeaters (SGRs) constitute a special class of neutron star systems (Mereghetti et al., 2002; Hurley, 2000; Woods & Thompson, 2006). They are identified mainly through their X-ray luminosities ($L_{\rm X} \sim 10^{34}-10^{36}$ erg s^{-1}), which are orders of magnitude higher than their rotational powers $\dot{E}_{rot} = -I\Omega\dot{\Omega}$. Their spin periods are clustered to a very narrow range ($2-12$ s). All five known SGRs and two of the eight known AXPs[2] show repetitive, short ($\lesssim$1s) super-Eddington bursts with luminosities up to 10^{42} erg s^{-1}. Three giant flares with peak luminosities $L_{\rm p} > 10^{44}$ erg s^{-1} and durations of a few minutes were observed from three different SGRs (Mazets et al., 1979, 1999; Hurley et al., 1999; Palmer et al., 2005).

The short timescales and the super-Eddington luminosities of these soft gamma-ray bursts strongly indicate a magnetar mechanism. The magnetar models (Duncan & Thompson, 1992; Thompson & Duncan, 1995, 1996) have strong magnetic fields with magnitudes $B_* > 10^{14}$ G on the stellar surface to explain the burst energetics. Are the burst energies stored in the dipole component or the higher multipoles of the magnetic field of the neutron star? In the current magnetar models, the dipole component of the magnetic field must be of magnetar strength to account for the spin-down properties of the AXPs and SGRs. In these models, persistent X-ray luminosities are explained by the magnetic field decay, while the magnetic dipole torque is taken to be the mechanism responsible for the spin-down rates of the

[2]Since the publication of this paper, bursts have been observed from all nine SGRs and six of the AXPs.

sources.

In the alternative fallback disk model (Chatterjee et al., 2000; Alpar, 2001), the source of the X-rays is the accretion onto the neutron star, while the optical/IR light originates from the accretion disk. The rotational evolution of the neutron star is determined by the interaction between the disk and the magnetosphere of the neutron star ($B_* \sim 10^{12} - 10^{13}$ G). Fallback disk models can account for the period clustering of AXPs and SGRs as the natural outcome of disk-magnetosphere interaction during their lifetimes (Alpar, 2001; Ekşi & Alpar, 2003). These models are consistent with magnetar fields on the neutron star provided that these fields are in higher multipole components of the magnetic field. As higher multipole fields rapidly decrease with increasing radial distance (as r^{-5} for the quadrupole component), it is the dipole component of the magnetic field that determines the interaction and the angular momentum transfer between the disk and the neutron star. In order to explain the period clustering of the AXPs and SGRs over their $\dot{M}$ (mass accretion rate) history, the strength of magnetic dipole field must be $B_0 \sim 10^{12} - 10^{13}$ G (Alpar, 2001; Ekşi & Alpar, 2003).

Fallback disk models can also explain the enhancements observed in the persistent luminosities of SGRs and AXPs. The X-ray enhancement of the SGR 1900+14 following its giant flare can be explained by the relaxation of a disk which has been pushed back by a preceding burst (Ertan & Alpar, 2003). The same model with similar disk parameters can also reproduce the correlated X-ray and IR enhancement of AXP 2259+58, which lasted for ~ 1.5 years, if this is triggered by a burst, with a burst energy estimated to have remained under the detection limits (Ertan et al., 2006b).

The suggestion of fallback disks has motivated observational searches for disk emission in the optical and IR bands, and has resulted in various constraints on the models. Some of the AXPs were observed in more than one IR band (Hulleman et al., 2001; Israel et al., 2002; Wang & Chakrabarty, 2002; Kaspi et al., 2003; Israel et al., 2003; Hulleman et al., 2004; Israel et al., 2004; Tam et al., 2004; Morii et al., 2005; Durant & van Kerkwijk, 2006b). AXP 4U 0142+61 is the source with the most extended observations, as it was also observed in the optical R and V bands (Hulleman et al., 2000, 2004; Dhillon et al., 2005), and recently in mid-IR bands with

the *Spitzer Space Telescope* (Wang et al., 2006). The discovery of modulation in the R band luminosity of 4U 0142+61 at the neutron star's rotation period P = 8.7 s, with a pulsed fraction of 27 % (Kern & Martin, 2002; Dhillon et al., 2005), is particularly significant. This fraction is much higher than the pulsed fraction of the X-ray luminosity of this source, indicating that the origin of the pulsed optical emission is not likely to be the reprocessed X-rays by the disk. Magnetospheric models for these pulsations can be built either with a dipole magnetar field or within a disk-star dynamo model (Cheng & Ruderman, 1991), in which magnetospheric pulsar activity is sustained by a stellar dipole field of $\sim 10^{12}$ G and a disk protruding within the magnetosphere. Ertan & Cheng (2004) showed that this pulsed optical component of the AXP 4U 0142+61 can be explained by both types of magnetospheric models. Thus, the presence of strong optical pulsations from the magnetosphere does not rule out the possibility of a fallback disk with a $10^{12} - 10^{13}$ G surface dipole magnetic field.

In the present work, we concentrate on the unpulsed optical/IR emission from the AXPs and SGRs in their persistent states, and we test the expectations of the irradiated accretion disk model through observations in different optical/IR energy bands (V, R, I, J, H, K, and K_s). The optical/IR emission expected from the irradiated fallback disks was first computed and discussed by Perna et al. (2000) and Hulleman et al. (2000). Using similar irradiation strengths, Perna et al. (2000) and Hulleman et al. (2000) found similar optical fluxes that remain well beyond those indicated by the observations of AXP 4U 0142+61 and AXP 1E 2259+586. To explain this result, Perna et al. (2000) suggested that the inner disk regions could be cut by an advection dominated flow, while Hulleman et al. (2000) concluded that the then existing optical data of the AXP 4U 0142+61 (in I, R, and V bands) can only be accounted for by an extremely small outer disk radius, around a few $\times 10^9$ cm. In the present work, we show that the optical/IR data of the AXPs can be explained by the irradiated accretion disk model without any implausible constraints on the outer and inner disk radii. The main reason for the difference between our results and those of earlier works is that both Hulleman et al. (2000) and Perna et al. (2000) assumed a particular irradiation strength, while we keep it as a free parameter, to address the broadband full data set. This approach is supported by the observations

of the low-mass X-ray binaries (LMXBs) that indicate varying irradiation strengths. Furthermore, model fits are sensitive to the interstellar reddening parameter $A_{\rm V}$, which was estimated to be between 2.6 and 5.1 for 4U 0142+61 (Hulleman et al., 2004). For this source, we obtain the best model fit with $A_{\rm V} = 3.5$, which turned out to be consistent with the recent result of $A_{\rm V} = 3.5 \pm 0.4$ (Durant & van Kerkwijk, 2006c). On the other hand, the test disk model with an unreasonably small outer disk radius requires $A_{\rm V} = 5.4$ (Hulleman et al., 2000). In this model, the optical emission comes from the outer disk, while in our model, it is the inner regions of an extended disk that emits substantially through the optical bands (see Section 2.3 for further discussion). We give the details of the disk model in Section 2.2. We discuss our results in Section 2.3, and summarize our conclusions in Section 2.4.

2.2 Optical/IR Emission from the Irradiated Disk

Model fits to the X-ray and IR enhancement data (Kaspi et al., 2003) of AXP 1E 2259+586 favor the irradiated disk model, although they do not exclude the nonirradiated thin disk model (Ertan et al., 2006b). We start by assuming that the AXP disks are irradiated and include the irradiation strength as a free parameter through our calculations.

When the disk is irradiated by the X-rays from the neutron star, both the intrinsic dissipation and the irradiation flux should be taken into account in calculations of the disk blackbody emission. A steady disk model is a good approximation for the present evolution of the AXP and SGR disks in their persistent states. For a steady thin disk, the intrinsic dissipation can be written as

$$D = \frac{3}{8\pi}\frac{GM\dot{M}}{R^3}, \tag{2.1}$$

where $\dot{M}$ is the disk mass flow rate, M is the mass of the neutron star and R is the radial distance from the neutron star (see, e.g., Frank et al., 2002). In the absence of irradiation, the effective temperature $T_{\rm eff}$ of the disk is proportional to $R^{-3/4}$ for a given $\dot{M}$. For an irradiated disk, the irradiation flux can be written as

$$F_{\rm irr} = \sigma T_{\rm irr}^4 = C\frac{\dot{M}c^2}{4\pi R^2}, \tag{2.2}$$

where c is the speed of light (Shakura & Sunyaev, 1973). Irradiation parameter C includes the albedo of the disk face, the disk geometry, and the conversion efficiency of the accretion into X-rays. Irradiation temperature $T_{\rm irr}= (F_{\rm irr}/\sigma)^{1/4}$ is proportional to $R^{-1/2}$ (Equation 2.2). For small radii, dissipation is the dominant source of the disk emission. At a critical radius R_c, the irradiation flux becomes equal to the dissipation rate, and beyond R_c, the disk emission is supported mainly by reprocessed X-rays. Equating $F_{\rm irr}$ to D (Equations 2.1 and 2.2), the critical radius is found to be

$$R_c = \frac{3}{2}\frac{GM_*}{Cc^2} \simeq \left(\frac{10^{-4}}{C}\right) 3 \times 10^9 \text{cm}. \tag{2.3}$$

The effective temperature profile of the disk can be obtained using

$$\sigma T_{\rm eff}^{1/4} = D + F_{\rm irr} \tag{2.4}$$

where σ is the Stefan-Boltzmann constant.

We adopt the observed magnitudes in the optical/IR bands, distances and the N_H values given by Woods & Thompson (2006) and references therein and convert the magnitudes to energy flux values. We calculate $A_{\rm V}$ values using $N_H = 1.79\times10^{21}$ $A_{\rm V}$ (Predehl & Schmitt, 1995). To find the model disk flux in a given observational band, we integrate the calculated blackbody emissions of all radial grids radiating in this band. For comparison with data, we calculate the model disk fluxes along the optical/IR bands V, R, H, I, J, K and K_s. For all sources, we set $\cos i = 1$ where i is the angle between the disk normal and the line of sight of the observer. We equate the disk mass flow rate $\dot{M}$ to the accretion rate onto the neutron star, thus assuming the mass loss due to the propeller effect is negligible. We first adjust $\dot{M}$ to obtain the observed X-ray flux. Next, using this value of $\dot{M}$ and taking the strength of the magnetic dipole field $B = 10^{12}$ G on the surface of the neutron star, we calculate the Alfvén radius $r_{\rm A}$, which we take to be the inner radius of the disk. Then, we look for a good fit to the overall available optical/IR data by adjusting the irradiation strength C within the uncertainties discussed in Section 2.3.

2.3 Results and Discussion

Our results are summarized in Table 2.1. For each source, the first column gives the unabsorbed flux data obtained from the observed magnitudes and the estimated A_V values (see Table 2.1) given in Woods & Thompson (2006), and the second column gives the model fluxes. For the AXP 4U 0142+61, the range of reddening quoted in earlier literature is $2.6 < A_V < 5.1$ (Hulleman et al., 2004). We obtain a good fit with $A_V = 3.5$. Table 2.1 shows that the irradiated steady disk model is in agreement with all the AXPs observed in the optical and IR bands. The parameters of the model for each source are given in Table 2.2.

At present, AXP 4U 0142+61, which has been observed in five different optical/IR bands from K to V in the same X-ray luminosity regime, seems to be the best source for studying the properties of AXPs in the persistent state. Earlier work by Hulleman et al. (2000) excluded the disk model for the AXP 4U 0142+61. They obtained an irradiation temperature profile by using a particular irradiation strength. The estimated optical flux for an extended disk with this irradiation efficiency remains above the optical data points of the AXP 4U 0142+61 (see Figure 3 in Hulleman et al., 2000). Considering the possibility that the optical flux might originate from the outermost disk region, Hulleman et al. (2000) tried to fit the then observed three data points in the I, R and V bands to the Rayleigh-Jeans tail of a blackbody spectrum with the extinction parameter $A_V = 5.4$. This placed an upper limit on the outer disk radius that is too small for a realistic disk. The key factor in the difference between the earlier results and our recent results is the irradiation efficiency, which we allow to vary in conjunction with A_V, to provide the best fit to the current broadband data. We note that the irradiation efficiency indicated by the observations of the low mass X-ray binaries varies from source to source. Even for the same source, the ratio of the irradiation flux to the X-ray flux may change with accretion rate (de Jong et al., 1996; Dubus et al., 1999; Ertan & Alpar, 2002). Taking these into account, we keep the irradiation efficiency as a free parameter for our model fits. With the parameters given in Table 2.2, the irradiated disk model can account for the optical/IR data of this source without setting any stringent constraints on the inner or outer disk radii. In our model, the optical luminosity is radiated from the inner disk, while longer wavelength IR emission comes from larger

Table 2.1: The Irradiated Disk Model and the Observational Flux Values
Note: The data flux values were calculated by using the magnitudes and A_V values given in the following references. For the AXP 4U 0142+61, a plausible range for reddening is $2.6 < A_V < 5.1$ (Hulleman et al., 2004); the data for this source here correspond to $A_V = 3.5$. The A_V values for the other sources are: $A_V = 7.8$ (J1708-40), $A_V = 6.1$ (1E 2259+58), $A_V = 8.4$ (1E 1841-045), $A_V = 5.6$ (1E 1048-59). REFERENCES: (J1708-40) Durant & van Kerkwijk 2006b, Rea et al. 2003; (1E 2259+586) Hulleman et al. 2001, Woods et al. 2004; (4U 0142+61) Hulleman et al. 2000, Hulleman et al. 2004, Patel et al. 2003, Morii et al. 2005; (1E 1841-45) Wachter et al. 2004, Morii et al. 2003; (1E 1048-59) Wang & Chakrabarty 2002, Mereghetti et al. 2004

	Flux (10^{-15} erg s^{-1} cm^{-2})									
	J1708-40		1E 2259+58		4U 0142+61		1E 1841-045		1E 1048-59	
Band	Data	Model	Data	Model	Data	Model	Data	Model	Data	Model
K_s	49	44	3.7	3.6	14	14	68	68	29	22
K		54		4.5	18	18		84		27
H	51	57		4.8	19	19		89	22	28
J	50	53		4.4	14	18		83	33	26
I		56	<15	4.4	18	21		88		24
R		65	<42	4.5	19	25	<380000	100		26
V		48		3.0	28	20		76		18

radii. A more detailed analysis of the AXP 4U 0142+61 with the new detections in the mid-IR *Spitzer* bands confirms the results here (Ertan et al., 2006b). The irradiation parameter C obtained from our model fits turned out to be in the range ($10^{-4} < C < 10^{-3}$) estimated from the observations of LMXBs and the disk stability analyses of the soft X-ray transients (de Jong et al., 1996; Dubus et al., 1999; Ertan & Alpar, 2002). Within the critical radius $R_{\rm c}$, given by Equation 2.4, dissipation is the dominant heating mechanism. For the disk model of the AXP 4U 0142+61, $R_{\rm c} \simeq 3 \times 10^9$ cm and $r_{\rm in} = 1 \times 10^9$ cm. The innermost disk emitting mostly in the UV bands also contributes to the optical emission. The radial distance at which the disk blackbody temperatures peak at the optical bands (R,V) is about 10^{10} cm; at this radial distance, about 35 % of the optical radiation is due to dissipation, and the rest is due to irradiation. Peak temperatures of the IR bands from I to $K_{\rm s}$ lie between $R \sim 2 \times 10^{10}$ cm and $R \sim 1.5 \times 10^{11}$ cm.

There are several uncertainties related to the inner disk emission characteristics of the AXPs, which are not possible to address by the irradiated thin disk model. First, emission properties of the innermost disk boundary interacting with the magnetosphere are not very clear. Second, the contributions from the magnetospheric pulsed emission, which is known to have a fraction of about 27 % in the R band for 4U 0142+61, is likely to be radiated from the other IR and optical bands as well. The relative amplitudes of these pulsed contributions radiated from different optical/IR bands are not known at present. Finally, there could be some X-ray−shielding effects depending on the details of the geometry of the innermost disk regions, which could also affect the optical/IR emission properties of these sources. For all the AXPs that were detected in the optical/IR bands, the optical and IR flux values of our models remain within about 30 % of all the data points, which is a reasonable fit considering the uncertainties discussed above.

For AXP J1708-40, Durant & van Kerkwijk (2006c) recently found that the previously reported IR data in the $K_{\rm s}$, H, and J bands are likely to be of a background star. They found another object within the positional error cycle and argued that this second object is more likely to be the IR counterpart to the AXP J1708-40. For this source, we adopt the IR ($K_{\rm s}$, H, J) data set reported by Durant & van Kerkwijk (2006c).

For the persistent state of the AXP 1E 2259+586, we use the pre-enhancement data (Hulleman et al., 2001). This source was detected in K_s band, and there are upper limits for I and R bands. Our model flux values are three and ten times below the upper limits reported for the I and R bands, respectively.

AXP 1E 1048-59 was detected in K_s, H and I bands (Wang & Chakrabarty, 2002). Observed X-ray fluxes from this source between 2000 December and 2003 January show a variation within a factor of 5 (Mereghetti et al., 2004). We use the X-ray flux obtained from the X-ray observation nearest to the date of the IR observations.

AXP 1E 1841 was detected only in the K_s band, and there is a high upper limit in the R band (Wachter et al., 2004). Model estimates in other optical/IR bands for this source (and the other AXPs) can be tested by future optical and IR observations.

Since there are no detections in short-wavelength optical bands for the AXPs (except for AXP 4U 0142+61), model fits are not sensitive to the chosen inner disk radii. We equate the inner disk radii to the Alfvén radii (Table 2.2) corresponding to a magnetic field with magnitude $B_* = 10^{12}$ G on the stellar surface and the accretion rates derived from the estimated X-ray luminosities (see Table 2.1 for references). For the AXP 4U 0142+61, optical data in R and V bands provide a constraint for the inner disk radius, thereby providing a constraint for the strength of the magnetic dipole field of this source (see Section 2.4).

2.4 Conclusion

We have shown that the optical, infrared and X-ray observations of the AXPs in their persistent states can be explained with irradiated disk models. Among the AXPs, 4U 0142+61 is currently the only source that provides an upper limit for the inner disk radius through its optical (R, V) data. For the best model fit for this source, which we have obtained with $A_V = 3.5$, the model inner disk radius ($\sim 10^9$ cm) is around the Alfvén radius for the accretion rate, estimated from the X-ray luminosity, together with a dipole magnetic field strength B $\simeq 10^{12}$ G on the neutron star surface. Nevertheless, it is possible to obtain reasonable fits by increasing the inner disk radius and decreasing the reddening accordingly. For $A_V =$

2.6, the minimum value of the reddening in the range $2.6 < A_{\rm V} < 5.1$ (Hulleman et al., 2004), we obtain the best fit with $r_{\rm in} \simeq 8 \times 10^9$ cm that corresponds to the maximum reasonable dipole field strength $B_0 \simeq 4 \times 10^{13}$ G on the pole and half of this value on the equator of the neutron star. We note that these limits could be increased depending on the amount of possible mass loss due to the propeller effect and/or on how much the inner disk radius penetrates inside the Alfvén radius (see Ertan et al., 2006a, for a detailed discussion for 4U 0142+61). On the other hand, even including these possibilities, very recent analysis concluding that $A_{\rm V} = 3.5 \pm 0.4$ (Durant & van Kerkwijk, 2006b) implies surface dipole magnetic field strengths less than about 10^{13} G. While the magnetar fields ($B_* > 10^{14}$ G) in multipoles are compatible with this picture, optical (R, V) data excludes a hybrid model involving a disk surrounding a magnetar dipole field. In the latter case, inner disk regions emitting in the optical would be truncated by the magnetar dipole field. High magnetic fields in multipoles, on the other hand, decrease rapidly with increasing radial distance, and they do not affect the disk-magnetosphere interaction.

Uncertainties in the source distances require modification of the model $\dot{M}$ values, and thereby the disk temperature profiles. For the AXP 4U 0142+61, new fits with similar quality can be obtained by slightly modifying the model inner disk radius and the irradiation parameter C as long as such distance corrections remain within a factor of ~ 3. In this case, surface dipole magnetic field should also be recalculated consistently with the newly obtained $\dot{M}$ and Alfvén radius, $r_{\rm A} \propto \dot{M}^{-2/7}\ B_0{}^{4/7}$. For the other AXPs, which were observed only in the IR bands, model fits at present are not sensitive to the inner disk radius, and in the case of distance corrections, similar fits can be obtained only by changing the irradiation strength. This is because IR radiation is emitted from the irradiation dominated outer disk regions, and therefore $\dot{M}$ corrections do not change the relative amplitudes of the fluxes in different IR bands. Future detections of these sources in the optical bands can constrain the inner disk radii together with the surface dipole field strengths.

On the other hand, existing IR data of the AXPs, including recent observations of 4U 0142+61 by *Spitzer* in 4.5 μm and 8 μm bands (Wang et al., 2006), do not put an upper limit for the extension of the outer disk radius $r_{\rm out}$. The lower limit for $r_{\rm out}$ provided by the longest wavelength IR data of the AXP 4U 0142+61 is

around 10^{12} cm. Further observations in the longer wavelength infrared bands by $SPITZER$ space telescope will provide us with valuable information about the structure and possibly the extension of the fallback disks around these systems. As a final remark, some AXPs and SGRs that are under the detection limits in some of the optical and IR bands could be observed in these bands if they exhibit phases of enhanced emission, as observed in the SGR 1900+14 and the AXP 1E 2259+586.

Table 2.2: The Parameters of the Irradiated Disk Model
Note: This model gives the optical/IR flux values seen in Table 2.1. For all the sources, we set cos $i = 1$, where i is the inclination angle between the disk normal and the line of sight of the observer, and we take the outer disk radius to be $r_{\rm out} = 5 \times 10^{12}$ cm (see Section 2.3 for details).

Parameter	1RXS J1708-40	1E 2259+58	4U 0142+61	1E 1841-045	1E 1048-59
$r_{\rm in}$(cm)	1.2×10^{9}	2.3×10^{9}	1.0×10^{9}	1.3×10^{9}	3.3×10^{9}
C	5.0×10^{-4}	1.6×10^{-4}	1.0×10^{-4}	7.2×10^{-4}	7.0×10^{-4}
d (kpc)	5	3	3	7	3
$\dot{M}$(g c^{-1})	1.0×10^{15}	9.1×10^{13}	4.8×10^{14}	2.2×10^{15}	1.3×10^{14}

Chapter 3

ON THE X-RAY OUTBURSTS OF TRANSIENT ANOMALOUS X-RAY PULSARS AND SOFT GAMMA-RAY REPEATERS

This chapter of the thesis was published in
The Astrophysical Journal, 2012, Volume 758, pp. 98 - 109
Şirin Çalışkan & Ünal Ertan

Abstract

We show that the X-ray outburst light curves of four transient anomalous X-ray pulsars (AXPs) and soft gamma-ray repeaters (SGRs), namely XTE J1810–197, SGR 0501+4516, SGR 1627–41 and CXOU J164710.2–455216, can be produced by the fallback disk model that was also applied to the outburst light curves of persistent AXPs and SGRs in our earlier work. The model solves the diffusion equation for the relaxation of a disk which has been pushed back by a soft gamma-ray burst. The sets of main disk parameters used for these transient sources are very similar to each other and to those employed in our earlier models of persistent AXPs and SGRs. There is a characteristic difference between the X-ray outburst light curves of transient and persistent sources. This can be explained by the differences in the disk surface-density profiles of the transient and persistent sources in quiescence indicated by their quiescent X-ray luminosities. Our results imply that a viscous disk instability operating at a critical temperature in $\sim 1300 - 2800$ K range is a common property of all fallback disks around AXPs and SGRs. The effect of the instability is more pronounced and starts earlier for the sources with lower quiescent luminosities, which leads to the observable differences in the X-ray enhancement light curves of transient and persistent sources. A single active disk model with the same basic disk parameters can account for the enhancement phases of both transient and persistent AXPs and SGRs. We also present a detailed parameter study to show the effects of disk parameters on the evolution of the X-ray luminosity of AXPs and SGRs in the X-ray enhancement phases.

3.1 Introduction

Anomalous X-ray pulsars (AXPs) and soft gamma-ray repeaters (SGRs) are a special population of young neutron stars whose rotational powers are not sufficient to account for their X-ray luminosities ($10^{34} - 10^{36}$ erg s^{-1}; see Mereghetti, 2008, for a recent review of AXPs and SGRs). The spin periods of all known AXP and SGRs are in the range of 2 – 12 s. These sources undergo short (< 1 s), super-Eddington soft gamma-ray bursts. Three out of four SGRs showed giant bursts with energies greater than 10^{44} erg. After a soft gamma ray burst episode, (it is likely that some

of these bursts were missed), these sources enter an X-ray outburst/enhancement phase characterized by a sharp increase and eventual decay in X-ray luminosity. Some of the AXPs and SGRs have very low X-ray luminosities ($\sim 10^{33}$ erg s^{-1}) in the quiescent phase, and were detected during these X-ray enhancement phases. These sources are called transient AXPs. During an outburst, X-ray luminosity, $L_{\rm X}$, of the transient sources increases from a quiescent level of $\sim 10^{33}$ erg s^{-1} to a maximum that remains in the $L_{\rm X}$ range of persistent AXP/SGRs (10^{34} – 10^{36} erg s^{-1}).

Energetics and time scales of the soft gamma-ray bursts which are very likely to have magnetic origin resulted in the classification of such objects as "magnetars" (Duncan & Thompson, 1992). In the magnetar model, the source of the X-ray luminosity is the magnetic field decay, and the rotation rate of the neutron stars in these systems is assumed to be slowing down by the magnetic dipole torques in vacuum. This requires that the dipole component of the magnetic field has magnetar strength ($B_0 > 10^{14}$ G) on the surface of the neutron star. The magnetar model has no explanation for the period clustering of AXP/SGRs. Explaining the optical and infrared (IR) observations of persistent and transient AXP/SGRs in quiescent and outburst (enhancement) phases within the magnetar model also poses problems.

The fallback disk model (Chatterjee et al., 2000; Alpar, 2001) was initially proposed to explain the spin periods and X-ray luminosities of AXPs and SGRs. It was suggested that the initial properties of fallback disks, together with magnetic dipole moment and initial spin period, could be responsible for the formation of the other young neutron star populations as well (Alpar, 2001). Later, it was shown that the optical, IR and X-ray observations of persistent AXPs and SGRs in both quiescent and enhancement phases can be explained consistently by the presence of active, accreting fallback disks in these systems (Ertan & Alpar, 2003; Ertan & Cheng, 2004; Ertan et al., 2006b; Ertan & Çalışkan, 2006). The detection of AXP 4U 0142+61 in mid-IR bands clearly indicates the presence of a disk around this source (Wang et al., 2006). This mid-IR data, together with earlier detections in optical and near IR bands, can be well fit by an irradiated active disk model, provided that the dipole field which interacts with the accretion disk has conventional values of $B_0 \simeq 10^{12} - 10^{13}$ G on the surface of the young neutron star (Ertan et al.,

2007). Coherently with these results, X-ray luminosity, period, period derivative, and statistical distribution of AXPs can also be produced by the evolution of the neutron stars with fallback disks and with dipole fields $B_0 < 10^{13}$ G (Ertan et al., 2009). Based on these constraints on B_0 indicated by our results, we proposed that the strong magnetic fields of AXPs must thus reside in multipoles which die rapidly in strength with increasing distance from the neutron star (Ekşi & Alpar, 2003; Ertan et al., 2007, 2009). Recently reported upper bound on the period derivative of SGR 0418+5729 unambiguously revealed that the dipole field strength of this source cannot be greater than $B \sim 7.5 \times 10^{12}$ G on the surface of the neutron star (Rea et al., 2010). This is in full agreement with our explanation, and clearly shows that the soft gamma-ray bursts do not require magnetar dipole fields. Furthermore, if the dipole field is below this upper limit, then the dipole spin down age would not be accurate and other torque and magnetic field effects would need to be taken into account. In the frame of the disk model, rotational properties and X-ray luminosity of this SGR can be reached simultaneously within the cooling timescale of a neutron star with $B_0 \simeq 10^{12}$ G (Alpar et al., 2011). Recently, Trümper et al. (2010) showed that the high-energy spectrum of AXP 4U 0142+61 can be produced in the accretion column of this source mainly by the bulk Comptonization process.

In the present work, we investigate the X-ray enhancement (outburst) light curves of persistent and transient AXPs. We pursue the results of the work by Ertan & Erkut (2008) on the X-ray outburst light curve and the spin evolution of the transient AXP XTE J1810–197. The X-ray outburst light curve of this source showed a different decay morphology than those of persistent sources (Ibrahim et al., 2004; Bernardini et al., 2009). By means of model fits to the X-ray enhancement data, Ertan & Erkut (2008) concluded that this difference could be due to a viscous disk instability (see e.g. Lasota, 2001, for a review of the disk instability model (DIM)) in the fallback disks at a critical temperature in the $\sim 1000 - 2000$ K range. The fallback disks around AXPs are expected to have similar chemical compositions. If one of the AXP disks undergoes a thermal-viscous disk instability at a particular critical temperature, then the others are also expected to show the same instability at the same temperature. Our aim is to test this idea by applying the same model to the X-ray outburst data of other transient AXPs.

There are some difficulties in testing our model when the observed X-ray luminosity is close to the quiescent level ($L_{\rm X} \sim 10^{33}$ erg s^{-1}) of the transient AXPs. As $L_{\rm X}$ decreases, temperature also decreases and thus effects of interstellar absorption increase. Furthermore, at these low temperatures, a significant fraction of the X-ray emission may come from outside the observational X-ray band and estimates of the bolometric luminosities are model dependent (Gotthelf & Halpern, 2007; Bernardini et al., 2009). Our model gives the total accretion luminosity without addressing the X-ray spectrum from the surface or the accretion column of the neutron star. For comparison with data, we assume that the observed $L_{\rm X}$ is a close representation of the total $L_{\rm X}$, which is a good assumption for the X-ray luminosities down to a few times 10^{33} erg s^{-1} but does not allow a reliable comparison for lower luminosities. Another difficulty at very low $L_{\rm X}$ arises due to the fact that the luminosity contribution from the intrinsic cooling of the neutron star (Page et al., 2006) could become comparable to the accretion luminosity depending on the age of the source. Keeping these uncertainties in mind, we extend the model curves to the quiescent luminosity levels to present the model predictions at low $L_{\rm X}$. As in other works on disk accretion, we do not perform χ^2 tests, since it is misleading due to the uncertainties in the disk, like the local instabilities close to the inner disk, that are not possible to address in the models.

Basic disk parameters, namely, the critical disk temperature, kinematic viscosity parameters, irradiation strength, and the radius dependence of the surface density of the extended disk are expected to be similar in the fallback disks of different AXPs. This forces us to a difficult task of producing the X-ray outburst light curves of AXPs with a single set of these basic parameters. We describe our model and discuss the effect of the disk parameters on the X-ray luminosity evolution in Section 3.2. Properties of the transient AXPs that were observed in X-ray enhancement phases are summarized in Section 3.3. We discuss the results of the model calculations in Section 3.4 and summarize our conclusions in Section 3.5.

3.2 The Numerical Model

3.2.1 Description of the Model Parameters

We solve the disk diffusion equation (see, e.g., Frank et al., 2002) in the way described in Ertan & Alpar (2003) and Ertan & Erkut (2008). In this model, it is assumed that a soft gamma-ray burst triggered on the surface of the neutron star pushes the inner disk matter outward. Some of this matter could escape from the system, while the remaining part creates a surface density gradient at the innermost disk. The resultant pile-up, centered at r_0, and the underlying disk distribution are represented by a Gaussian $\Sigma = \Sigma_{\rm max}$ exp $[-(r - r_0)^2/\Delta r^2]$ and a power-law $\Sigma = \Sigma_0$ $(r_{\rm in}/r)^p$ surface density profile respectively as the initial condition of the model.

We assume that the surface density profile of the innermost disk in the quiescent state is close to the standard thin disk profile $\Sigma \propto r^{-3/4}$, and the disk matter from $r_{\rm in}$ to a radius r_1, with mass δM, is initially pushed out to a narrow radial region at radius r_1 by the burst. As the matter with a range of specific angular momentum mixes and piles up at r_1, the angular momentum is redistributed rapidly due to mixing and the narrow radial extent of the pile-up. The required timescale for the sharing of angular momentum is of the order of a few h/v_K, where v_K is the Keplerian velocity close to r_1 and h is the thickness of the disk, typical lengthscale for efficient viscous interaction, at r_1. Taking $h(r_1) \sim 10^{-2} r_1$ and $r_1 \sim 10^{10}$ cm, $h/v_K \simeq 10^{-2}\Omega_K^{-1}$ is found to be a fraction of a second. This implies that the angular momentum is effectively shared during the formation of the pile-up. After the burst episode, this matter circularizes at a radius between $r_{\rm in}$ and r_1 depending on the mean specific angular momentum of the pile-up. The matter spreading from this circularization radius to both inner and outer radii with a surface density peak close to the circularization radius is represented by a Gaussian as the initial mass distribution in our model. The center r_0 of the Gaussian in the model could be assumed to represent this circularization radius.

Our model light curves do not sensitively depend on r_0 or the details of the Gaussian distribution. Similar model light curves could be produced with different r_0 values (within a factor of a few), provided that δM contained in the Gaussian

distribution remains the same. This density gradient leads to an abrupt rise in the mass-flow rate at the innermost disk. The rise phase of the X-ray light curve is produced by the enhanced mass-flow rate to the Alfvén radius and subsequently onto the surface of the neutron star. Since the exact position of the inner disk radius, $r_{\rm in}$, does not change the rate of mass inflow, for simplicity we take $r_{\rm in}$ constant and equal to the inner disk radius in quiescence. The mass accretion rate in the decay phase of the light curve is governed by the viscous relaxation of the inner disk matter. At the end of the decay phase, the luminosity converges to the quiescent X-ray luminosity level of the source. The X-ray luminosity produced by the inner disk through viscous dissipation is negligible compared to the luminosity powered by mass accretion onto the surface of the neutron star.

The evolution of the disk is determined by solving the diffusion equation (see, e.g., Frank et al., 2002). While δM is important in the evolution of the X-ray luminosity, the detailed shape of the Gaussian does not significantly affect the model light curve in the long term (Ertan et al., 2006b). For a viscously evolving disk, the power index p of the extended surface density profile is expected to be $\sim 3/4$ (Frank et al., 2002); we take $p = 3/4$ in our calculations.

We keep the inner radius of the disk $r_{\rm in}$ constant at a value near the Alfvén radius for a dipole magnetic field with strength $B_0 = 10^{12}$ G on the surface of the neutron star. Since the model fits are not sensitive to $r_{\rm in}$, we are not able to constrain B_0. Our results are not sensitive to the value of the outer disk radius $r_{\rm out}$ either, since the viscous timescale along the disk is much longer than the enhancement episodes of AXPs. In our calculations we take $r_{\rm out} = 10^{13}$ cm.

Irradiation parameter C represents the efficiency of X-ray irradiation flux $F_{\rm irr} = (C\dot{M}c^2)/(4\pi r^2)$ (Shakura & Sunyaev, 1973) where $\dot{M}$ is the mass accretion rate onto the neutron star. Infrared and optical data of the persistent AXPs can be accounted for by an active disk model with C in the range 10^{-4} – 10^{-3} (Ertan & Çalışkan, 2006) similar to those estimated for low-mass X-ray binaries. Total X-ray luminosity is related to the mass accretion rate through $L = GM\dot{M}/r$. We take $f = \dot{M}/\ \dot{M}_{\rm in} = 1$, where $\dot{M}_{\rm in}$ is the mass-flow rate arriving at the innermost radius of the disk. Actually, f could be less than unity, that is, a fraction of $\dot{M}_{\rm in}$ can escape the system or may not return back to the disk. Employing lower f values in the

calculations does not change our qualitative results, but requires a modification of some other disk parameters. This will be discussed in Section 3.4. For comparison of the model with observations, we take the X-ray luminosities in the observational bands to represent the total X-ray luminosity of the source.

Different viscosity states prevail in the hot ($T > T_{\rm crit}$) and cold ($T < T_{\rm crit}$) regions of the disk. For the kinematic viscosity, we use the α-prescription (Shakura & Sunyaev, 1973) with $\alpha = \alpha_{\rm cold}$ and $\alpha = \alpha_{\rm hot}$ in the cold and hot viscosity states respectively. For a review of the DIMs, see e.g. Lasota (2001). The disk evolution model we use here is the same as DIMs of LMXBs and dwarf novae (DNs). The difference is the value of the critical temperature, $T_{\rm crit}$. In LMXB and DN disks, the thermal-viscous instability operates around the ionization temperature of hydrogen ($T_{\rm crit} \sim 10^4$ K). In the case of AXPs, both the temperature profile and the chemical composition of the disk are different from the hydrogen disks of LMXB and DNs. In AXP disks, metallicity is likely to be much higher than in an LMXB disk. We should also note that the hottest, innermost parts of the LMXB disks do not exist in AXP disks due to stronger dipole fields of AXPs that cut the disk at a relatively larger radius ($\sim 10^9$cm).

The critical temperatures depend sensitively on the details of the ionization properties of the disk matter. Independent of these details, if the disk undergoes a global disk instability at a particular temperature, the resultant evolution of the disk produces a light curve which can be easily distinguished from the pure viscous decay curve (not affected by instabilities). Furthermore, fallback disks around AXPs are likely to have similar chemical compositions and similar critical temperatures.

In our model, there are five main disk parameters, namely, $T_{\rm crit}$, $\alpha_{\rm cold}$, $\alpha_{\rm hot}$, p, and C, which govern the evolution of the accretion disk for a given initial mass distribution. Among these, $T_{\rm crit}$ and C are degenerate parameters. There is a constraint on the range of C obtained in our earlier work on the persistent AXPs (Ertan & Çalışkan, 2006). These basic disk parameters are very likely to have similar values for fallback disks of different AXPs. In Section 3.2.2, we investigate the effects of model parameters on the evolution of the disk to clarify the subsequent discussion on the light curves of persistent and transient sources.

3.2.2 Parameter Study

Observations of X-ray outburst (enhancement) light curves of different AXPs with different energetics and time-scales provide an opportunity for a detailed test of the fallback disk model and also for constraining the model parameters. In this section, we investigate the effect of important disk parameters on the X-ray outburst light curves of model sources.

3.2.2.1 Different burst energies

Soft gamma-ray bursts of AXPs are likely to have magnetic origin and to occur close to the neutron star. Assuming an isotropic emission, a small fraction $\delta E/E_{\rm tot} \sim H_{\rm in}/r_{\rm in}$ of the total burst energy, $E_{\rm tot}$, is absorbed by the disk where δE is the part of the burst energy illuminating the disk and $H_{\rm in}$ is the half-thickness of the disk at $r = r_{\rm in}$. H/r is roughly constant along the disk and is about 10^{-3} in the accretion regime of AXPs. When the inner disk is pushed back and heated by δE, part of the inner disk matter could escape the system, while the remaining part piles up, forming a surface density gradient at the inner disk (see Ertan et al., 2006b, for details). In our model, the Gaussian surface density distribution represents the inner pile-up and the power-law surface density distribution stands for the outer extended disk that is expected to remain unaffected by the soft gamma-ray burst. The position r_0 and the total mass δM of the pile-up, for a given δE, depend on the inner disk radius $r_{\rm in}$ and the mass distribution of the inner disk just before the burst event. In steady state, the surface density profile of the inner disk-magnetosphere boundary is not well known. Assuming that the inner disk conditions are similar for fallback disks of AXPs, it is expected that a higher burst energy pushes the inner disk to a larger radius, and creates a greater density gradient at the inner disk.

In the quiescent state, the mass-flow rate, $\dot{M}$, decays very slowly and therefore can be taken as constant in the models. In this steady state, $\dot{M} \propto \Sigma\ \nu$ where $\nu = \alpha\ c_S\ H$ is a function of temperature and radius, and depends also on the ionization properties of the disk matter. The pressure-scale height of the disk $H \simeq c_S/\Omega_K$, then $\nu \propto T\ r^{3/2} \propto r^{3/4}$ (see, e.g., Frank et al., 2002) where T is the mid-plane temperature of the disk. The irradiation temperature $T_{\rm irr} \propto r^{-1/2}$ modifies the effective temperatures and the stability criteria of the disk without significantly

affecting the mid-plane temperatures in the accretion regime of AXPs and SGRs (e.g. Dubus et al., 1999). Then, in the quiescent state, the surface density of the disk $\Sigma \propto r^{-p}$ with $p = 3/4$. The main role of the irradiation is to slow down the decay of the X-ray luminosity, preventing the rapid propagation of the cooling front inward. This will be investigated in detail in Section 3.2.2.3.

We first illustrate X-ray enhancement light curves of a model source with different δM values representing the evolution of the same source with different burst energies. In the first exercise, we compare the model curves without invoking the instability (pure viscous evolution) with $\alpha = 0.1$, $r_{\rm in}= 10^9$ cm, and $r_{\rm out}= 10^{13}$ cm. Three different illustrative light curves presented in Figure 3.1 are obtained with different δM values that give peak luminosities of 1×10^{36}, 3×10^{36}, and 1×10^{37} erg s^{-1}. The quiescent $L_{\rm X}$ of all these sources are close to 10^{35} erg s^{-1}, a typical luminosity of a persistent AXP. It is seen that the X-ray luminosities follow almost the same decay curve after $\sim$ a few months and eventually reach their quiescent level. For the first several weeks of the outburst both the fluences and the functional forms of the decay curves are very different from each other. For this initial decay phase, the model curves can be fit by a power law $L = L_{\rm peak}\ (t/t_{\rm peak})^{-n}$ with power-law indices of 0.88, 0.68 and 0.46. The minimum burst energy imparted to the disk can be estimated from δM using $\delta E \simeq G\ M\ \delta M\ (r_{\rm in}^{-1} - r_0^{-1}) \simeq G\ M\ \delta M\ /\ r_{\rm in}$. For these illustrative models, $\delta M = 4.9 \times 10^{22}$, 2.1×10^{22}, and 8.9×10^{21} g, and the estimated δE values are 9.2×10^{39}, 3.8×10^{39}, and 1.7×10^{39} erg, respectively. Note that actually a higher δE accumulates a greater δM at a larger r_0. Since the chosen r_0 does not significantly affect the light curve, for simplicity, we take r_0 constant (5×10^9 cm) for all these illustrative simulations.

We repeat the same calculations for a model source with a quiescent luminosity around 10^{33} erg s^{-1}, typical for transient AXPs. In Figure 3.2, we present three different light curves produced by pure viscous evolution of the disk for three different δM values, without changing the other parameters. In this case, estimated δE values are 4.5×10^{38} erg, 2.3×10^{38} erg and 1.2×10^{38} erg respectively. For these sources, first $\sim$ 100 days of the decay curves can be fitted by power laws with indices 0.91, 0.73, and 0.59. In Figure 3.2, like the model sources given in Figure 3.1, the sources with higher δM show higher peak luminosities and sharper decay

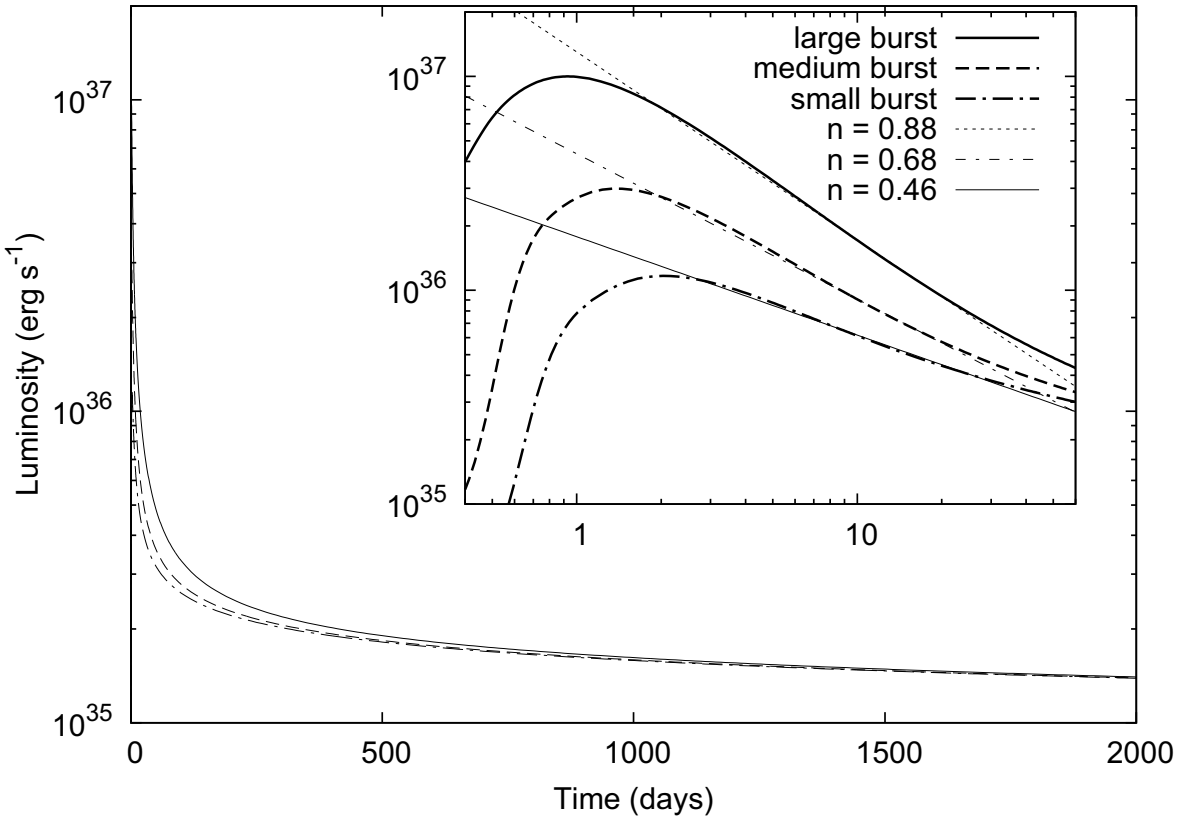

Figure 3.1: Model light curves produced by pure viscous evolution of disks for three different δE values. The short-term light curve, in the inset, shows peak luminosities of 10^{37} erg s^{-1}, 3×10^{36} erg s^{-1}, and 10^{36} erg s^{-1}, which all decay to the same quiescent luminosity in the long term. The δM values are 4.9×10^{22} g, 2.1×10^{21} g, and 8.9×10^{20} g and the estimated δE values are 9.2×10^{39} erg, 3.8×10^{39} erg, and 1.7×10^{39} erg respectively. The model light curves can be fitted with power laws in the early decay phase ($\sim$ a few weeks). The values of power indices (n) are given in the inset.

curves in this early phase of evolution.

In these examples, the model light curves are produced by pure viscous evolution of the disk without any instability. Comparing Figures 3.1 and 3.2, we might conclude that the sources with similar $L_{\rm X}$ in quiescence could show decay curves with rather different power-law indices, while it is also possible that sources with different quiescent luminosities could give similar decay curves in the early decay phase of the outburst. In Section 3.2.2.2, we show that this early phase of the X-ray light curves can indeed be produced by pure viscous evolution of the disk for both transient and persistent sources. This pure viscous evolution model gives similar long-term curves for all model sources (Figures 3.1 and 3.2), which would be the case if there were no critical temperature leading to viscous instability in the disk. In the following sections, we show how the presence of a critical temperature leads to systematic differences in the functional form of the decay curves depending on the X-ray luminosities in quiescence.

3.2.2.2 Quiescent X-ray luminosity and critical temperature

The main characteristics of X-ray outbursts of soft X-ray transients (SXTs) and DNs can be successfully accounted for by DIMs (see, e.g., Lasota, 2001, for a review). In these systems, the viscous instability manifests itself at temperatures around 10^4 K which corresponds to the ionization temperature of hydrogen. In the DIMs, disk regions with temperatures higher and colder than this critical temperature are in hot and cold viscosity states respectively. Different α parameters are employed in the cold and hot states ($\alpha_{\rm hot} \sim 0.1$ and $\alpha_{\rm cold} \sim 0.01 - 0.05$, see Section 3.2.2.4) to obtain reasonable model fits to the X-ray outburst light curves of SXTs and DNs. We note that these viscosities are turbulent in both hot and cold states.

We now investigate the effect of viscous instability with different critical temperatures on the model X-ray light curves of two illustrative sources with quiescent X-ray luminosities of 10^{33} and 10^{35} erg s^{-1} as representatives of transient and persistent AXPs. For both model sources, we take $C = 1 \times 10^{-4}$. The results are seen in Figure 3.3. Panel (a) shows the luminosity evolution of a persistent source, for three different $T_{\rm crit}$ values, as well as the pure viscous decay (no viscous instability). Similarly, panel (b) shows the evolution of a transient source. For a given source, the

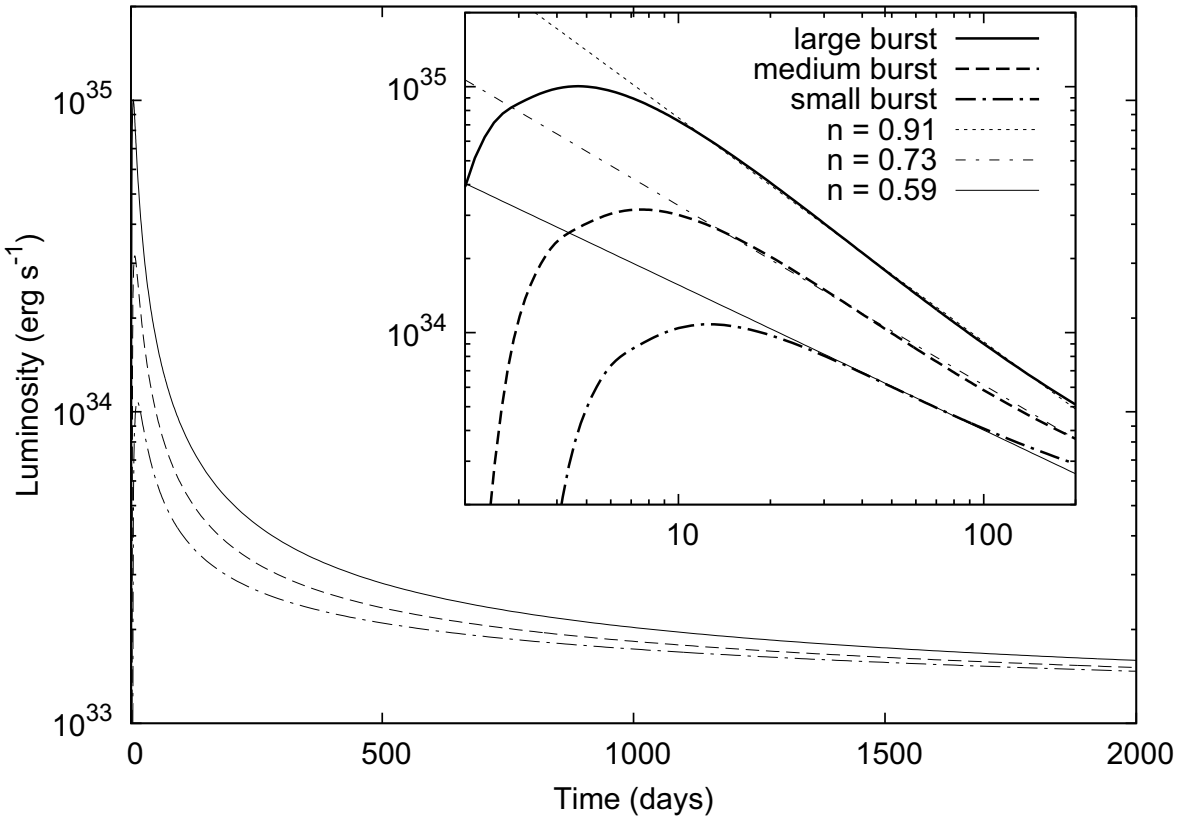

Figure 3.2: Short-term and long-term model light curves of a typical transient source for three different δE values. For these models, δM values are 2.4×10^{21} g, 1.2×10^{21} g, and 6.4×10^{20} g and estimated δE values are 4.5×10^{38} erg, 2.3×10^{38} erg, and 1.2×10^{38} erg respectively. The decay phases of the light curves can be fitted with power laws for the first ~ 100 days (inset). The values of power indices (n) are given in the inset.

model curves with higher $T_{\rm crit}$ values diverge from pure viscous decay curve earlier. Comparing Figures 3.3(a) and 3.(b), we see that for a particular $T_{\rm crit}$, the light curve of the persistent sources (high quiescent luminosity) deviate from the pure viscous decay curve much later than the transient sources (low quiescent luminosity). For instance, for $T_{\rm crit} = 2000$ K, the light curve of the transient source deflects from the pure viscous decay curve at $t \sim 100$ days. For the persistent source with the same $T_{\rm crit}$, the deviation starts at $t \sim 200$ d and the luminosity decreases much slower compared to the transient source. For $T_{\rm crit} \sim 1500$ K, the light curve of the persistent source is indistinguishable from the pure viscous decay until $t \sim 400$ days, while for the transient source, the deviation starts as early as $t \sim 200$ days (Figure 3.3). This characteristic difference in the light curve morphologies of high and low-luminosity AXPs in the decay phase is mainly due to the differences in the surface density and temperature profile of the disks in the quiescent states. These properties could be estimated from the X-ray luminosities in quiescence, which scales with the accretion rate onto the neutron star.

3.2.2.3 X-Ray irradiation

Another factor that plays an important role in the evolution of the disk and the X-ray luminosity is the X-ray irradiation of the disk. The irradiation flux can be written as $F_{\rm irr} = C\dot{M}c^2/4\pi r^2$ where irradiation efficiency C depends on the albedo of the disk faces and the irradiation geometry (Shakura & Sunyaev, 1973). The critical temperature discussed in Section 3.2.2.2 and C are degenerate parameters. The results of our earlier work on the X-ray and IR data of AXPs constrain the value of C to the range $10^{-4} - 7 \times 10^{-4}$ (Ertan & Çalışkan, 2006), which remains in the range of the estimated irradiation efficiencies of SXTs ($10^{-4} - 10^{-3}$; de Jong et al., 1996; Dubus et al., 1999; Tuchman et al., 1990).

The effective temperature of a steady disk at a radial position is determined by the dissipation rate given by $D = 9\ \nu\ \Sigma\ \Omega_K^2\ /\ 8$, where Ω_K is local Kepler velocity, and by the X-ray irradiation flux $F_{\rm irr}$. Including $F_{\rm irr}$, the effective temperature can be written as $\sigma T_{\rm eff}^4 \simeq D + F_{\rm irr}$. Since $\nu\Sigma \propto \dot{M}$, both $F_{\rm irr}$ and D have the same $\dot{M}$ (and thus $L_{\rm X}$) dependence. The irradiation flux and the dissipation rate decrease with radial distance as r^{-2} and r^{-3} respectively. Equating $F_{\rm irr}$ to D, we find $r \sim 2 \times 10^9$

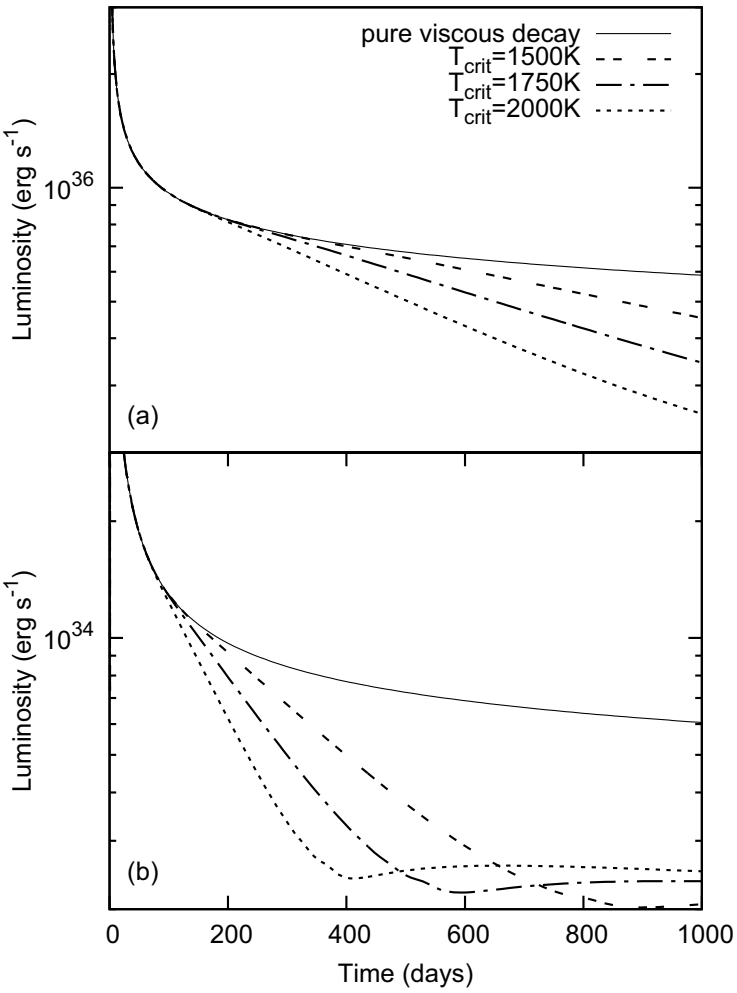

Figure 3.3: Model light curves for persistent (a) and transient (b) sources, for $T_{\rm crit}$= 1500 K, 1750 K, and 2000 K. Solid curves illustrate the pure viscous decay with the same initial conditions for comparison. For a given $T_{\rm crit}$, comparing (a) and (b), the difference between the model curves of the transient and persistent sources is clearly seen.

cm which does not depend on $\dot{M}$. For smaller radii, D dominates $F_{\rm irr}$, while $F_{\rm irr}$ is the dominant source of heating beyond this radius (see, e.g., Frank et al., 2002).

The radius $r_{\rm h}$ of the hot inner disk is determined by the strength of the X-ray irradiation ($T(r{=}r_{\rm h}) = T_{\rm crit}$). Increasing (decreasing) $F_{\rm irr}$ increases (decreases) the effective temperatures at all radii, and $r_{\rm h}$ is situated further out (in). This implies that the sources with higher X-ray luminosity have greater $r_{\rm h}$. This is actually the main reason that leads to different X-ray light curve morphologies in the enhancement phases of transient and persistent sources. The rate of mass accretion which powers $L_{\rm X}$ is determined by the surface density profile of the disk. The sources with higher surface densities have higher accretion rates, higher X-ray irradiation fluxes, and thus greater $r_{\rm h}$. To illustrate, for $T_{\rm crit} = 1500$ K and $C = 1.5 \times 10^{-4}$, we find $r_{\rm h} = 1.4 \times 10^{11}$ cm for $L_{\rm X} = 10^{35}$ erg s^{-1} and $r_{\rm h} = 1.4 \times 10^{10}$ cm for $L_{\rm X} = 10^{33}$ erg s^{-1}.

At the beginning of the X-ray enhancement phase, the innermost disk that was emptied by the burst is refilled rapidly due to high density gradients, leading to a sharp rise in X-ray luminosity. The mass-flow rate in the inner disk, the accretion rate onto the neutron star, and thereby the X-ray luminosity, $L_{\rm X}$, and $r_{\rm h}$ reach their maximum values. Subsequently, $r_{\rm h}$ decreases gradually at a rate governed by the decreasing X-ray flux.

In the quiescent phase, the mass-flow rate at the inner hot disk depends on the conditions at the cold outer disk. The hot disk easily transfers all the mass flowing from the outer cold disk toward $r_{\rm in}$. During an enhancement, the mass-flow rate is determined mainly by the viscous processes at the hot inner disk. Just before the onset of the X-ray outburst, the total amount of mass that remains within $r_{\rm h}$, the position of $r_{\rm h}$ and the rate at which it moves inward all affect, and also depend on the evolution of $L_{\rm X}$.

Initially, the light curve mimics that of a pure viscous decay, since the information from $r_{\rm h}$ moving inward reaches the inner disk after a viscous time-scale across the hot disk. With decreasing $r_{\rm h}$, the total hot mass contributing to the accretion with high viscosity also decreases. After the conditions at $r_{\rm h}$ start to modify $\dot{M}_{\rm in}$, $L_{\rm X}$ decreases more rapidly and diverges from the pure viscous decay curve.

In Figure 3.4, we give the model curves with different C values, keeping $T_{\rm crit} =$

1750 K for all the simulations. Comparing with Figure 3.3, it is seen that the light curves for different C values are similar to those obtained with different $T_{\rm crit}$ values, keeping C constant. It is also seen that the viscous instabilities triggered at the same $T_{\rm crit}$ and with the same C produce very different light curves for transient and persistent sources.

3.2.2.4 Viscosity parameter

For both transient and persistent AXPs, the rise, turnover and early decay phase (several weeks to months) of the X-ray light curve are produced by the evolution of the hot inner disk matter and the resultant accretion onto the neutron star. In all our calculations, we take $\alpha_{\rm hot} = 0.1$ as in our earlier works. For all the sources, this initial phase of the light curve is indistinguishable from that produced by a pure viscous evolution of the disk, that is, the evolution of a disk remaining in the same viscosity state at all radii. By illustrative model light curves (Figures 3.3 – 3.5), we have shown that the deviation from this pure viscous decay phase starts much earlier in transient AXPs which have relatively low luminosities in the quiescent phase. After the instability starts to affect the accretion rate, the value of $\alpha_{\rm cold}$ has an important role in the evolution of the X-ray luminosity $L_{\rm X}$. From the DIMs of SXTs and DNs, $\alpha_{\rm cold}$ is estimated to be $\sim 0.01 - 0.05$ (Lasota, 2001). From model fits to X-ray enhancement light curve of XTE J1810–197, Ertan & Erkut (2008) found that $\alpha_{\rm cold} \sim 0.03$ with $T_{\rm crit} \sim 1500$ K produce reasonable model curves. In the present work, we also refine the model parameters of Ertan & Erkut (2008) through a comparative study with the X-ray enhancement light curves of other transient AXPs, including the new data points of XTE J1810–197 (Section 3.3).

Keeping all the other parameters constant, we see that small variations in $\alpha_{\rm cold}$ could lead to significant changes in the light curve at the end of the decay phase. To illustrate this effect, we present model curves with different $\alpha_{\rm cold}$ values in Figure 3.5. The depths of the minima at the end of the model light curves of the model sources depend mainly on the values of $\alpha_{\rm cold}$. It is seen in Figure 3.5 that the model light curves settle down to the quiescent level following quite different morphologies even for small changes in $\alpha_{\rm cold}$.

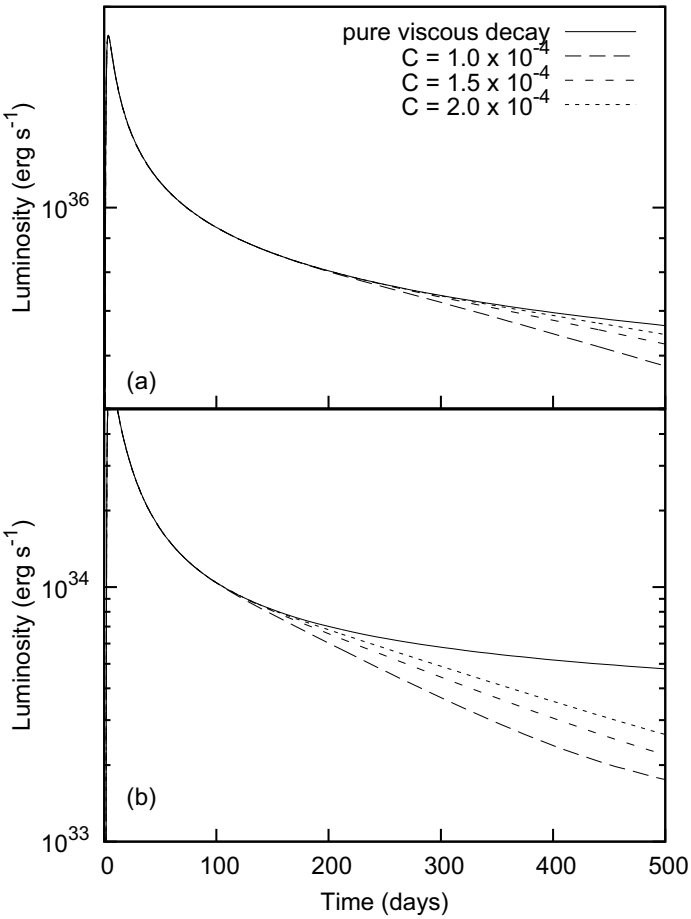

Figure 3.4: Top panel shows the model light curves of a persistent source for different C values, and the bottom panel shows the light curves for a transient source, for the dame parameter values. The model curves representing pure viscous decay are given with solid lines and $T_{\rm crit} = 1750$ K for the other models. It is seen that the evolution of persistent sources diverges from the pure viscous decay curve much later than transients.

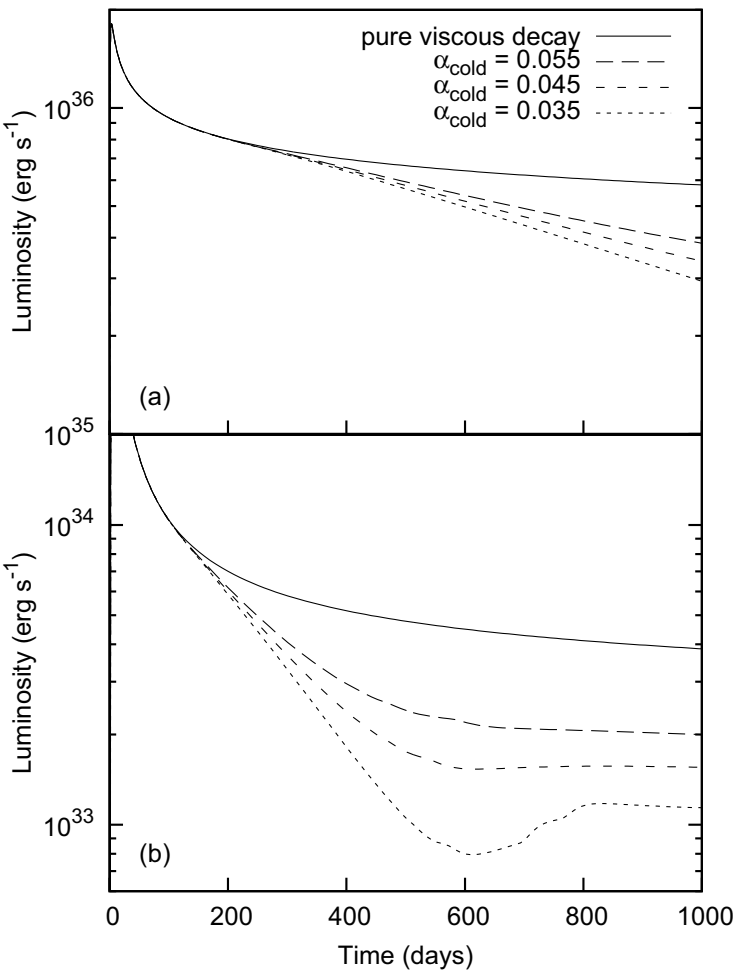

Figure 3.5: Top panel shows the light curve of a persistent source for different $\alpha_{\rm cold}$ values, and the bottom panel shows the light curves for a transient source, for the same parameter values. The pure viscous decay curves are also presented (solid lines) for comparison. For the other models, we take $T_{\rm crit} = 1750$ K and $C = 1 \times 10^{-4}$.

The physical reason producing the minima in the model curves can be summarized as follows: after the formation of the pile-up at the inner disk, the accretion rate abruptly increases in the hot disk region ($r < r_{\rm h}$) due to newly formed density gradients. The resultant increase in $L_{\rm X}$ pushes $r_{\rm h}$ to larger radii, causing part of the previously cold disk region to enter the hot viscosity state. Due to the density gradients and more efficient kinematic viscosity in the hot state, the inner disk matter is depleted at a rate much higher than the mass-flow rate provided by the outer disk. As a result, surface density profile $\Sigma(r)$ of the inner disk decreases below the extrapolation of $\Sigma(r)$ of the cold outer disk. Meanwhile, $L_{\rm X}$ decreases due to both decreasing Σ of the inner disk and the propagation of $r_{\rm h}$ inward with decreasing $L_{\rm X}$.

The rate of refilling of the innermost disk regions sensitively depends on the value of $\alpha_{\rm cold}$. It is seen in Figure 3.5 (bottom panel) that the minimum in the model light curves becomes more pronounced for smaller $\alpha_{\rm cold}$ values. This is because the surface density gradients are smoothed out more rapidly with higher kinematic viscosity. Observed X-ray enhancement light curves provide an opportunity to constrain the value of $\alpha_{\rm cold}$. Nevertheless, the limitation for testing the models can also be clearly seen in Figure 3.5 (bottom panel). The accretion luminosity of the transient AXPs might decrease even below the intrinsic cooling luminosity of the neutron star depending on the age of the source.

3.2.2.5 Outer disk radius

The outer disk radius, $r_{\rm out}$, defines the extent of the active accretion disk and depends on the minimum disk temperature at which the disk becomes inactive. X-ray luminosity, rotational and statistical properties of AXPs can be explained by the long-term evolution of neutron stars evolving with fallback disks that become inactive at low temperatures around ∼100–200 K (Ertan et al., 2009). In this model, $r_{\rm out}$ gradually decreases in time with slowly decreasing quiescent X-ray luminosity of the source.

The evolution of $r_{\rm out}$ has an important effect on the long-term (10^3 – 10^5 yr) evolution of AXPs. Nevertheless, the position of $r_{\rm out}$ does not affect the X-ray enhancement light curves of AXPs, which last from months to several years, . The outer radii of the fallback disks of known AXPs are estimated to be greater than

about a few $\times$ 10^{12} cm (Ertan et al., 2007). Viscous timescale across the disk is longer than the duration of the enhancement phase. In our calculations, we set $r_{\rm out}$ = 10^{13} cm. We note that the radius $r_{\rm h}$ of the hot disk which is the border between low and high viscosity regions of the disk should not be confused with $r_{\rm out}$.

3.3 Application of the Model to the X-ray Enhancement Light Curves of Transient AXPs

Our model parameters and their effects on the evolution of the sources are described in detail in Section 3.2. Now, we test this model, performing model fits to the X-ray outburst light curves of the sources XTE J1810–197, SGR 1627–41, CXOU J164710.2–455216 and SGR 0501+4516 (Figures 3.6 – 3.9). The model parameters are presented in Table 3.1. All these sources were detected in the decay phases of their X-ray outbursts. The rise and turn-over phases of the outburst were missed.

The X-ray flux of XTE J1810–197 in quiescence (during 1993 – 1999) was 5.5 $\times$ 10^{-13} erg cm^{-2} s^{-1} (Gotthelf et al., 2004) and increased to about 5.5 $\times$ 10^{-11} erg cm^{-2} s^{-1} during the outburst (Ibrahim et al., 2004). Most recent distance and the corresponding peak luminosity estimates for this source are d = 5 kpc, $L_{\rm X}$ = 1.3 $\times$ 10^{36} erg s^{-1} (Ibrahim et al., 2004), d = 3.3 kpc, $L_{\rm X}$ = 5.8 $\times$ 10^{35} erg s^{-1} (Lazaridis et al., 2008) and d = 3.5 kpc, $L_{\rm X}$ = 6.6 $\times$ 10^{35} erg s^{-1} (Bernardini et al., 2009). In our calculations, we take d = 3.5 kpc. For the model fits, we use 2 – 10 keV XTE data (Ibrahim et al., 2004) and 0.6 – 10 keV XMM data (Bernardini et al., 2009). The XMM data were converted to 0.1 – 10 keV unabsorbed flux with *WebPIMMS*, using the 3BB model described in their paper. The XTE data, given in counts s^{-1} PCU^{-1}, were converted to unabsorbed flux using a conversion factor. The factor was chosen so as to align the first XMM data with the corresponding XTE data (in 2003 September). Our model curve is given in Figure 3.6. For all the sources, together with the best model fits, we also plot the pure viscous decay curves for comparison.

The transient SGR 1627–41 underwent an X-ray outburst in 1998 and its decay curve is also similar to those of other transient sources (Mereghetti et al., 2006b). The peak luminosity of SGR 1627–41 was 9.5 $\times$ 10^{34} d_{11}^2 erg s^{-1} during the outburst and the distance was measured as 11.0 $\pm$ 0.3 kpc (Corbel et al., 1999). The source

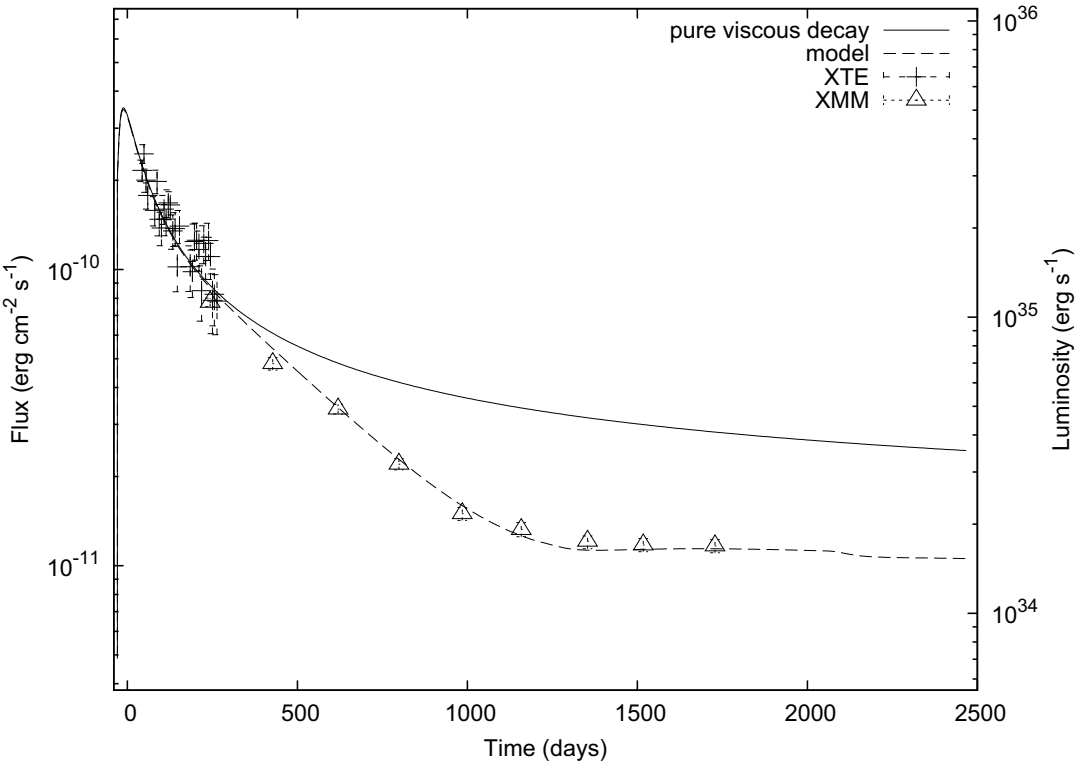

Figure 3.6: 0.1 – 10 keV unabsorbed X-ray flux and luminosity data of XTE J1810–197. The absorbed 0.6 – 10 keV XMM data (Bernardini et al., 2009) were converted to unabsorbed 0.1 – 10 keV flux using the 3BB model described in their paper. The XTE data were given in counts s^{-1} cpu^{-1} with a conversion factor for 2 – 10 keV absorbed flux (Ibrahim et al., 2004), with no spectral fits. The XTE data were rescaled by a factor of 2.3 to match the first XMM data, taken in 2003 September (see the text for details). The luminosity is calculated assuming $d = 3.5$ kpc. For this model, $\delta M \sim 1 \times 10^{23}$ g and the estimated $\delta E \sim 1 \times 10^{40}$ erg.

subsequently decayed to quiescence with $L_{\rm X} \sim 3.9 \times 10^{33}$ d_{11}^2 erg s^{-1} (Kouveliotou et al., 2003). In 2008 May, a new X-ray outburst was observed in SGR 1627–41 (Palmer et al., 2008). The absorbed 2–10 keV flux was $\sim$1.3 $\times$ 10^{-12} erg cm^{-2} s^{-1}, corresponding to a luminosity of $L_{\rm X} \sim 3 \times 10^{34}$ d_{11}^2 erg s^{-1} (Esposito et al., 2009a). There is an uncertainty in estimating the unabsorbed flux of this source due to high interstellar absorption with $N_{\rm H} \sim 10^{23}$ cm^{-2} (Mereghetti et al., 2009b). We take d = 11 kpc to estimate the luminosity. Our model curve is seen in Figure 3.7.

A soft gamma-ray burst from CXOU J164710.2–455216 was detected with *Swift* BAT on 2006 September 21 (Krimm et al., 2006). It was observed for $\sim$ 20 ms with total energy $\sim 3 \times 10^{37}$ erg (15 – 150 keV, for d = 5 kpc; Muno et al., 2007). The observed maximum X-ray flux data point was reported 1.6 days after the burst. The X-ray flux data of AXP CXOU J164710.2–455216 cover about 150 days on the decay phase of its outburst in 2006 September (Israel et al., 2007; Woods et al., 2011). The X-ray luminosity of the source increased from $\sim 1 \times 10^{33}$ d_5^2 erg s^{-1} to more than 1 $\times$ 10^{35} d_5^2 erg s^{-1} during the outburst (Muno et al., 2007). The distance of CXOU J164710.2–455216, located in a star cluster, was estimated as 2 kpc $< d \leq$ 5.5 kpc (Clark et al., 2005). We convert the flux data to luminosity using d = 5 kpc. The data seen in Figure 3.8 seem to be taken in the early decay phase of this source, and therefore does not constrain $T_{\rm crit}$ yet.

Another transient source that was discovered in an outburst is SGR 0501+4516 (Barthelmy et al., 2008). Subsequently, the source was observed with *XMM – Newton*, *Swift* and *Suzaku* in the decay phase, starting from a maximum absorbed 1 – 10 keV flux of 4.1 $\times$ 10^{-11} erg cm^{-2} s^{-1} (Rea et al., 2009, Figure 3.9). The distance of SGR 0501+4516 is not very well determined, with estimates d = 1.5 kpc (Aptekar et al., 2009), d = 4 kpc (Nakagawa et al., 2011), d = 5 kpc (Rea et al., 2009) and d = 10 kpc (Enoto et al., 2009; Kumar et al., 2010). The pre-outburst quiescent (0.1 – 2.4 keV) flux of this source was reported as $\sim$ 4.1 $\times$ 10^{-12} erg cm^{-2} s^{-1} (Rea et al., 2009), which corresponds to a 1 – 10 keV flux of 1.3 $\times$ 10^{-12} erg cm^{-2} s^{-1}. Assuming a distance of 5 kpc, the maximum and quiescent luminosities are 1.2 $\times$ 10^{35} erg s^{-1} and 4 $\times$ 10^{33} erg s^{-1} respectively. We take d = 5 kpc in our calculations. This source also does not constrain $T_{\rm crit}$ yet.

The transient AXP 1E 1547.0–5408 at the end of the $\sim$ 100 days of decay, showed

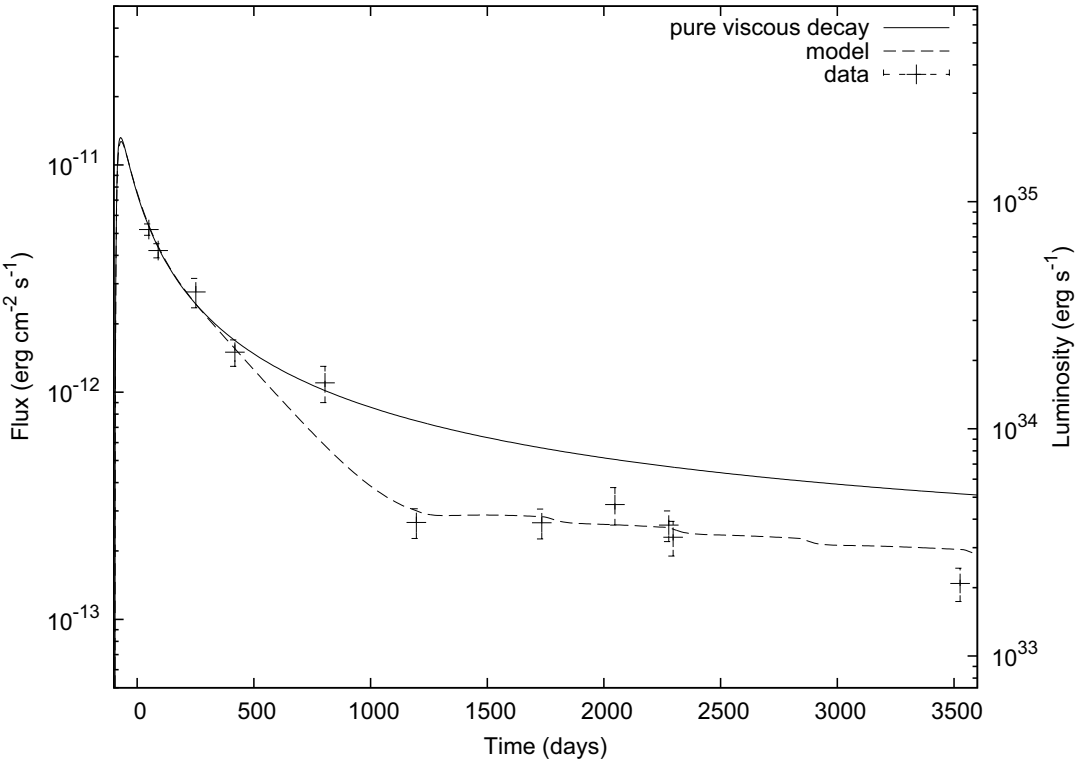

Figure 3.7: Unabsorbed 2 – 10 keV flux and luminosity data of SGR 1627–41 (Mereghetti et al., 2006b). The parameters of the model curve, given by the dashed line, are listed in Table 3.1. The solid curve represents pure viscous decay with the same initial conditions. These model curves are obtained with $\delta M \sim 4 \times 10^{22}$ g, which gives $\delta E \sim 4 \times 10^{39}$ erg with the chosen $r_{\rm in}$ (see the text for details). The luminosity is calculated assuming $d = 11$ kpc.

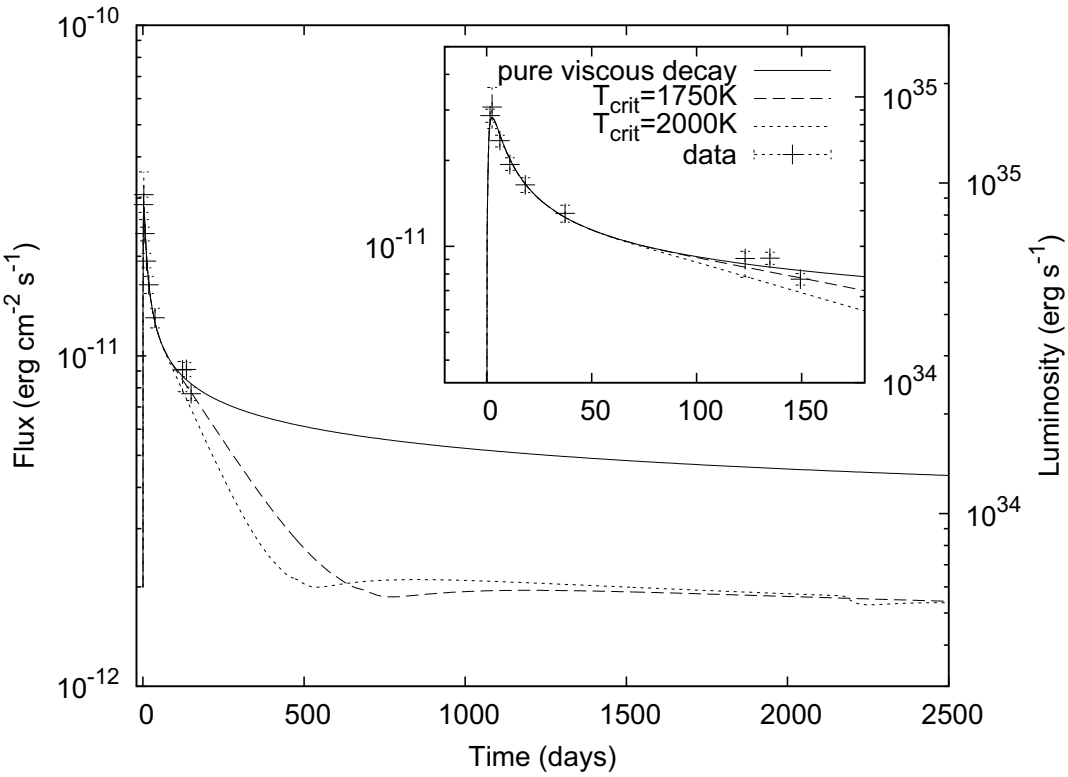

Figure 3.8: Unabsorbed 2 – 10 keV flux data of CXOU J164710.2–455216 (Israel et al., 2007; Woods et al., 2011). The long term model light curves are obtained with $T_{\rm crit} = 1750$ K, and $T_{\rm crit} = 2000$ K. For these models, $\delta M \sim 2 \times 10^{21}$ g and the estimated $\delta E \sim 2 \times 10^{38}$ erg. The luminosity is calculated assuming $d = 5$ kpc.

re-brightening (Camilo et al., 2008), possibly due to another soft gamma-ray burst, which we could not address in the model. Long-term behavior of this source can be studied by future observations. The source showed SGR-like flaring activity in 2009 January, observed by *INTEGRAL* and *Swift* (Savchenko et al., 2010).

The X-ray flux data of the candidate transient AXP AX J1845–0258 cover a period of longer than 10 years. Tam et al. (2006) argue that the recent flux data of AX J1845–0258 may be from another unrelated source within the error circles. Because of this ambiguity, we did not include this source in the present work.

The decay timescales of XTE J1810–197 and SGR 1627–41 are a few years (see Figures 3.6 and 3.7). The transient sources CXOU J164710.2–455216 and SGR 0501+4516 seem to have been observed while still in their early decay phases ($t \sim 150$ days). In Figures 3.8 and 3.9, we also present the estimated evolution of these sources in the future for different $T_{\rm crit}$ values. We note that the decay characteristics of the model light curves depend on the quiescent level of X-ray luminosity or accretion rate. Any corrections in distance measurements may require a revision of some model parameters.

3.4 Results and Discussion

Our model calculations show that the idea proposed by Ertan & Erkut (2008) to explain the X-ray enhancement light curve of XTE J1810–197 can be extended to other transient AXPs as well. This idea could be summarized as follows: there is a critical temperature, $T_{\rm crit} \sim 2000$ K, that prevails in the fallback disks of all AXPs. In the X-ray enhancement phase, the viscous instability created at this temperature governs the X-ray luminosity starting from a certain time of the decay phase, depending mainly on the disk properties in quiescence. The properties of the extended disk, in particular the surface density profile, can be estimated from the X-ray luminosity in quiescence, which is different in low-luminosity transient and high-luminosity persistent AXPs. Because of these differences in the disk properties, the effect of the instability on the decay curve is more pronounced and starts earlier in the transient AXPs than in persistent AXPs (see Section 3.2.2 and Figures 3.3 – 3.5).

A self-consistent explanation of the observed X-ray light curves requires that

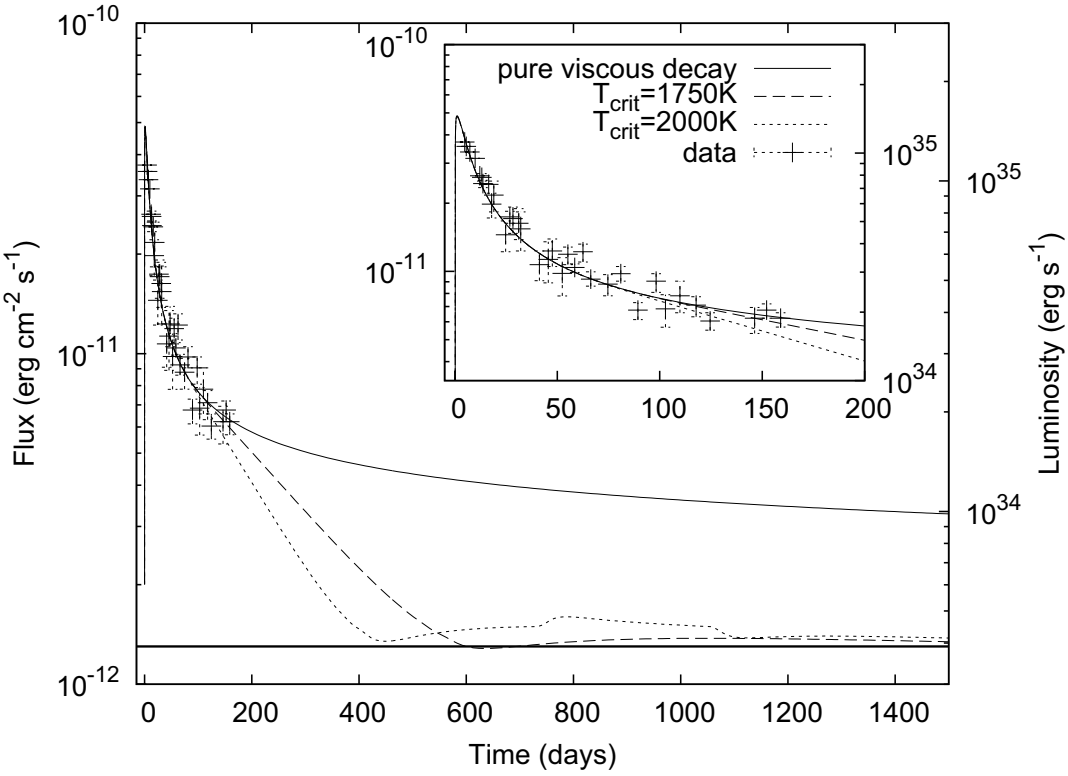

Figure 3.9: Absorbed 1–10 keV flux and luminosity data of SGR 0501+4516 (Rea et al., 2009). The model light curves are obtained with $T_{\rm crit}$= 1750 K, and $T_{\rm crit}$= 2000 K. The horizontal line shows the estimated quiescent flux of the source (1.3×10^{-12} erg cm^{-2} s^{-1}), obtained from *ROSAT* observations in 1992, extrapolated to the 1–10 keV band assuming a blackbody emission Rea et al. (2009). The luminosity is calculated assuming $d = 5$ kpc. These model curves are obtained with $\delta M \sim 3 \times 10^{21}$ g. We estimate $\delta E \sim 2 \times 10^{38}$ erg. It is seen that the source is about to diverge from the pure viscous decay curve (solid curve).

the basic model parameters obtained for the different enhancement light curves of AXPs should be similar within the uncertainties of the fallback disks. These basic parameters, which are described in detail in Section 3.2.2 are the viscosity parameters in the cold and hot state of the disk ($\alpha_{\rm cold}$, $\alpha_{\rm hot}$), the irradiation parameter (C), the critical temperature ($T_{\rm crit}$) and the power index (p) of the initial surface density profile, $\Sigma \propto r^p$, of the extended disk. It is seen in Table 3.1 that these parameters of our model for different AXPs are the same, except for C, which is very close to each other. With these parameters, the model X-ray light curves for four different transient AXPs are in good agreement with observations (Figures 3.6 – 3.9).

X-ray enhancement of persistent AXPs can also be fit well by the pure viscous evolution model (Ertan & Alpar, 2003; Ertan et al., 2006b). This is consistent with our results, since the critical temperatures found here do not significantly affect the enhancement light curves of persistent AXPs (Section 3.2).

The model that we use in the present work was first proposed by Ertan & Alpar (2003) for the SGR 1900+14. The only difference in our work is that we introduce a critical temperature ($T_{\rm crit}$). It is the presence of this $T_{\rm crit}$ that leads to viscous instability during the enhancement phase. In the model, this instability does not produce an X-ray outburst, but changes the evolution of the disk mass-flow rate and thereby the X-ray luminosity in the decay phase of the X-ray enhancement. In the disk, at temperatures below and above $T_{\rm crit}$ we use different alpha parameters ($\alpha_{\rm hot}$ and $\alpha_{\rm cold}$) to represent different viscosity states like in the models of SXTs. Over the decay phase, in the disk, the radius with $T = T_{\rm crit}$ (cooling front) propagates inward as we explained in Sections 3.2.2.3 and 3.2.2.4. In this phase, the rapid motion of the cooling front with varying X-ray luminosity is a viscous instability since it changes the viscosities along the radii it propagates. On the other hand, in the model, the observed X-ray enhancement is produced by the mass density and temperature gradients at the inner disk.

The effect of this propagation of the cooling front on the X-ray light curve is remarkably different in low-luminosity transient and high-luminosity persistent systems like SGR 1900+14 and this was discussed in detail with illustrative model curves in the paper. All X-ray enhancement light curves of AXP/SGRs mimic the light curve produced by a pure viscous decay in the early phase of evolution, but

later, they diverge from the pure viscous decay curve due to ongoing viscous instability in the disk (Figures 3.3–3.5). The same $T_{\rm crit}$ exists in all fallback disks, nevertheless the effect of the cooling-front propagation in the decay phase is more prominent and observed earlier from the systems that have lower luminosities in the quiescent state. In the present work, we also present the model curves produced by pure viscous decay just to show, by comparison, the effect of the instability on the luminosity evolution of the sources.

The fact that Ertan & Alpar (2003) can fit to the enhancement light curve of SGR1900+14 with a single alpha parameter ($\alpha_{\rm hot} \sim 0.1$), without using a $T_{\rm crit}$, indicates that the information from the cooling front could not communicate to the innermost disk during the observation period of this source. That is, when $T_{\rm crit}$ with values obtained in our work is inserted in Ertan & Alpar (2003), their model curve does not change. This shows the self consistency of our results with the earlier work, and could also be tested by the future observations of these sources. Since the critical temperature depends on the details of the chemical composition of fallback disks which is not well known, it could only be estimated from the model fits. Considering that this critical temperature must be an intrinsic property of the fallback disks, its value must be the same in all AXP/SGR systems. In the present work, we also constrain this critical temperature, trying to find solutions that can fit the light curves of all these transient sources with a similar $T_{\rm crit}$ along with other similar sets of intrinsic disk parameters (Table 3.1).

In the quiescent state, the position of the cooling front remains almost constant and is determined by the current X-ray irradiation flux. In quiescence, back and forth motion of the cooling front in a narrow radial region of the disk could create variations in the local mass-flow rate (and could still be called viscous instability), but those are smoothed out on the way to the Alfvén radius and does not cause variations in the X-ray luminosity. Therefore, we expect to observe the effect of the viscous instability in the decay phase of the X-ray luminosity.

We note that, in the present work, we have also refined the model parameters obtained by Ertan & Erkut (2008) for XTE J1810–197 considering the newly reported last three data points of this source (Bernardini et al., 2009). Illustrative model

curves given in Ertan & Erkut (2008) can produce the 2 – 10 keV absorbed data[3] for a particular $\alpha_{\rm cold}$. Nevertheless, these model curves are seen to remain above the new data points by a factor of three. We notice that the interstellar absorption significantly affects the light curve of the source close to the quiescent level of the X-ray luminosity. Here, we have repeated the calculations using unabsorbed data including the new data points of the source (Bernardini et al., 2009). For also the other sources, except for SGR 0501+4516, we have used unabsorbed data (Ibrahim et al., 2004; Bernardini et al., 2009; Mereghetti et al., 2006b; Israel et al., 2007; Woods et al., 2011; Rea et al., 2009). Since SGR 0501+4516 is in the early decay phase of the X-ray outburst (Figure 3.9), its absorbed data can be safely used to test our model. The model curves presented in Figures 3.6 – 3.9 are obtained with degenerate parameters $T_{\rm crit} = 1750$ K and $C \simeq 1 \times 10^{-4}$. For the maximum possible value of C ($\sim 7 \times 10^{-4}$), indicated by our earlier work, reasonable light curves could be obtained by increasing $T_{\rm crit}$ by a factor of ~ 1.6. This constrains $T_{\rm crit}$ to the $\sim$ 1700 – 2800 K range. This is not a strong constraint, since this result was obtained with a particular $f = \dot{M}/\dot{M}_{\rm in} = 1$ (see Section 3.2.1). Reasonable model curves can also be obtained with lower f values; nevertheless this requires modification of the model parameters. For instance, using $f = 0.1$, a model curve that fits well to X-ray enhancement data of XTE J1810–197 can be obtained with $\alpha_{\rm cold} = 0.039$ and 1350 K $< T_{\rm crit} <$ 2100 K, corresponding to $1 \times 10^{-4} < C < 7 \times 10^{-4}$.

In Figures 3.6 – 3.9, we also give the estimated mass δM of the pile-up for each of the sources. Our results sensitively depend on δM. Estimated amount of burst energy δE imparted to the inner disk depends on δM, $r_{\rm in}$ and r_0. Relative positions of $r_{\rm in}$ and r_0 also affect the model light curves, while similar results could be obtained with different $r_{\rm in}$ values, adjusting r_0 and surface density without changing δM. There is an uncertainty in estimated δE because of the uncertainties in $r_{\rm in}$ and surface density profile of the innermost disk in quiescence.

In the case of SGR 0501+4516, the distance is rather unconstrained (see Section 3.3). This source seems to be in the early phase of evolution, at a time the information from the cooling front has not reached the innermost disk by the viscous processes yet. This is the phase over which the light curve mimics that of a

[3]There is a misprint in the label of Figure 1 in Ertan & Erkut (2008). The data in their Figure 1 are absorbed flux.

pure viscous decay. That is, changing the initial surface density profile at all radii by a constant multiplicative factor, it is possible to obtain different model light curves that have the same functional forms that differ only in amplitudes. Since any change in distance will modify all data points with the same multiplicative factor, we can obtain a similar model fit without modifying the intrinsic disk parameters. Nevertheless, after the viscous instability deviates the light curve from that of pure viscous decay, any correction in distances could require a modification of the critical temperature parameter to obtain a similar model fit to data, or possibly the model could fail in producing the observed light curve.

We should also note the possibilities of different burst geometries. We assume that the soft gamma-ray burst energy is emitted isotropically. This might not be the case, at least for some of the bursts. For instance, only a certain angular segment of the disk could be illuminated by the burst energy. This leads to a rather different post-burst surface density profile than we assume here. Even in this case, the resultant enhancement light curves are likely to be similar to those produced by an isotropic burst, provided that the burst creates a sufficient surface density gradient. These possibilities put further uncertainties on the estimated burst energy. For instance, in some cases it is possible that we observe an X-ray enhancement without observing the triggering burst whose anisotropic emission pattern evaded us. Another possibility is that we could observe bursts that are not followed by an enhancement in X-rays, if the solid angle of this particular burst does not cross the disk.

Independent of the details of burst geometries, subsequent X-ray outburst light curves of different AXPs provide a good test for the fallback disk model. For given quiescent and peak X-ray luminosities in an enhancement phase, there is a single decay curve estimated by the disk model. To put it in other words, all the observed enhancement light curves of AXPs should be reproduced by a single set of main disk parameters.

In comparison of the model curves with data, there are some uncertainties that we encounter at very low luminosities ($L_{\rm X} \sim 10^{33}$ erg s^{-1}): (1) due to very low temperatures, a significant fraction of the X-ray luminosity of the source is expected to be emitted below the observed X-ray band that we take to represent the total

luminosity of the source. (2) Absorption effects considerably increase for the soft radiation emitted at these low temperatures. (3) Depending on the age, the cooling luminosity of the source could have significant contribution to the total quiescent luminosity of the source. (4) It is possible that some small bursts could be emitted in the decay phases and affect the secular decay characteristics of the light curves. It is not possible to address these effects in the model. For instance, the data point that remains above the model light curve of SGR 1627-41 (Figure 3.7) might be due to such a small burst.

Within these uncertainties, our model curves are in agreement with the X-ray enhancement data of four transient AXPs (Figures 3.6 – 3.9). We have succeeded to obtain reasonable model curves with almost the same basic disk parameters, given in Table 3.1.

3.5 Conclusions

We have shown that the X-ray outburst (enhancement) light curves of AXPs and SGRs can be explained by the evolution of an irradiated disk after the inner disk is pushed back to larger radii by a soft gamma-ray burst. A viscous instability created at a critical temperature, $T_{\rm crit}$, seems to be a common property of all AXP/SGR disks. For the extreme values of X-ray irradiation efficiency obtained from our earlier work (Ertan & Çalışkan, 2006), we estimate that $T_{\rm crit}$ is in 1300 – 2800 K range.

Characteristic differences between the enhancement light curves of transient and persistent AXP/SGRs can naturally be accounted for by their different pre-burst (quiescent) conditions of the disks implied by the X-ray luminosity of the sources in quiescence. X-ray outburst light curve of a persistent AXP/SGR could not be distinguished from a light curve produced by a pure viscous (without any instability) evolution of the disk for a few years. For a transient source, the outburst light curve could diverge from the pure viscous evolution within months after the onset of the outburst (Figures 3.6 – 3.9). These results are consistent with our earlier work on the X-ray outburst light curves of persistent AXP/SGRs (see, e.g., Ertan et al., 2006b) which were explained by pure viscous evolution of the disk.

Basic properties of the fallback disks are likely to be similar in the fallback disks of all AXP/SGRs. Through a large number of simulations, we have obtained a single

Table 3.1: The parameters for the model curves presented in Figures 3.6–3.9. Note that the parameters $\alpha_{\rm hot}$, $\alpha_{\rm cold}$, p and $T_{\rm crit}$ are expected to be similar for all AXPs and SGRs. Irradiation efficiency, C, which could change with accretion rate is also likely to be similar for the sources in the same accretion regimes. In quiescence, Σ_0 scales with accretion rate. The width of the Gaussian pile-up is represented by Δr. The parameters Δr, r_0, and $\Sigma_{\rm max}$ could vary from source to source, depending on the burst energy and geometry. The values of inner disk radius $r_{\rm in}$ are close to the Alfvén radii of the sources with $B_0 \simeq 10^{12}$ G. We set $r_{\rm out} = 10^{13}$ cm and $f = \dot{M}/\dot{M}_{\rm in} = 1$ for all our models.

Parameter	XTE J1810-197	SGR 1627-41	CXO J164710.2-455216	SGR 0501+4516
$r_{\rm in}$ (cm)	2×10^9	2×10^9	1.8×10^9	3×10^9
r_0 (cm)	7×10^9	2.3×10^{10}	5×10^9	6×10^9
Δr (cm)	9×10^9	6×10^8	6×10^8	1.4×10^9
$\Sigma_{\rm max}$ (g cm^{-2})	20	60	13	10
Σ_0 (g cm^{-2})	10	1	7.6	5
$\alpha_{\rm hot}$	0.1	0.1	0.1	0.1
$\alpha_{\rm cold}$	0.045	0.045	0.045	0.045
$T_{\rm crit}$ (K)	1750	1750	1750	1750
C	1×10^{-4}	1.6×10^{-4}	1×10^{-4}	1×10^{-4}
p	0.75	0.75	0.75	0.75

set of these basic parameters (Table 3.1) that can produce reasonable model fits to the enhancement light curves of four transient AXP/SGRs (Figures 3.6 – 3.9).

The predictions of our model could be tested by future observations of AXPs and SGRs in the X-ray enhancement phases.

Chapter 4

SGR 0418+5729 - HOW DOES A YOUNG NEUTRON STAR SPIN DOWN TO A 9 S PERIOD WITH A DIPOLE FIELD LESS THAN 10^{13} G ?

This chapter of the thesis was published in
The Astrophysical Journal Letters, 2011, Volume 732, pp. 4 - 7
Mehmet Ali Alpar, Ünal Ertan & Şirin Çalışkan

Abstract

The period derivative bound for SGR 0418+5729 (Rea et al., 2010) establishes the magnetic dipole moment to be distinctly lower than the magnetar range, placing the source beyond the regime of isolated pulsar activity in the $P - \dot{P}$ diagram and giving a characteristic age $> 2 \times 10^7$ years, much older than the 10^5 year age range of SGRs and AXPs. So the spindown must be produced by a mechanism other than dipole radiation in vacuum. A fallback disk will spin down a neutron star with surface dipole magnetic field in the 10^{12} G range and initial rotation period $P_0 \sim 100$ ms to the 9.1 s period of SGR 0418+5729 in a few 10^4 to $\sim 10^5$ years. The current upper limit to the period derivative gives a lower limit of $\sim 10^5$ years to the age that is not sensitive to the neutron star's initial conditions. The total magnetic field on the surface of SGR 0418+5729 could be significantly larger than its 10^{12} G dipole component.

4.1 Introduction

The recently discovered SGR 0418+5729 (van der Horst et al., 2010) has a period $P = 9.1$ s (Göğüş et al., 2009) in the narrow range of AXP and SGR periods (Mereghetti, 2008). The spin-down rate has not been measured yet (Kuiper & Hermsen, 2009; Woods et al., 2009; Esposito et al., 2010; Rea et al., 2010). The best period derivative upper limit, $\dot{P} < 6 \times 10^{-15}$ s s^{-1} (Rea et al., 2010), evaluated as dipole spin-down of an isolated star, gives a surface dipole magnetic field $B_0 < 1.5 \times 10^{13}$ G at the poles, much lower than fields previously deduced from spin-down rates of magnetars[4]. The characteristic age $P/(2\dot{P}) > 2.5 \times 10^7$ years, while AXPs and SGRs, some of which are associated with SNR (Esposito et al., 2009b; Mereghetti, 2008, and references therein) are believed to be young neutron stars with ages $\sim 10^5$ years. SGR 0418+5729 is similar to other AXPs and SGRs in all observed properties except for $\dot{P}$. The energy in its soft gamma-ray bursts requires a total magnetic field $\sim 10^{12}$ G on the neutron star surface, but if all SGRs have super-outbursts occasionally, so far observed from SGR 1806-20, SGR 0526-66 and

[4]Rea (2012) reported a preliminary measurement of $\dot{P} = 5 \times 10^{-15}$ s s^{-1}, which gives a dipole magnetic field $B_0 = 1.4 \times 10^{13}$ G, but these values have not been confirmed yet.

SGR 1900+14, the total surface magnetic field $B_{\rm total} \sim 10^{14} - 10^{15}$ G according to the magnetar model (Duncan & Thompson, 1992; Thompson & Duncan, 1995). If SGR 0418+5729 is a standard magnetar, it provides a clear counterexample to the proposition that for magnetars the dipole component of the magnetic field is of the same order as the total field.

If the spindown to the present period was achieved by magnetic dipole radiation SGR 0418+5729 would be an exceptional object, mimicking all SGR and AXP properties while not belonging to the class. Its position in the $P - \dot{P}$ diagram, beyond the so called death-valley, makes it exceptional also among the rotation powered isolated pulsars: the only other source located similarly in $P - \dot{P}$ is the radio pulsar PSR J2144-3933. Furthermore, if SGR 0418+5729 is older than 2.5×10^7 years as its characteristic age $P/(2\dot{P})$ suggests, its quiescent X-ray luminosity cannot be explained by cooling, reheating or magnetic field decay, let alone explaining soft gamma-ray outbursts occurring at such old age. If SGR 0418+5729 is much younger than its characteristic age with dipole spin-down, its initial rotation period would have to be close to the present 9.1 s period, again making this source unique, standing far out from the initial period distribution inferred from population synthesis (Faucher-Giguère & Kaspi, 2006).

The dipole component of the field B_0 determines torques due to electromagnetic radiation and interactions with the environment. Estimates of B_0 from spin-down rates depend on the torque mechanism. The total surface magnetic field is derived from measurements of cyclotron lines (Ibrahim et al., 2002) and the spectral continuum (Güver et al., 2007, 2008). Historically, the dipole field measurements came first (Kouveliotou et al., 1998). The field inferred with the dipole spin-down torque was in the magnetar range, supporting the magnetar model which had been proposed to explain the SGR bursts and other SGR and AXP properties including spindown to long periods at a young age (Duncan & Thompson, 1992; Thompson & Duncan, 1995). The identification of the dipole component with the total field has been taken for granted.

We proceed, by Occam's razor, to posit that SGR 0418+5729 is a member of the same class of young neutron stars as the other SGRs and AXPs, but its spin down is not due to magnetic dipole radiation. So there must be matter around the star,

in a bound state, therefore carrying angular momentum. For *isolated* neutron stars a fallback disk, which can be formed in some supernovae (Michel, 1988; Chevalier, 1989; Lin et al., 1991) will provide this. The fallback disk model was proposed by Chatterjee et al. (2000) for AXPs, and independently by Alpar (2001) as a possible way of explaining the different classes of young neutron stars, including the X-ray dim isolated neutron stars (XDINs) and compact central objects (CCOs) as well as AXPs and SGRs. The prime motivation was to address the period clustering which strongly suggests a regulating store of angular momentum. For a given value of $\dot{P}$ the dipole moment inferred with fallback disk model is generally less than that derived assuming isolated dipole spin-down. The differences in $\dot{P}$ between sources of similar period are not primarily due to differences in magnetic dipole moment, with the fallback disk also playing a critical role in evolution. The model indicates surface dipole fields $\sim 10^{12} - 10^{13}$ G. The bursts may be powered by strong total magnetic fields $B_{\rm total} \sim 10^{14} - 10^{15}$ G as in the magnetar model- implying that the dipole field is smaller than the total field. The discovery of a disk around AXP 0142+61 (Wang et al., 2006) gave strong support to the fallback disk model. Ertan et al. (2007) showed that the entire non-pulsed optical to mid-IR spectrum can be understood as emission from a gaseous disk, while the pulsed optical signal is produced in the magnetosphere (Ertan & Cheng, 2004; Cheng & Ruderman, 1991).

This work investigates evolutionary scenarios for SGR 0418+5729 employing a fallback disk. We show that the period derivative as well as the period and X-ray luminosity in quiescence are explained quite naturally, and a fallback disk can spin down the neutron star to a period of 9.1 s in a few 10^4 to $\sim 10^5$ years.

4.2 Evolution With a Fallback Disk

The mass and mass inflow rate of the fallback disk decay through viscous dynamics, modified by irradiation from the neutron star. The fallback disk, though truncated at the inner radius, follows the self-similar solutions with power law decay in time (Pringle, 1974) quite closely as long as the entire disk is viscous (Ertan et al., 2009). Viscous activity stops when the local temperature falls below a critical temperature $T_p \sim 100$ K, becoming too cold for sufficient ionization for the magneto-rotational instability to generate viscosity and sustain mass inflow (Inutsuka & Sano, 2005).

Such passive regions grow starting from the outer disk. Irradiation by the star can keep the outer disk at temperatures higher than T_p for a while, delaying the passive phase, keeping a larger part of the disk active. This interaction between the gradual transition to a final passive phase, and the effect of irradiation to prolong the active phase determines the evolution in a complicated way. To calculate the irradiation flux impinging on the disk we employ the same irradiation efficiency as in our best fits for the disk observed around AXP 0142+61 (Ertan et al. 2007, see Ertan & Çalışkan 2006 for the other AXPs).

At each step in the evolution a solution for the entire disk is constructed taking all these effects into account. The mass inflow rate $\dot{M}_{\rm in}$ arriving at the inner disk is obtained and the inner disk radius $r_{\rm in}$ is determined as the Alfvén radius

$$r_{\rm A} = 10^9 \text{ cm } \mu_{30}^{4/7} (\dot{M}_{\rm in15})^{-2/7} (M/M_\odot)^{-1/7} \tag{4.1}$$

Here $M_\odot$ is the solar mass, $\dot{M}_{\rm in15}$ is the mass inflow rate in 10^{15} g s^{-1}, and μ_{30} is the dipole magnetic moment in 10^{30} G cm^3. The important distance scales are the light cylinder radius $r_{\rm LC} = {\rm c}/\Omega$, the co-rotation radius ${\rm r_{co}} = ({\rm GM})^{1/3}/\Omega^{2/3}$ and $r_{\rm A}$. The fallback disk will effect the evolution when the disk's inner radius is within the neutron star's light cylinder. The effect of the disk will decrease drastically when the disk moves outside the light cylinder.

Throughout the evolution $r_{\rm A} > {\rm r_{co}}$, so the neutron star is a fast rotator, and the torque applied by the disk is always a spin-down torque. The neutron star is in the propeller regime (Illarionov & Sunyaev, 1975). In contrast to the original propeller picture the fallback disk model takes some portion $\dot{M}_{\rm acc}$ of the mass inflow $\dot{M}_{\rm in}$ to be accreting onto the neutron star during spin-down (Chatterjee et al., 2000; Alpar, 2001). Rappaport et al. (2004) have shown from general considerations of accreting neutron stars that partial accretion must be taking place. This provides the X-ray luminosity in the fallback disk model thoughout most of the evolution, when ${\rm r_{co}} < r_{\rm A} < r_{\rm LC}$. The luminosity evolution is determined by the unknown fraction $\dot{M}_{\rm acc}/\dot{M}_{\rm in}$ and the initial fallback disk mass ${\rm M_d}$ which effects the evolution of $\dot{M}_{\rm in}$.

The spin-down rate of a neutron star under disk torques is given by

$$I\dot{\Omega} = \dot{M}_{\rm in} (GMr_{\rm A})^{1/2} F(\omega) \tag{4.2}$$

where I is the moment of inertia, $\dot{\Omega}$ the spin-down rate, Ω the rotation rate, $\dot{M}_{\rm in}$ the mass inflow rate arriving from the disk at its inner boundary, and M is the star's mass. $F(\omega)$ is the dimensionless torque which depends on the fastness parameter $\omega \equiv \Omega/\Omega_K(r_A)$, $\Omega_K(r_{\rm A})$ being the Keplerian rotation rate at $r_{\rm A}$. A dimensionless disk torque

$$F(\omega) = (1 - \omega^2) \cong -\omega^2 \tag{4.3}$$

is indicated by our earlier results (Ertan et al., 2009; Ertan & Erkut, 2008). This torque is due to the azimuthal bending of magnetic field lines from the co-rotating magnetosphere at $\rm r_{co}$to the slower rotating inner disk at $r_{\rm A} > \rm r_{co}$. Equations (1)-(3) show that the torque is independent of $\dot{M}_{\rm in}$. ($F(\omega) \cong -\omega^{2+\delta}$ gives a weak dependence $\propto \dot{M}_{\rm in}{}^{-3\delta/7}$). We integrate $\dot{\Omega}$ to get Ω, reconstruct the disk, with current $r_{\rm A}$ and $r_{\rm LC}$, irradiated by the current luminosity, and proceed by iteration.

As $\dot{M}_{\rm in}$ decreases and the star spins down, $r_{\rm A}$ increases with time faster than $r_{\rm LC}$ does. Near and beyond the light cylinder $r_{\rm LC}$ the electromagnetic field gradually changes from the dipole magnetic field to wave fields. The inner disk radius is somewhat larger than $r_{\rm A}$ in this region. Ekşi & Alpar (2005) have studied the transition towards the wave zone. They show that the disk is stable beyond the light cylinder as long as the inner disk radius r_{in} remains within a critical distance which depends on the angle between the rotation and magnetic axes of the star, ranging from 2.5 $r_{\rm LC}$ for a perpendicular rotator to many $r_{\rm LC}$ for an almost aligned rotator. The torque and luminosity should drop within a narrow range of $r_{in} \cong r_{\rm LC}$ – the disk can be stable far beyond $r_{\rm LC}$, but is causally disconnected from the star and magnetosphere. Cooling or energy dissipation in the neutron star account for a much reduced X-ray luminosity. For the torque we consider two distinct models: (i) We assume that the disk remains undetached from the light cylinder and set r_{in} = $r_{\rm LC}$. This can be qualitatively justified as mass lost by the disk cannot penetrate into the magnetosphere, but will tend to pile up around the light cylinder. As the disk inner radius reaches $r_{\rm LC}$ from inside the mass pile-up is likely to keep r_{in} from detaching from $r_{\rm LC}$. (ii) The minimal torque is the dipole radiation torque taking over immediately when $r_{in} \geq r_{\rm LC}$. The actual torque should show a transition from disk torque to dipole radiation torque.

4.3 Spin and Luminosity Evolution of SGR 0418+5729

We have carried out a detailed investigation of SGR 0418+5729 using the code developed earlier (Ertan & Erkut, 2008; Ertan et al., 2009) which successfully generated AXP and SGR properties at their likely ages by luminosity and spindown evolution driven by a fallback disk. Many combinations of initial conditions were tried in search for a scenario to produce the present day SGR 0418+5729. Each calculation starts with a choice of dipole moment and initial rotation period for the neutron star, and an initial disk mass.

The disk around SGR 0418+5729 cannot still be inside the light cylinder at present: if it were, $\dot{P}$ would be approximately (or exactly, in our torque model) independent of $\dot{M}_{\rm in}$ in this epoch, so that the age estimate would be given by $\sim P/\dot{P} = 5 \times 10^7$ years, an untenably old age. We find that SGR 0418+5729 was spun-down to its period with efficient disk torques in a past epoch when the inner disk was within the light cylinder, $\dot{P}$ having subsequently decreased to its present value in the present epoch when the disk is at or beyond $r_{\rm LC}$.

Figures 4.1 and 4.2 show evolutionary tracks for luminosity, period and period derivative, producing the present properties of SGR 0418+5729 for numerous combinations of the initial conditions. Figure 4.1 shows the evolutionary models with $P_0 = 150$ ms for $B_0 = 1.2, 1.4, 1.6 \times 10^{12}$ G, with initial disk masses $M_d = 5.6, 2.2, 1.3 \times 10^{-5}$ $M_\odot$ respectively. In Figure 4.2, we show evolutionary tracks with $B_0 = 1.2 \times 10^{12}$ G and $P_0 = 70 - 300$ ms, with $\rm M_d \simeq 6 \times 10^{-5}$ $M_\odot$. A reference luminosity $L_x = \rm GM\dot{M}_{in}/R$ is plotted throughout the past epoch when the inner disk was inside the light cylinder. The true luminosity was less by the unknown fraction $\dot{M}_{\rm acc}/\dot{M}_{\rm in}$. This uncertainty does not influence the evolutionary models because its effect on the disk is folded into the irradiation efficiency. We took B_0 in the $10^{11} - 10^{13}$ G range of dipole fields for most young pulsars, which worked in earlier applications (Ertan et al., 2009). All AXPs and SGRs have $L_x \lesssim 10^{36}$ erg/s, giving an upper limit for M_d in our searches. $\rm M_d$ is calculated for disk models extending to an outer radius $r_{\rm out} = 5 \times 10^{14}$ cm at the start. For given B_0, disks lighter than a certain M_d can never penetrate the light cylinder, and so cannot produce an AXP/SGR. For each B_0 - M_d choice, there is a minimum P_0 for the inner disk to ever lie within $r_{\rm LC}$. The degeneracy of initial conditions producing SGR 0418+5729

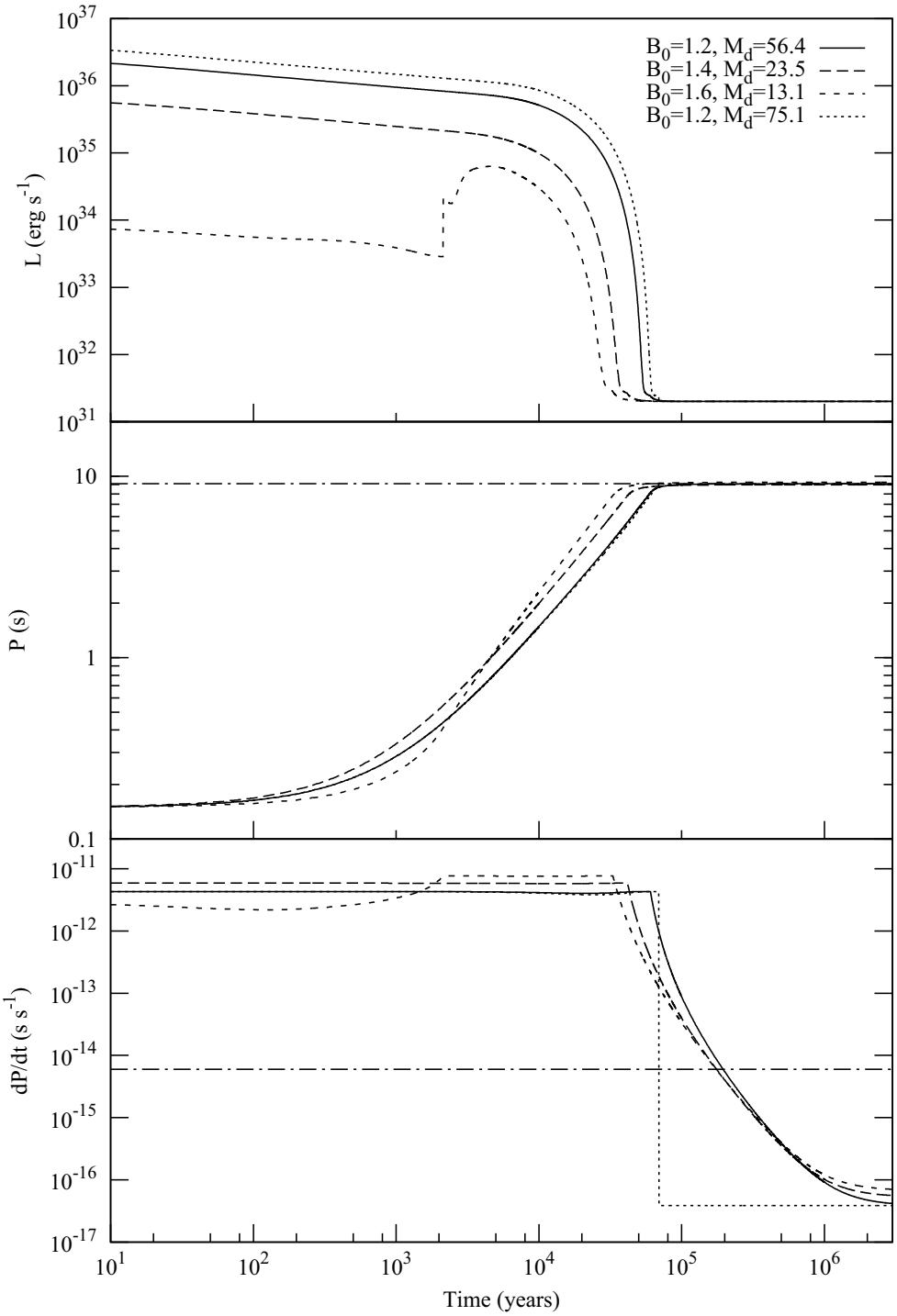

Figure 4.1: Luminosity, period and period-derivative evolution of model sources for an initial period $P_0 = 150$ ms. Values of the initial disk mass (in units of 10^{-6} $M_\odot$) and the magnetic field (in 10^{12} Gauss) at the poles of the neutron star are given in the figure. The horizontal lines correspond to the period (9.1 s) and the present upper limit on the period-derivative of SGR 0418+5729 (6×10^{-15} s s^{-1}). We also present the minimal torque case (dotted curve) where the disk torque is assumed to vanish when $r_A \geq r_{LC}$.

shows that these correlations between workable initial conditions are not very strict constraints. For most B_0 and M_d, models start off with the inner disk within the light cylinder. (Models with stronger B_0 and lower M_d show different early evolution, with $r_{\rm A} > r_{\rm LC}$ initially. Starting off under the dipole spin-down torque, the low luminosity $\sim 10^{34} - 10^{35}$ erg s^{-1} in the initial phases is due to cooling (Page, 2009) and dissipative dynamics inside the neutron star (Alpar, 2007). These models show sudden luminosity and torque increase at $\sim 10^3$ years when the inner disk enters the light cylinder.)

Between 10^4 and 10^5 years, there is a turnover to fast luminosity decay with rapid spin-down until the period settles to its present value of 9.1 s. The fall-back disk is evolving towards its final passive phase. As $\dot{M}_{\rm in}$ drops, so does the rate of viscous heating. Effects of irradiation also start to drop as the accretion luminosity decreases with mass inflow rate. Starting from the outermost parts, more and more sections of the disk are cooling below the critical temperature $T_{\rm p}$. As this continues, $\dot{M}_{\rm in}$ arriving at the inner disk to provide for accretion decreases even more rapidly. The positive feedback leads to a luminosity turnover and eventual cutoff. Throughout this phase, $r_{\rm A}$ is inside the light cylinder and the disk torque remains in effect. The light cylinder recedes as the star spins down, but the inner disk recedes more rapidly with the accelerated decay of $\dot{M}_{\rm in}$, and finally reaches $r_{\rm LC}$. The $\dot{P}$ now starts dropping very rapidly and the period remains almost constant from this point on. The luminosity is down to the cutoff luminosity, which we take to be 2×10^{31}erg s^{-1}, three times less than the slowly decaying present luminosity quoted by Rea et al. (2010) for a distance of 2 kpc, and consistent with the standard cooling luminosity range of neutron stars at ages of $10^5 - 10^6$ years. The choice of luminosity cutoff does not effect the evolution.

The optical and infrared emission of the disk around SGR 0418+5729 at present is much weaker than for other AXPs and SGRs. We expect luminosities in K_s and 4.5 μm bands about 10^3 and 10^5 times less than the corresponding luminosities of AXP 0142+61. The disk luminosity is even lower in the R band, since the magnetosphere truncates the inner disk of SGR 0418+5729.

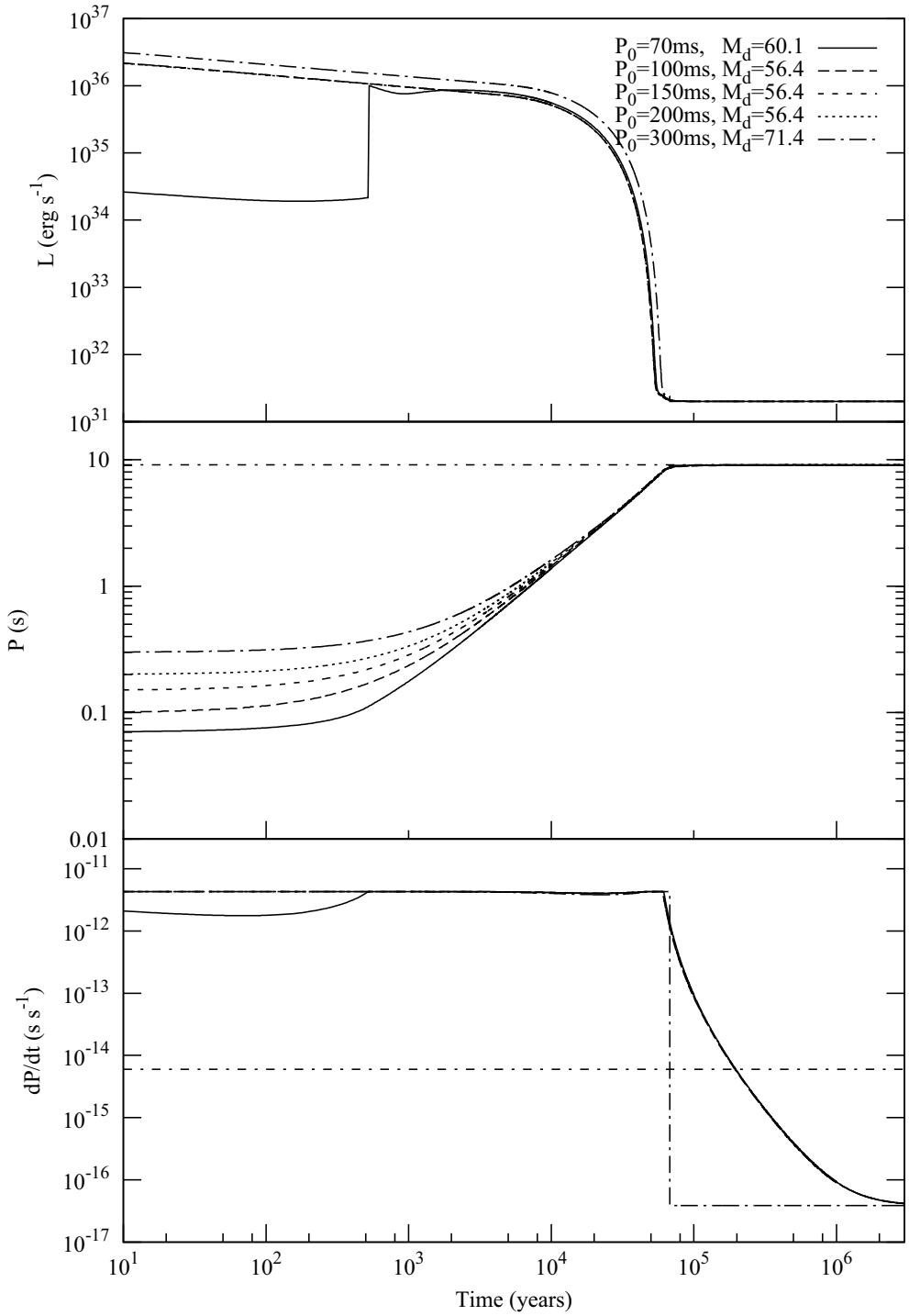

Figure 4.2: Luminosity, period and period-derivative evolution of model sources for a polar magnetic field of $B_0 = 1.2 \times 10^{12}$ G on the surface of the neutron star. Values of the initial disk mass (in units of 10^{-6} $M_\odot$) and initial period are given in the figure. The horizontal lines show the present period and upper-limit on $\dot{P}$. The period derivative curves converge to a final value of $\sim 4 \times 10^{-17}$ s s^{-1}, a lower limit given by the dipole spin-down torque when the disk becomes inactive. The dipole spin-down case is given by the dotted-dashed curve.

4.4 Discussion and Conclusions

SGR 0418+5729 was spun down to its present period in an earlier epoch when the inner disk was within the light cylinder. The present state of exceedingly low spindown rate was reached when the disk retreated to or beyond the light cylinder. Initial parameters $B_0 \simeq 1-2\times10^{12}$ G, $\mathrm{M_d} \simeq 4\times10^{-6}$ $M_\odot$to $\mathrm{M_d}\simeq 6\times10^{-5}$ $M_\odot$ and $P_0 > 70$ ms work well, giving the period $P_0 = 9.1$ of SGR 0418+5729, consistently with the upper limit $\dot{P} < 6\times10^{-15}$ s s^{-1} at ages greater than about 2×10^5 years. For the present epoch with the disk inner edge at or beyond the light cylinder tracks with a sustained disk torque are shown, as well as evolution reduced to dipole spin-down. The luminosity is due to partial accretion until $t \sim 3-6\times10^4$ years. For simplicity we show only a reference luminosity calculated for full accretion; the actual luminosity in this past epoch was smaller by an unknown fraction $\dot{M}_{\rm acc}/\dot{M}_{\rm in}$. The period $P = 9.1$ s is reached as an eventual constant period, already at $3-6\times10^4$ years, together with a drop in period derivative.

Figures 4.1 and 4.2 show that the present $\dot{P}$ upper limit gives a lower limit of $\sim 2\times10^5$ years if the disk torque is still operating. If the disk is already out of contact with the star, the dipole spin-down track gives a lower limit of $\sim 10^5$ years. A future measurement of $\dot{P}$ will give a rough estimate of the age, between this lower bound and the age at which the disk torque models give the observed $\dot{P}$. A measurement of $\dot{P} \sim 4\times10^{-17}$ s s^{-1} will establish dipole spin-down prevails at present. An even lower $\dot{P}$ measurement would signal dipole spin-down driven by $B_0 < 10^{12}$ G.

We conclude that the very low period derivative upper limit for SGR 0418+5729 can be naturally explained in terms of spindown by a fallback disk. The neutron star has initial rotation period in the range expected for young neutron stars (Faucher-Giguère & Kaspi, 2006). The dipole component of the surface field is in the 10^{12} G range. The higher multipoles and the total surface field could be much larger. Indeed, the X-ray spectrum of SGR 0418+5729 indicates a total surface field of 1.1×10^{14} G (Güver et al., 2011). Comparative investigation of total and surface dipole magnetic fields by different methods is likely to provide important clues to properties and evolution of magnetars, pulsars and young neutron stars.

Chapter 5

ON THE EVOLUTION OF THE RADIO PULSAR PSR J1734-3333

This chapter of the thesis was accepted for publication in
Monthly Notices of the Royal Astronomical Society, 2013
Şirin Çalışkan, Ünal Ertan, Mehmet Ali Alpar, Joachim E. Trümper & Nikos D. Kylafis

Abstract

Recent measurements showed that the period derivative of the 'high-B' radio pulsar PSR J1734−3333 is increasing with time. For neutron stars evolving with fallback disks, this rotational behavior is expected in certain phases of the long-term evolution. Using the same model as employed earlier to explain the evolution of anomalous X-ray pulsars and soft gamma-ray repeaters, we show that the period, the first and second period derivatives and the X-ray luminosity of this source can simultaneously acquire the observed values for a neutron star evolving with a fallback disk. We find that the required strength of the dipole field that can produce the source properties is in the range of $10^{12} - 10^{13}$ G on the pole of the neutron star. When the model source reaches the current state properties of PSR J1734−3333, accretion onto the star has not started yet, allowing the source to operate as a regular radio pulsar. Our results imply that PSR J1734−3333 is at an age of $\sim 3 \times 10^4 - 2 \times 10^5$ years. Such sources will have properties like the X-ray dim isolated neutron stars or transient AXPs at a later epoch of weak accretion from the diminished fallback disk.

5.1 Introduction

The discovery of several new classes of isolated neutron stars, namely the anomalous X-ray pulsars (AXPs) and soft gamma-ray-burst repeaters (SGRs), the X-ray dim isolated neutron stars (XDINs), the compact central objects in certain supernova remnants (CCOs), and the rotating radio transients (RRATs), has brought into focus the question of possible evolutionary links (see, e.g., Kaspi, 2010; Popov, 2008). The existence of radio pulsars with large inferred dipole magnetic moments, close to, and in fact partly overlapping with, the range of magnetar fields inferred for AXPs and SGRs ($\gtrsim 10^{14}$ G), and the observation of radio pulses from some AXPs and SGRs, further highlight the possibility of links and raise questions about the similarities and differences among these sources. The locations and evolutionary tracks of pulsars in the $P - \dot{P}$ diagram hold the keys to deciphering the links. The recent measurement of the peculiar braking index $n = 0.9 \pm 0.2$ of PSR J1734−3333, the lowest among the measured braking indices of young pulsars, with period $P =$

1.17 s and period derivative $\dot{P} = 2.28 \times 10^{-12}$ s s^{-1} (Espinoza et al., 2011) is an exciting new clue.

Analyzing the $P - \dot{P}$ diagram of all isolated pulsars in terms of evolution by rotationally powered dipole radiation into the vacuum, starting with the initial rotation rate and the magnetic dipole moment at birth, and assuming that the dipole moment remains constant, fails to explain the distribution of all young pulsars on the $P - \dot{P}$ diagram or to shed light on the possible connections of the distinct classes. Evolution of the magnetic-dipole moment and its angle with the rotation axis is one direction of extending the picture, as suggested in the work reporting the braking index of PSR J1734−3333 (Espinoza et al., 2011). Magnetic-field evolution and amplification to lead to magnetar strength $10^{14} - 10^{15}$ G surface fields have been invoked to explain the bursts of SGRs and AXPs (Duncan & Thompson, 1992). This does not require that the magnetar strength fields are necessarily in the *dipole* component that controls the spin-down of the pulsar and thereby its evolution on the $P - \dot{P}$ diagram. Indeed, the recently published $\dot{P}$ upper limit of SGR 0418+5729 (Rea et al., 2010) has shown that the surface dipole field of this pulsar is at most 7.5×10^{12} G at the equator (1.5×10^{13} G at the poles). This has been interpreted in terms of the decay of the magnetar dipole moment of this SGR (Turolla et al., 2011). All measured braking indices (Becker, 2009) deviate from the n = 3 value, characteristic for dipole radiation in vacuum. Braking indices n < 3 imply a growing magnetic dipole moment (or growth of the dipole moment component perpendicular to the rotation axis). Thus, to understand the behavior of pulsars and magnetars in different parts of the $P - \dot{P}$ diagram requires growth, or decay, of the magnetic dipole moment perpendicular to the rotation axis, at rates depending on the sources.

An alternative avenue for a more general picture of isolated pulsar evolution is to allow for the possibility of interaction with matter around the star, so that the emission is not dipole radiation in vacuum. An effective possibility is that some matter left over from the supernova explosion is actually bound to the neutron star, in the form of a 'fallback' accretion disk, as it necessarily carries angular momentum, as proposed by Chatterjee et al. (2000) to explain the properties of AXPs. Alpar (2001) suggested that the presence or absence, and the initial mass, of a fallback disk could be the third initial condition, complementing the initial rotation rate and

dipole magnetic moment, to determine the subsequent evolution of different classes of neutron stars. A first simple application of this idea to pulsar braking indices and motion across the $P - \dot{P}$ diagram was presented by Alpar et al. (2001). Discoveries of radio pulsars with long periods and large period derivatives suggested that these sources could have evolutionary links with AXPs and SGRs (Kaspi 2010; Espinoza et al. 2011; see, e.g., Mereghetti 2008 for a recent review of AXPs and SGRs).

In the present paper we apply the fallback disk model in detail to the evolution of PSR J1734−3333 and show that the model can explain all the properties of this source, including its braking index. In Section 5.2 we outline the model and examine evolutionary tracks for a neutron star with a fallback disk to search for scenarios leading to the present properties (P, $\dot{P}$, $\ddot{P}$, and $L_{\rm X}$) of PSR J1734–3333. We trace all possible initial conditions, namely the initial period, dipole field, and disk mass, that can produce the source properties. We discuss the results of our model calculations in Section 5.3, and summarize our conclusions in Section 5.4.

5.2 The Model

In the fallback disk model (FDM) (Chatterjee et al., 2000; Alpar, 2001) the period and luminosity evolution are determined by the interaction between the neutron star and a fallback disk around it. The mid-infrared detections from the AXPs 4U 0142+61 (Wang et al., 2006) and 1E 2259+586 (Kaplan et al., 2009) are consistent with the presence of fallback disks around these sources (Ertan et al., 2007). It was shown by Ertan & Çalışkan (2006) that the observed near-IR luminosities and the upper limits of AXPs/SGRs are compatible with the expectations of FDM. The values of the dipole-field strength at the pole of the neutron star B_0, indicated by FDM fits to optical/IR data of 4U 0142+61 (Ertan et al., 2007) and by the results of the work explaining the long-term P, $\dot{P}$, and X-ray luminosity, $L_{\rm X}$, evolution of AXPs and SGRs, are less than 10^{13} G in all cases (Ertan et al., 2009; Alpar et al., 2011). It was proposed in these papers that the magnetar strength fields needed to power the bursts must be residing in quadrupole and higher multipole components. The higher multipole fields fall off with distance from the star more rapidly than the dipole field does, leaving the dipole field to determine the interaction with the disk and the resulting torques.

The interactive evolution of the neutron star and the fallback disk can have epochs with accretion as well as radio pulsar epochs. The neutron star enters the accretion regime and experiences an efficient torque if and when the inner edge of the fallback disk penetrates into the light cylinder. The neutron star can then spin down to long periods of several seconds on timescales from $\sim 10^3$ to $\sim 10^5$ yr, depending on the disk torques, the dipole-field strength B_0 and the disk mass $\mathrm{M_d}$. The first (ejector) phase of evolution without accretion could last from several years to more than 10^5 yr depending on B_0, $\mathrm{M_d}$, and initial period P_0. During this phase, the neutron star is a radio pulsar. In the present work, we show that PSR J1734−3333 is likely to be in the radio pulsar phase without accretion at present and that the accretion epoch could start at a future time. In the accretion phase, at a time depending on the initial parameters, the inner disk will reach the light cylinder and the accretion will stop. After the accretion phase, the disk could remain attached to the light cylinder and the disk torque could still remain active while its efficiency gradually decreases to the level of the dipole radiation torque. Unlike a steady-state disk in a binary, where the accreting stage can be sustained on the evolutionary timescales of the binary and the companion, the fallback disk around an isolated neutron star will diminish. From the beginning, the outermost parts of the disk are always at low temperatures. Eventually, temperature even in the inner disk becomes too low to sustain viscosity. The disk then becomes passive, mass inflow and disk torques terminate. The decreasing luminosity and disk torque together lead to the observed period clustering (see Ertan et al., 2009; Alpar et al., 2011, for details).

For PSR J1734−3333, we investigate the evolution mainly in the initial radio pulsar phase. We address the peculiar braking index of PSR J1734−3333, thereby exploring the effect of a possible fallback disk on the evolution of isolated radio pulsars across the P - $\dot{P}$diagram. The recent measurement of the second derivative of the period, $\ddot{P} = 5.3 \times 10^{-24}$ s s^{-2} (Espinoza et al., 2011), provides an opportunity to test FDM evolutionary scenarios more stringently than before, checking for the first time for simultaneous agreement of $\ddot{P}$with P, $\dot{P}$, and X-ray luminosity, L_{X}. The X-ray luminosity of the source is $7.3 \times 10^{31} - 6.6 \times 10^{32}$ erg s^{-1}, taking into account the 25% error margins for the distance estimate (Olausen et al., 2013). It is interesting that the $\ddot{P}$ of PSR J1734−3333 is positive. This means that the

pulsar is evolving towards the upper right corner, the AXP/SGR region, of the P - $\dot{P}$ diagram. For an isolated neutron star evolving by magnetic-dipole radiation in vacuum, this would require a dipole field growing in time. Note that the toroidal and dipole fields of AXPs/SGRs, starting from the early phase of evolution, should *decrease* rather rapidly with time in the magnetar model (see, e.g., Turolla et al., 2011).

The model we employ for PSR J1734−3333 is the same as the one we used to investigate the long term evolution of AXPs/SGRs in our earlier work. The details of the model are described in Ertan et al. (2009) and Alpar et al. (2011). We start with an initially extended disk with an inner radius equal to the Alfvén radius

$$r_A = (GM)^{-1/7}\ \mu^{4/7}\ \dot{M}_{in}^{-2/7}, \tag{5.1}$$

where $\dot{M}_{\rm in}$ is the rate of mass flow arriving at the inner disk, G is the gravitational constant, M and μ are the mass and the magnetic-dipole moment of the neutron star. When the inner disk radius $r_{\rm in}$, calculated by Equation 5.1, exceeds the light cylinder radius $r_{\rm LC}$, we set $r_{\rm in} = r_{\rm LC}$ (Alpar et al., 2011). This assumes that the inner disk remains linked on the closed field lines when it cannot enter the light cylinder. In this phase, accretion is not possible, and pulsed radio emission is allowed. In the phase of spin-down with accretion, when the inner disk is inside the light cylinder and greater than the co-rotation radius ($\rm r_{co} < r_{in} < r_{LC}$) , a fraction of the matter could be propelled from the system while the remaining fraction accretes onto the neutron star.

In the accretion phase, we calculate the disk torque acting on the neutron star using

$$N = \frac{1}{2}\ \dot{M}_{in}\ (GMr_{in})^{1/2}\ (1-\omega_*^2) = I\ \dot{\Omega}_* \tag{5.2}$$

(Ertan & Erkut, 2008), where I is the moment of inertia of the neutron star. The fastness parameter is defined as $\omega_* = \Omega_*/\Omega_{\rm K}(r_{\rm in})$, where $\Omega_{\rm K}(r_{\rm in})$ is the angular frequency of the disk at $r_{\rm in} = r_{\rm A}$ and Ω_* is the angular frequency of the neutron star. Using Equations 5.1 and 5.2, it is found that $\dot{P} \propto {\rm B}^2$, independent of $\dot{M}$ and P when the system is not close to rotational equilibrium. This indicates that $\dot{P}$ is constant and $\ddot{P} = 0$ in this phase. When a high-luminosity AXP/SGR is approaching

(or receding from) rotational equilibrium $\ddot{P}$ is negative (positive). In the early radio phase, the magnetic dipole radiation torque could dominate the disk torque for fast born pulsars ($P_0 \lesssim 50$ ms) for $B_0 \sim 10^{12}$ G. We calculate the total torque including also the magnetic dipole torque $N_{dip} = -2\mu^2{\Omega_*}^3/3c^3$.

In our model calculations, we find that over the spin history of PSR J1734−3333, the dipole radiation torque remains 2−3 orders of magnitude weaker than the disk torque for an initial period $P_0 \sim 300$ ms. For a given field strength, the ratio of the torques depends on the chosen disk torque model and the initial period P_0. For instance, our results agree with the results of Yan et al. (2012), who found that for slow-born pulsars (with $\mathrm{P}_0 \sim 300$ ms) the disk torque dominates for the first $\sim 10^5$ years. In their model, for fast-born pulsars ($\mathrm{P}_0 \sim 5$ ms), the dipole torque is the dominant mechanism for the first $\sim 10^5$ years. The disk torque we employ in our model is more efficient than that used in Yan et al. (2012), and depending on the disk mass, it could start to dominate the dipole torque in an earlier phase of the evolution for fast-born pulsars (which probably represent a small set among newborn neutron stars, lying in the tail of a Gaussian distribution with mean 300 ms and standard deviation 150 ms, according to the simulations of Faucher-Giguère & Kaspi 2006).

The mass flow rate at the inner disk is calculated at each evolutionary step by solving the diffusion equation with an initially thin disk surface density profile (e.g., Ertan et al., 2009). Initially, for numerical reasons, we set the outer disk radius at $r_{\rm out}= 5 \times 10^{14}$ cm. After the first time step, $r_{\rm out}$ has a dynamical evolution such that the temperature at $r_{\rm out}$ remains equal to $T_{\rm p}$, and beyond this radius the disk is assumed to be in a viscously inactive phase. Because of decreasing irradiation flux, temperatures and $r_{\rm out}$ also decrease gradually with time. The initial disk mass is found by integrating the initial surface density profile. Since the position of the initial outer disk radius is not well known, our $\mathrm{M_d}$ values may not reflect the actual full disk mass. In this phase, we substitute $r_{\rm in} = r_{\rm LC}$ to calculate the disk torque (Equation 5.2). When the dipole torque is negligible, we find $\dot{P} \propto \dot{M}_{\rm in}\mathrm{P}^{7/2}$ in this phase. We perform numerical calculations to follow the evolution of $\dot{M}_{\rm in}$ together with corresponding P, $\dot{P}$, and $\ddot{P}$ at each time step (Ertan et al., 2009; Alpar et al., 2011). We repeat the calculations until we identify the initial conditions that can

produce the observed P, $\dot{P}$, $\ddot{P}$ and also, in the present case, $L_{\rm X}$ of PSR J1734−3333 simultaneously, at an age when the disk does not penetrate the light cylinder, allowing for radio pulsar activity.

In the radio pulsar phase, for a neutron star with the properties of PSR J1734−3333 the source of the X-ray luminosity is very likely to be the cooling luminosity. For the fast born pulsars, the dipole radiation luminosity could remain well above the cooling luminosity until the periods increase to a few 100 ms. We include the cooling and dipole luminosities in addition to dissipation due to magnetic and disk torques (Alpar, 2007) in the calculation of the total luminosity in the radio phase. In the long-term evolution of AXPs/SGRs and XDINs, when the sources reach long periods of a few seconds, the presence of cooling luminosity extends the life time of the disk by providing irradiation even in the absence of accretion luminosity. During the initial radio phase, it does not have a significant effect on the evolution, but, through the effect of irradiation on the disk evolution and disk torques, it affects the time at which the model source acquires the observed rotational properties (P, $\dot{P}$, $\ddot{P}$) simultaneously. In our model, we employ the intrinsic cooling luminosity evolution calculated by Page et al. (2006) with the assumption of an isothermal neutron star with radius 12 km and mass 1.4 $M_{\odot}$. The results are not sensitive to the choice among standard cooling scenarios.

5.3 Results and Discussion

The model curves that can account for the properties of PSR J1734−3333 are seen in Figures 5.1 - 5.4. Performing many simulations tracing the initial conditions, we obtain reasonable results for the range of disk masses $\mathrm{M_d} = 9.0 \times 10^{-8} - 1.5 \times 10^{-6}$ $M_{\odot}$ and for dipole fields with $B_0 = 9 \times 10^{11} - 1 \times 10^{13}$ G. The model is in very good agreement with P, $\dot{P}$, $\ddot{P}$, and $L_{\rm X}$ of the source with $B_0 \simeq 2 \times 10^{12}$ G (solid curve in Figure 5.1). For the solid curve in Figure 5.1, the disk mass $\mathrm{M_d} = 3 \times 10^{-7}$ $M_{\odot}$ and the initial period $P_0 = 300$ ms. In Figure 5.1, we also present illustrative model curves (dashed and dot-dashed) that cannot represent the evolution of PSR J1734−3333. For the viable model in Figure 5.1, and all three viable models shown in Figure 5.2, the source is powered by intrinsic cooling when the observed properties of PSR J1734−3333 are attained. For this radio pulsar, considering all reasonable

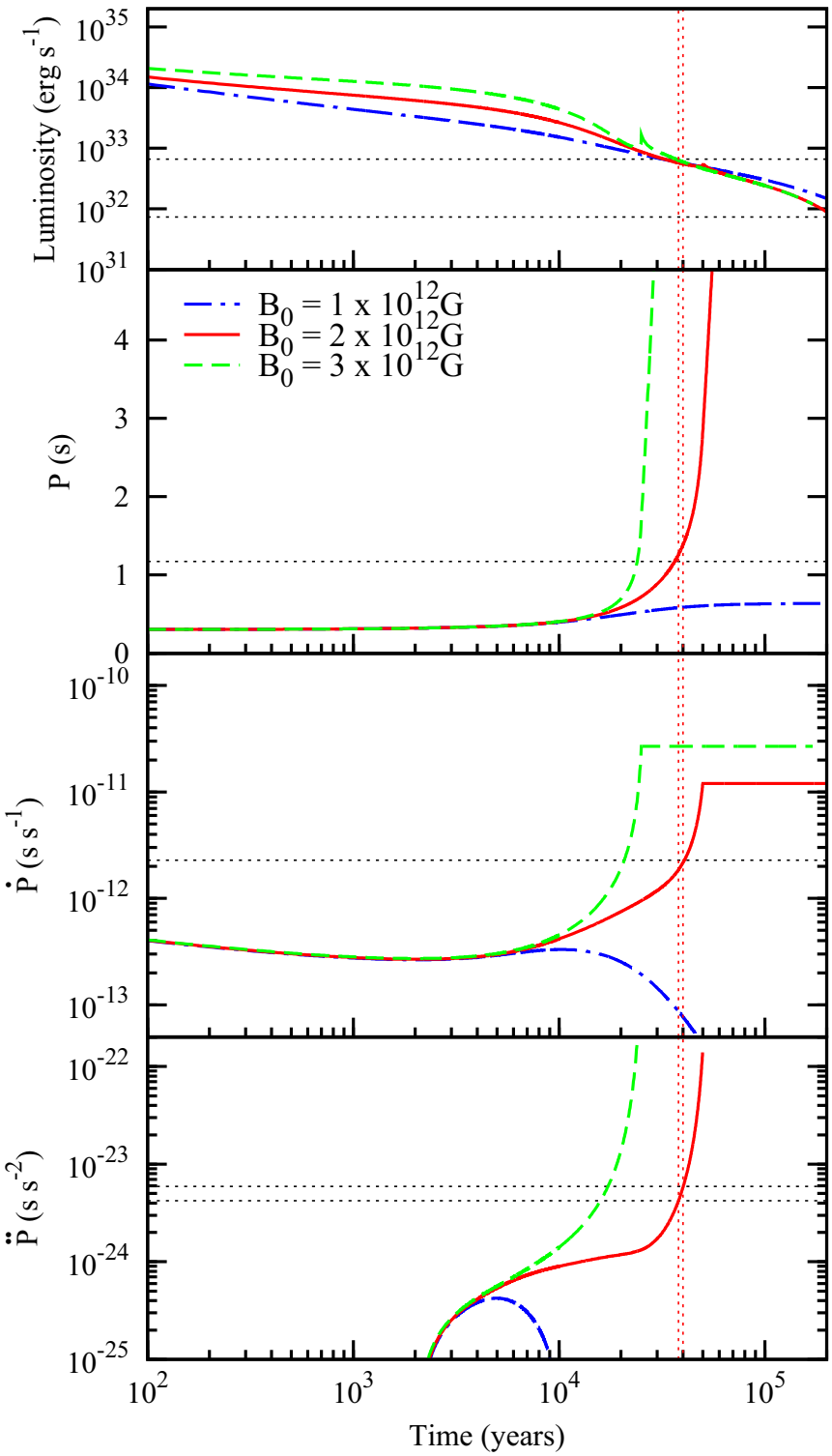

Figure 5.1: Evolution of the luminosity, period, first and second period derivatives of the model sources. Horizontal lines show the properties of PSR J1734−3333, with the observational uncertainties in L_X and $\ddot{P}$. The vertical lines are to show the time period over which the solid (red) model curve traces the uncertainty range of $\ddot{P}$. Values of B_0 are given in the second panel. For these calculations, we have taken $M_d = 3 \times 10^{-7}\ M_\odot$ and $P_0 = 300$ ms. In the accretion phase, sources enter the constant $\dot{P}$ phase and $\ddot{P}$ becomes 0 (see text for details).

model curves, the simultaneous agreement with all these model parameters leads to a model estimate of the present age $\sim 3\times10^4 - 2\times10^5$ years. At an epoch later than the present age of PSR J1734−3333, the disk eventually penetrates the light cylinder. Accretion then starts, and the star enters a constant $\dot{P}$ phase. This is also observed as a small abrupt rise in the luminosity curve. There is no substantial increase in the luminosity when accretion starts, because the mass-flow rate has already decreased to low levels by the time the inner disk penetrates the light cylinder. Reasonable model curves indicate that accretion will start at a future time of order $\sim 10^4$ yr from the present. For other model source histories, accretion can start at earlier times and the accretion luminosity can be orders of magnitude greater than the cooling luminosity. Evolutionary curves for such models do not simultaneously produce all the observed properties of PSR J1734−3333.

Figure 5.1 shows that $\ddot{P}$ reaches values of order $\sim 2\times10^{-22}$ s s^{-2} at the end of the radio pulsar epoch. Before the accretion phase, from t $\sim 10^3$ years to the present age, the braking index for model sources varies from ~ 5 to ~ -1. In the accretion phase, $\ddot{P} = 0$, $\dot{P}$ becomes constant and the braking index remains ~ 2 when the source is not very close to rotational equilibrium.

The mass accretion from the disk starts at a time that depends on the initial period P_0, as well as on B_0 and $\mathrm{M_d}$ (Ertan et al., 2009). A large range of P_0 values are allowed for producing the source properties. In Figure 5.2, for a given dipole field ($B_0 = 2\times10^{12}$ G), we present three illustrative model curves with initial periods of 50, 100 and 300 ms. To obtain acceptable models, smaller P_0 values require greater $\mathrm{M_d}$. All model curves given in Figure 5.2 produce the X-ray luminosity and the rotational properties of PSR J1734−3333 at different epochs. In the early radio-pulsar phase, the source of the luminosity is either the intrinsic cooling or magnetic dipole radiation of the neutron star, depending on B_0 and P_0. Reasonable model curves indicate that current luminosity of PSR J1734−3333 is produced by the intrinsic cooling luminosity while the source is slowing down by the disk torques. We find that the rates of dissipation inside the star due to dipole and disk torques (Alpar, 2007) do not contribute significantly to the total luminosity in the radio-pulsar phase of this source at present. A part of the dipole luminosity is emitted in the X-ray band. For model sources that have low P_0 and/or high B_0 values, the

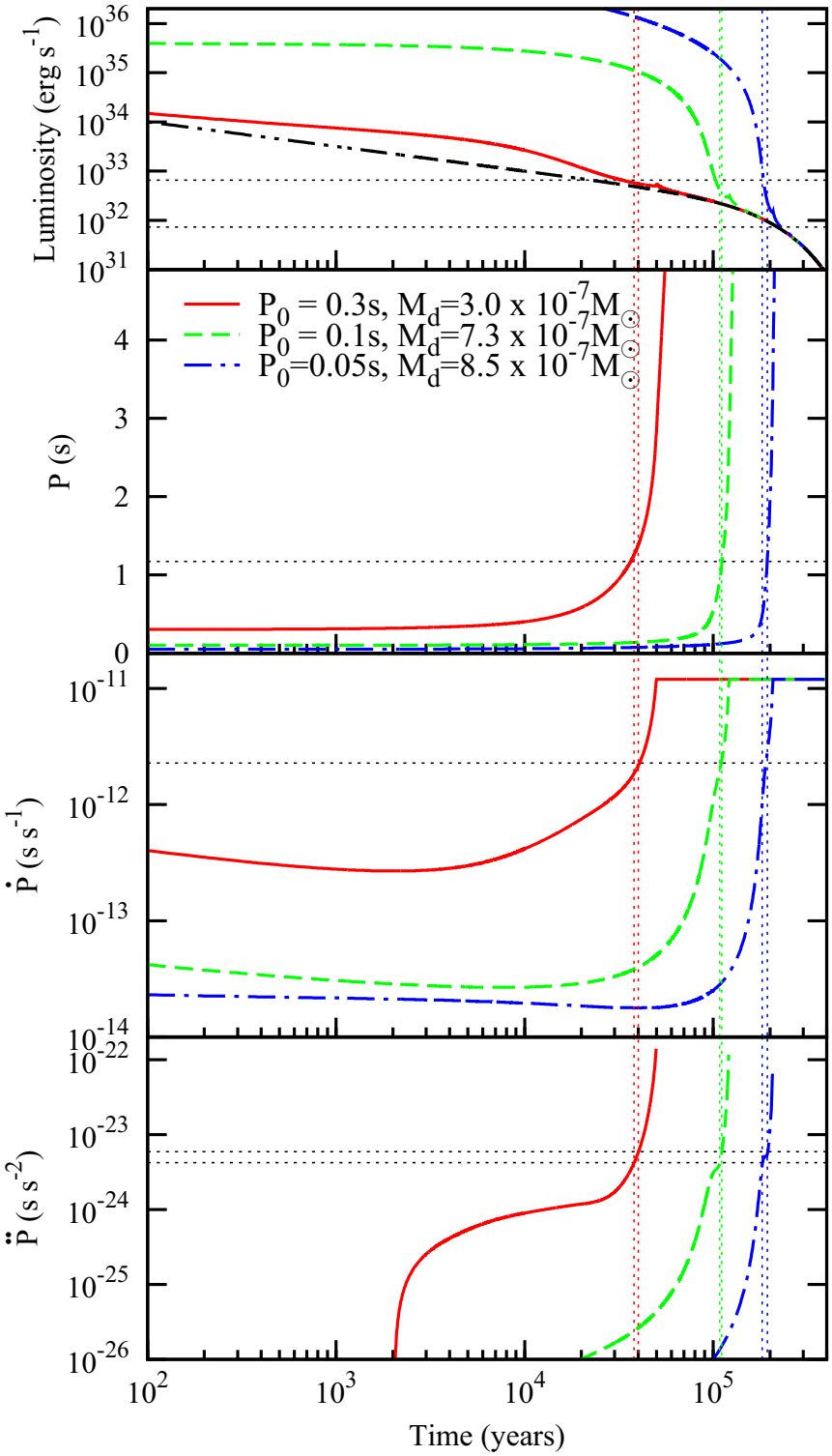

Figure 5.2: Evolution of the luminosity, period, first and second period derivatives of model sources. Horizontal dotted lines represent the properties of PSR J1734−3333 with the range of uncertainties in L_X and $\ddot{P}$. These illustrative model curves are obtained for $B_0 = 2 \times 10^{12}$ G. The values of initial period and disk mass are given in the second panel. The cooling luminosity is shown with the dot-dot-dashed (black) curve. It is seen that the source properties could be well reproduced with different initial periods. Between the vertical lines given with the same color, the model sources trace the uncertainty range of $\ddot{P}$ (see text for details).

dipole radiation could be the dominant luminosity in the early phases of evolution. For instance, for initially fast-rotating model sources with $B_0 = 2 \times 10^{12}$ G, the luminosity of magnetic dipole radiation dominates the intrinsic cooling luminosity until the period increases to beyond $\sim$ 200 ms (see Figure 5.2). For $B_0 \gtrsim 10^{13}$ G, the dipole luminosity remains above the upper limit of the observed luminosity when the rotational properties of PSR J1734−3333 are acquired. We note that the blackbody nature of the X-ray spectrum (Olausen et al., 2013) also indicates that the source of the observed luminosity is likely to be the intrinsic cooling rather than magnetic dipole radiation. For the model sources with $B_0 \lesssim 9 \times 10^{11}$ G, accretion starts before the current rotational properties of PSR J1734−3333 are reached. To sum up, the luminosity, P, $\dot{P}$ and $\ddot{P}$ values of PSR J1734−3333 can be acquired by the model sources only for B_0 values in $\sim 9 \times 10^{11} - 1 \times 10^{13}$ G range. The two model curves with the minimum and maximum allowed values of B_0 and $\mathrm{M_d}$ are given in Figure 5.4.

The important parameters that affect the long-term evolution of the model sources are the initial period P_0, the minimum temperature of the active disk T_p, which is degenerate with the irradiation efficiency C, (but C is restricted by optical and IR observations of AXPs; Ertan & Çalışkan, 2006), the disk mass $\mathrm{M_d}$, and the dipole magnetic field strength B_0 on the surface of the star. In our earlier work and in the present paper, we take $T_\mathrm{p} \simeq 100 - 200$ K. Since T_p together with C determine the end of the active disk phase, they have almost no effect on the evolution during the initial radio phase. The initial period can affect the time of onset of accretion, but similar long term evolutionary curves could be found for a large range of initial periods. To follow the evolution of model sources in the initial radio phase, there remain only two important parameters: $\mathrm{M_d}$ and B_0. We repeat the simulations tracing $\mathrm{M_d}$ and B_0 to find the entire allowed ranges of these parameters that can produce the properties of PSR J1734−3333 simultaneously.

Our results indicate that PSR J1734−3333 could be at an age in the range $\sim 3 \times 10^4 - 2 \times 10^5$ yr depending on the actual initial conditions of the star. For $B_0 = 2 \times 10^{12}$ G and $P_0 = 300$ ms, $\mathrm{M_d} = 3 \times 10^{-7}\ M_\odot$ gives the observed properties of PSR J1734−3333 simultaneously, while for $P_0 = 100$ ms the disk mass is $\mathrm{M_d}$= $7.3 \times 10^{-7}\ M_\odot$ and for $P_0 = 50$ ms $\mathrm{M_d} = 8.5 \times 10^{-7}\ M_\odot$. For $B_0 = 2 \times 10^{12}$ G

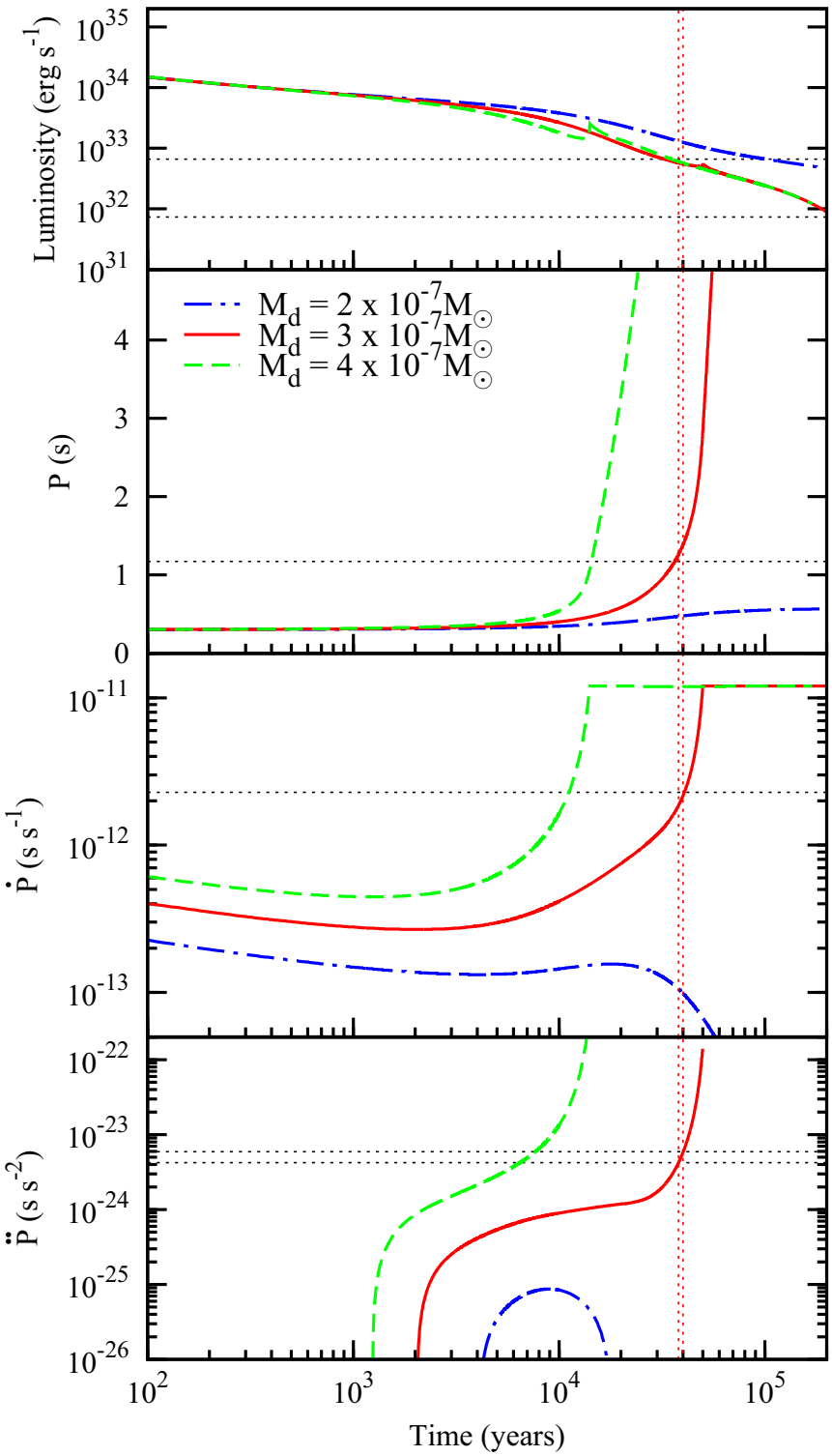

Figure 5.3: Evolution of the luminosity, period, first and second period derivatives, for models that do not work for PSR J1734–3333. Horizontal dotted lines show the properties of PSR J1734−3333, with the uncertainties in L_X and $\ddot{P}$. These model curves are obtained with $B_0 = 2 \times 10^{12}$ G and $P_0 = 300$ ms. The solid lines are the same as the solid lines in Figures 5.1 and 5.2, for the model that works. We also present two illustrative model curves for smaller and greater M_d that cannot represent the evolution of PSR J1734−3333 (see text for details).

and $P_0 = 300$ ms, illustrative model curves obtained with different disk masses are given in Figure 5.3. The solid (red) curve is the same as the tracks given in Figures 5.1 and 5.2 with the same B_0 and P_0. It is seen that the model with the greatest $\mathrm{M_d}$ starts the accretion phase earlier, while the source with the smallest $\mathrm{M_d}$ never enters the accretion phase. These models, represented by dashed and dot-dashed curves in Figure 5.3, cannot produce all present properties of PSR J1734−3333 simultaneously.

In later phases of evolution, radio pulsars similar to PSR J1734−3333 are likely to be observed either as transient AXPs in the accretion phase, if they are detected by means of soft gamma-ray bursts, or as XDINs after the termination of the accretion phase, while the disk torques are still effective. We also present the evolution of these model sources on the P - $\dot{P}$ diagram in Figure 5.5. A paper on the evolution of XDINs is in preparation (Ertan et al., 2013).

Our long-term evolution model of neutron stars with fallback disks differs from earlier fallback disk models described in Chatterjee et al. (2000) and Menou et al. (2001b), as well as Alpar (2001) and Alpar et al. (2001) in two crucial ingredients of the models: (1) the minimum temperature (T_p) at which the viscous activity stops and the disk becomes passive, and (2) the torque expression employed in the models, which determine the $\dot{M}$ dependence and spin evolution of the neutron star.

According to the fallback disk model proposed by Menou et al. (2001b), the disk becomes inactive at accretion rates at which the disk cools through the thermal viscous instability. To explain the braking indices of young neutron stars with high X-ray luminosities, Menou et al. (2001a) employed the same model. In this model, the minimum mass-flow rate for the disk to remain active and interact with the magnetic field is a few times 10^{14} g s^{-1}. The properties of the transient AXPs, discovered later with inferred quiescent accretion rates much lower than the minimum critical limit of Menou et al. (2001b), seem hard to be explained together with persistent sources in a single coherent picture. Another difficulty arises when applying this model to PSR J1734−3333 and to other pulsars with low luminosities. At present, the inner disk of PSR J1734−3333 cannot enter the light cylinder, and therefore the pulsed radio emission is allowed, provided that the mass-flow rate of the disk is less than about 10^{13} g s^{-1} (even for a relatively low dipole field strength

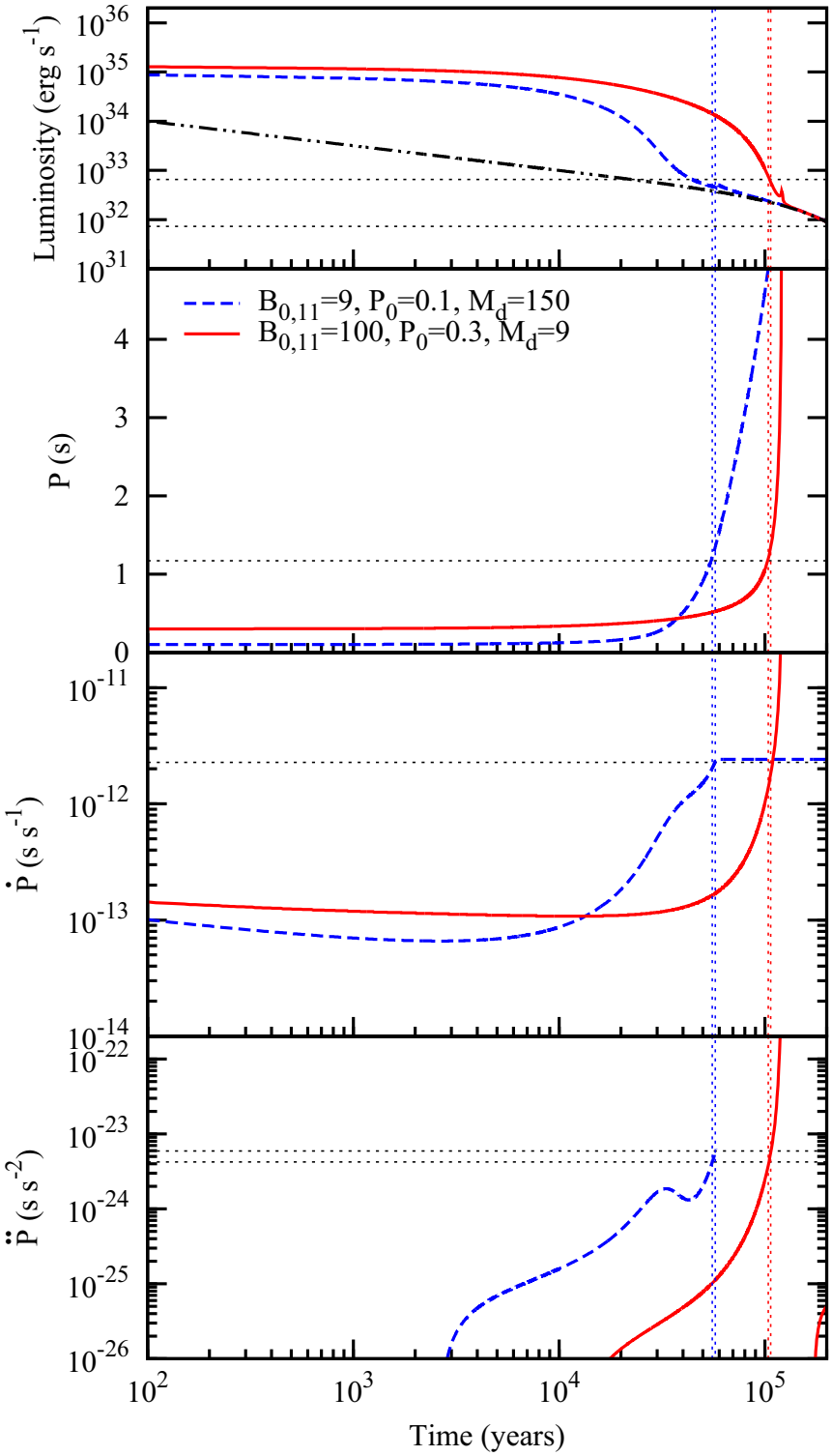

Figure 5.4: Evolution of the luminosity, period, first and second period derivatives, for model sources with the lowest and highest allowed B_0 values. The magnetic field is given in units of 10^{11} G, the initial period is in seconds and the disk mass is given in units of 10^{-8} $M_\odot$. The cooling luminosity is shown with the dot-dot-dashed (black) curve.

of 10^{12} G). With this mass-flow rate, the disk is not active in this model. To put it in other words, the model used in Menou et al. (2001b) cannot be applied to PSR J1734−3333. A similar problem emerges in the fallback disk model used in Chatterjee et al. (2000), since the disk is assumed to make a transition to ADAF regime at mass inflow rates even higher than the minimum critical rates given in Menou et al. (2001b). In Chatterjee et al. (2000) the disk is assumed to have no contribution to the torque in the radio phase, that is, this model cannot be applied to PSR J1734−3333 either. In our model we do not encounter this problem: the disk becomes passive at low temperatures $T_{\rm p} \sim 100 - 200$ K, in accordance with theoretical work by Inutsuka & Sano (2005), starting from the outermost disk as described in detail in Ertan et al. (2009) and Alpar et al. (2011).

The evolutionary model curves of the rotational properties of neutron stars and their dependence on mass flow rate of the disk are sensitive to the disk torque models employed in the calculations. The motivation leading us to the particular torque model employed in earlier work (Ertan & Erkut, 2008; Ertan et al., 2009; Alpar et al., 2011) and in the present work was the peculiarity of the contemporaneous X-ray luminosity and period evolution of the transient AXP XTE J1810-197 in the X-ray enhancement/outburst phase. Nevertheless, the observations of XTE J1810-197 (Gotthelf & Halpern, 2007) show that in the range of accretion rates from a few 10^{13} to 10^{15} g s^{-1}, the torque remains almost independent of mass-inflow rate. We use the same torque model that is in good agreement with this observation, in all subsequent work on spin evolution of neutron stars with fallback disks. This behaviour, observed in XTE J1810-197, cannot be accounted for by earlier disk torque models.

5.4 Conclusions

We have shown through detailed analysis that the observed period, the first and second period derivatives, and the X-ray luminosity of PSR J1734−3333 can be simultaneously reached by a neutron star evolving with a fallback disk. The model is compatible with the pulsed radio emission of the source, since the present source properties are reached at a time when the accretion of matter from the disk is not allowed yet.

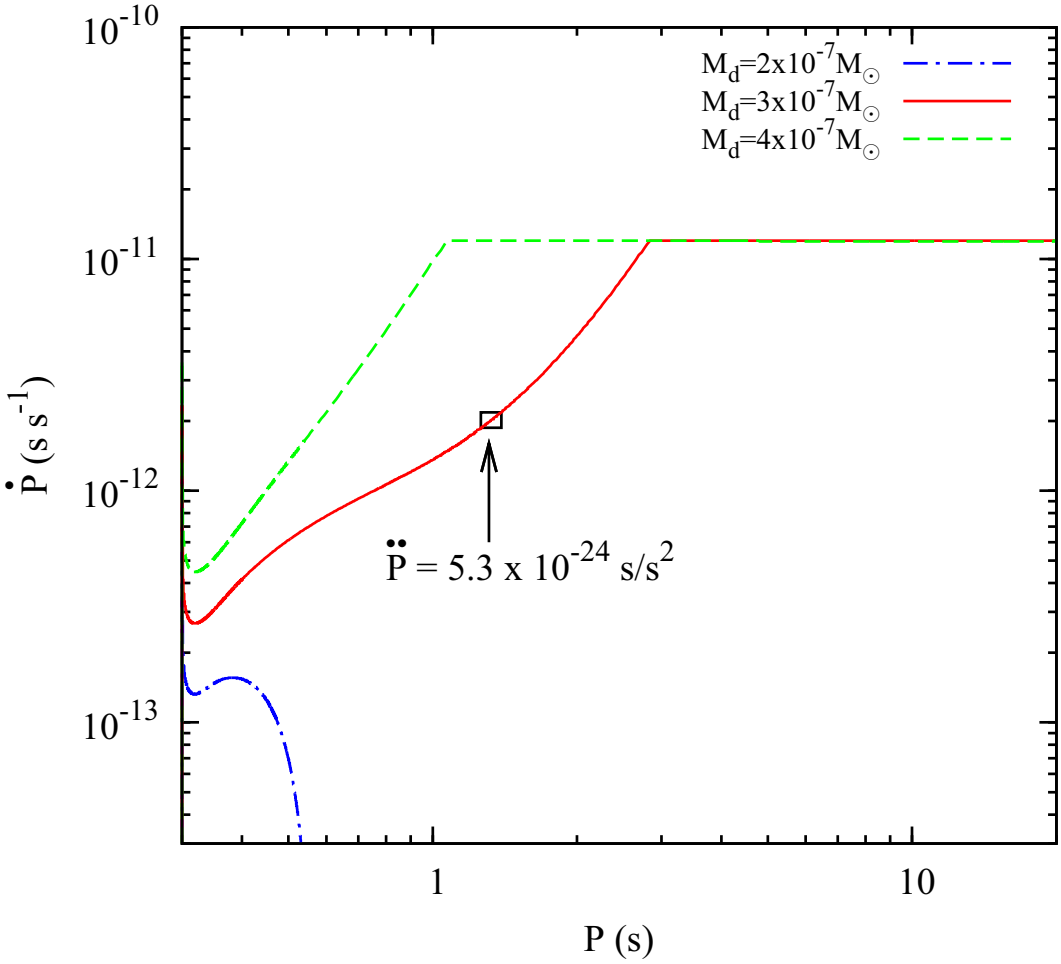

Figure 5.5: The evolution of the three model sources of Figure 5.3 on the P - $\dot{P}$ diagram. The values of initial disk mass M_d are shown in the Figure. All sources start with P_0 = 300 ms. The model source with the lowest M_d (blue) never enters the accretion regime and its period converges to $\sim$ 0.5 s. The model source with the highest M_d (green) enters the accretion regime early on and after 10^5 years it has P > 30 s. The model represented by the solid curve can reproduce the properties of PSR J1734−3333 (see Figure 5.3). The rectangle shows the current position of the source on the P - $\dot{P}$ diagram. The size of the rectangle represents the uncertainty in the measured $\ddot{P}$ value.

The observed properties of PSR J1734−3333 can be obtained at an age of $\sim 3 \times 10^4 - 2 \times 10^5$ years, with a range of initial periods and with disk masses ($9 \times 10^{-8} M_\odot < \mathrm{M_d} < 1.5 \times 10^{-6} M_\odot$), relatively low compared to those estimated for AXPs/SGRs. Dipole fields with strength in the range $9 \times 10^{11} - 1 \times 10^{13}$ G, together with appropriate disk masses and initial periods, give reasonable model curves.

PSR J1734−3333 has not been observed in IR to the best of our knowledge. A search for IR emission from the fallback disk in PSR J1734−3333 will be of great interest. The infrared emission from the disk depends on several factors, like inclination angle of the disk, irradiation efficiency, outer and inner disk radii. As a continuation of this research topic, we will calculate the expected IR emission from PSR J1734−3333 and sources similar to it in detail, together with a discussion of the assumed parameters.

We expect that PSR J1734−3333 will evolve into the accretion phase within another $\sim 10^4$ years (see Figures 5.1 and 5.2). By the onset of the accretion phase, the mass-flow rate of the inner disk will have decreased to a very low level such that accretion does not significantly contribute to the total X-ray luminosity. Radio pulsars following evolutionary curves similar to that of PSR J1734−3333 could be detected in the accretion phase if they show soft gamma-ray bursts like AXPs/SGRs - these would be identified as transient AXPs. Such sources are not likely to emit radio waves, having spun down to long periods by this late stage of evolution. Only if they are sufficiently close to Earth we could detect and identify them as XDINs. Some of these sources could evolve to periods longer than the AXP/SGR periods (Ertan et al., 2009). It is hard to detect them due to low X-ray luminosities. In short, sources like PSR J1734−3333 may evolve to become transient AXPs or XDINS. Our work on the evolution of XDINS and their connection with AXP/SGRs is in progress.

Chapter 6

SUMMARY AND OUTLOOK

We have investigated some basic and connected properties of young neutron star systems under the topics: (1) Optical and infrared properties of AXPs and SGRs in persistent states, (2) Enhancement light curves of transient and persistent AXP and SGRs, (3) Long term evolution of the "low-field" magnetar SGR 0418+5729, (4) Long term evolution and anomalous braking index of the radio pulsar PSR J1734-3333. Long term luminosity and rotational evolution of these systems, leading to the observed properties at present, have been explained by a self consistent fallback disk model.

In this model, a young neutron star with a conventional dipole field ($B_0 < 10^{13}$ G) evolves with a fallback disk. The disk, heated by X-ray irradiation, evolves with turbulent viscosities. The heat injected to the disk by viscous dissipation and irradiation is emitted in the form of a multi-color blackbody (disk blackbody) radiation, depending on the effective temperature profile of the disk. In the model, this emission from the disk surface is the source of the broad band spectrum from optical to mid-infrared wavelengths.

The dynamical outer radius ($r_{\rm out}$) of the active disk extends to a radius at which the effective temperature decreases to $\sim 100 - 200$ K. With gradually decreasing X-ray irradiation flux and disk temperatures, $r_{\rm out}$ also decreases in time. There is a continuous mass flow from the outer active disk region towards the inner disk. The interaction between the inner disk and the magnetic dipole field of the star remains as the dominant torque mechanism over the observable history of the source, even in the phases when accretion is not possible.

In the model, the accretion of matter onto the star is allowed if the inner disk can penetrate the light cylinder. In the propeller regime, part of the inner disk

matter could be expelled from the system while the remaining part accretes onto the star. For simplicity, we take the accretion rate to be equal to the mass-flow rate. In the accretion phase, the source of the X-ray luminosity is the mass-flow onto the surface of the neutron star. When the inner disk cannot penetrate the light cylinder, intrinsic cooling of the neutron star produces the X-ray luminosity depending on the age of the source.

For certain ranges of initial parameters, model sources cannot enter the accretion phase in the very early stage of evolution, but start to accrete matter at later times ($\sim 10^3 - 10^4$ years). We call this initial phase of evolution the "radio phase", since pulsed radio emission can be produced while accretion does not take place. It is also possible that some model sources can never accrete matter, depending on the initial conditions, and remain as radio pulsars until they cross the pulsar death line.

In our model, accretion is not allowed when the calculated Alfvén radius is found to be greater than the light cylinder radius ($r_{\rm LC}$). In these phases, we take $r_{\rm in} = r_{\rm LC}$. After the long lasting accretion periods, whether the source can act as a radio pulsar depends on the strength of the dipole field and the current period of the star. It is possible that some sources could find themselves below the pulsar death line, while others may have still sufficiently low periods to emit radio pulses after the accretion stops.

In the radio phases and after the accretion epochs, the disk torque is less efficient than in the accretion phase. Nevertheless, in most cases, it continues to prevail as the dominant torque mechanism over the observable life of the source.

First, we have applied the outlined model to five persistent AXPs (Chapter 2) and showed that fallback disks around these sources can produce the observed luminosities and upper limits in the optical and infrared bands, while the disk is illuminated by the X-rays produced by the accretion of disk matter onto the neutron star. The disk is heated by X-ray illumination and viscous dissipation. The inner parts of the disk, with higher effective temperatures, emit in the UV and optical bands, while the outer parts emit in the infrared bands. We have also found that the required X-ray irradiation efficiency of these sources remain in the same range as that of low mass X-ray binaries.

Secondly, we have investigated the X-ray enhancement light curves of AXP/SGRs

in detail. The enhancement light curves of four transient AXP/SGRs can be produced by the relaxation of an accreting fallback disk that has been pushed back by a soft gamma-ray burst. The X-ray enhancement light curves of transient sources show a characteristic difference in comparison with those of persistent sources. This difference can be explained by a thermal disk instability that is triggered at the same temperature in all systems. Nevertheless, the difference in the quiescent surface density profiles of persistent and transient sources, leads to different light-curve morphologies. To sum up, the X-ray enhancement light curves of transient and persistent AXP/SGRs could be explained by a single active disk model that is consistent with our long term evolution model.

Since our results are insensitive to the exact position of the inner disk radius, these model fits cannot constrain the field strength. We could obtain the model curves for all the sources with the same set of model parameters (cold and hot state viscosity parameters, irradiation efficiency and critical temperature). Other disk parameters could differ from source to source. For example, the inner radius of the disk and the current disk mass-flow rate depends on the magnetic dipole field of a given source. The initial disk masses do not need to be the same, since different amounts of disk matter could be left over from the supernova explosion and the sources could be at different ages. The disk surface density profiles after the soft gamma-ray bursts depend on the burst energy imparted on the disk and on the pre-burst surface density profiles. On the other hand, basic parameters like the critical temperature causing the viscous instability and the viscosities of the hot and cold regions of the disk are expected to be similar in all AXP/SGRs, since the fallback disks of these sources are likely to have similar chemical compositions.

General luminosity and rotational properties of AXP/SGRs can be produced by the fallback disk model (Ertan et al., 2009). The upper limit on the period derivative of the newly discovered SGR 0418+5729 showed that the source has a dipole field weaker than 7.5 $\times 10^{12}$ G on the surface of the star. The evolution of this source can be explained with extreme initial toroidal and dipole field magnitudes in the frame of the magnetar model. We have shown that SGR 0418+5729 is an ordinary source in the frame of the fallback disk model (Chapter 4). Like other AXPs, its properties can be acquired by a neutron star evolving with a conventional dipole

field (B $\sim 1-2\times10^{12}$ G) and a fallback disk. Our results indicate that the source has completed its accretion phase and slows down by the disk torques at present.

Next, we worked on the radio pulsar, PSR J1734−3333, which seems completely different from known AXP/SGRs. It is interesting that this radio pulsar is evolving toward the AXP/SGR region in the P-$\dot{P}$ diagram, hinting at a possible evolutionary link between some of the radio pulsars and AXP/SGRs. Its very low braking index does not agree with the conventional magnetar model. We have shown that its rotational properties and X-ray luminosity can be achieved through evolution with a fallback disk (Chapter 5). Our results suggest that this source has a conventional magnetic field strength (B $\sim 1-5\times10^{12}$ G), and that it is evolving in the early radio phase. Accretion has not started yet for this source. From the model results, we estimate that the age of the source is $\sim$ a few $\times10^4$ years and that it could enter the accretion phase on a timescale of $\sim 10^4$ years.

The magnetar model requires extremely strong initial toroidal fields ($\gtrsim 4\times10^{16}$ G) and a rapid decay of the dipole component of the magnetic field to explain the observed properties of SGR 0418+5729 (Turolla et al., 2011). The positive period second derivative of PSR J1734−3333 puts the source in the class of AXP progenitors. In the magnetar model, the properties of this source require a dipole field growth, which is in sharp contrast with the scenario proposed for the rotational and field history of SGR 0418+5729. In the fallback disk model, there is no need for extreme initial conditions; the properties of these pulsars can be reproduced with dipole magnetic field strengths in the range $\sim 10^{11}-10^{12}$ G.

During the X-ray enhancement and subsequent decay, the critical temperature at which viscous instability occurs ($T_{\rm crit}$) and the irradiation parameter (C) are degenerate. Nevertheless, our earlier results suggest that C lies in the range $\sim 10^{-4}-7\times10^{-4}$ (see Chapter 2). If C is increased from the minimum to the maximum value of this range, a similar evolution is obtained by increasing $T_{\rm crit}$ by only a factor of ~ 1.6 (see Chapter 3 for a detailed discussion). In the long term evolution of neutron stars with fallback disks, the irradiation parameter is degenerate with the passive disk temperature $T_{\rm p}$. This degeneracy is also removed by the constraint on C. With two extreme values of C, similar evolutionary curves can be obtained by changing $T_{\rm p}$ by a factor less than 2. This means that our results constrain $T_{\rm p}$ to

low temperatures ($\lesssim$ 300 K). Using the same irradiation parameter in both the long term evolution and the X-ray enhancement studies, we find that $T_{\rm p} \sim 100 - 200$ K, in agreement with the theoretical work of Inutsuka & Sano (2005), which indicates that the disk should be active at T $\simeq$ 300 K.

Our model light curves for the X-ray enhancements of AXPs do not depend on the exact position of the inner disk. Therefore, the model fits to the X-ray enhancements of AXPs do not constrain the dipole magnetic field. The dipole magnetic field strength is constrained by the results of the long term evolution models (Ertan et al., 2009, and Chapters 4 and 5) and by the model fits to optical/infrared data of the AXP 4U 0142+61 (Ertan et al., 2007).

The difference of our fallback disk model from the earlier models (Chatterjee et al., 2000; Menou et al., 2001b; Alpar, 2001) lies in the addition of a minimum temperature ($T_{\rm p}$) below which viscous activity stops, and the expression for the disk torque acting on the star. The model proposed by Menou et al. (2001b) assumes that the disk becomes inactive at high accretion rates and cannot explain the low luminosity transient AXP/SGRs. Because of the same reason, this model cannot account for the properties of pulsar PSR J1734−3333 (see Chapter 4). In the model used by Chatterjee et al. (2000), the disk torques do not operate in the radio phase and the model cannot be applied to PSR J1734−3333. Ekşi et al. (2005) argued that in most cases the disk formed around a neutron star would be quickly destroyed. This does not agree with the results of Ekşi & Alpar (2005), who showed that stable solutions can be found for $r_{\rm A} > r_{\rm LC}$. The disk torque model we employ was proposed by Ertan & Erkut (2008) to explain the period and X-ray luminosity evolution of the transient AXP XTE J1810-197 during its X-ray enhancement phase. This model was later found to be successful in explaining the general properties of AXP/SGRs (Ertan et al., 2009).

The details of the interaction between the inner disk and the magnetosphere, and in particular the conditions starting true propeller phase are not clear yet (Rappaport et al., 2004; D'Angelo & Spruit, 2010). This is also a limitation of fallback disk models.

The results that we obtain in this thesis support the idea proposed by Alpar

(2001): The properties of different young neutron star populations could be explained if the properties of fallback disks are included in the initial parameters of the models in addition to the magnetic moment and the initial period of the neutron star. The two pulsars, PSR J1734−3333 and SGR 0418+5729 represent two different evolutionary stages of young neutron stars with fallback disks: one where accretion has not yet started and the other where accretion has already stopped. Our work on the optical/infrared emission and the X-ray enhancements of AXP/SGRs involves the sources in the intermediate evolutionary stage, when accretion is still going on. This model covers *all* three phases of fallback disk evolution and self-consistently explains the properties of different sources in different evolutionary phases.

New detections of such systems in optical and infrared bands will further constrain the model parameters. Relative fluxes in optical/infrared bands could vary depending on the current position of inner and outer disk radii of the active disk, which are, for a given field strength, determined by the current mass inflow rate and $T_{\rm p}$ respectively. A detailed calculation of the spectrum of fallback disks around young neutron stars for different field strengths and X-ray luminosity regimes will be the subject of our subsequent work.

In continuation of the present work, we will also investigate the possible evolutionary links between AXP/SGRs and other young neutron star systems (XDINs, RRATs, CCOs, young radio pulsars). Through a detailed study of these sources, our aim is to explain the evolutionary and statistical properties of all these young neutron star systems in a single, self-consistent, coherent picture.

Bibliography

Alpar, M. A. 2001, ApJ, 554, 1245

—. 2007, Ap&SS, 308, 133

Alpar, M. A., Ankay, A., & Yazgan, E. 2001, ApJL, 557, L61

Alpar, M. A., Cheng, A. F., Ruderman, M. A., & Shaham, J. 1982, Nature, 300, 728

Alpar, M. A., Ertan, Ü., & Çalışkan, Ş. 2011, ApJL, 732, L4

Aptekar, R. L., Cline, T. L., Frederiks, D. D., et al. 2009, ApJL, 698, L82

Baade, W., & Zwicky, F. 1934, Proceedings of the National Academy of Science, 20, 259

Barthelmy, S. D., Baumgartner, W. H., Beardmore, A. P., et al. 2008, The Astronomer's Telegram, 1676, 1

Becker, W. 2009, in Astrophysics and Space Science Library, Vol. 357, Astrophysics and Space Science Library, ed. W. Becker, 91

Bernardini, F., Israel, G. L., Dall'Osso, S., et al. 2009, A&A, 498, 195

Bibby, J. L., Crowther, P. A., Furness, J. P., & Clark, J. S. 2008, MNRAS, 386, L23

Camilo, F., Reynolds, J., Johnston, S., Halpern, J. P., & Ransom, S. M. 2008, ApJ, 679, 681

Camilo, F., Cognard, I., Ransom, S. M., et al. 2007a, ApJ, 663, 497

Camilo, F., Ransom, S. M., Peñalver, J., et al. 2007b, ApJ, 669, 561

Chatterjee, P., Hernquist, L., & Narayan, R. 2000, ApJ, 534, 373

Cheng, K. S., & Ruderman, M. 1991, ApJ, 373, 187

Chevalier, R. A. 1989, ApJ, 346, 847

Clark, J. S., Negueruela, I., Crowther, P. A., & Goodwin, S. P. 2005, A&A, 434, 949

Corbel, S., Chapuis, C., Dame, T. M., & Durouchoux, P. 1999, ApJL, 526, L29

D'Angelo, C. R., & Spruit, H. C. 2010, MNRAS, 406, 1208

Davies, B., Figer, D. F., Kudritzki, R.-P., et al. 2009, ApJ, 707, 844

de Jong, J. A., van Paradijs, J., & Augusteijn, T. 1996, A&A, 314, 484

Dhillon, V. S., Marsh, T. R., Hulleman, F., et al. 2005, MNRAS, 363, 609

Dhillon, V. S., Marsh, T. R., Littlefair, S. P., et al. 2009, MNRAS, 394, L112

—. 2011, MNRAS, 416, L16

Dib, R., Kaspi, V. M., & Gavriil, F. P. 2007, ApJ, 666, 1152

—. 2008, ApJ, 673, 1044

—. 2009, ApJ, 702, 614

Dib, R., Kaspi, V. M., Scholz, P., & Gavriil, F. P. 2012, ApJ, 748, 3

Dubus, G., Lasota, J.-P., Hameury, J.-M., & Charles, P. 1999, MNRAS, 303, 139

Duncan, R. C., & Thompson, C. 1992, ApJL, 392, L9

Durant, M., & van Kerkwijk, M. H. 2005, ApJ, 627, 376

—. 2006a, ApJ, 650, 1070

—. 2006b, ApJ, 650, 1082

—. 2006c, ApJ, 648, 534

Ekşi, K. Y., & Alpar, M. A. 2003, ApJ, 599, 450

—. 2005, ApJ, 620, 390

Ekşi, K. Y., Hernquist, L., & Narayan, R. 2005, ApJL, 623, L41

Enoto, T., Nakagawa, Y. E., Rea, N., et al. 2009, ApJL, 693, L122

Ertan, Ü., & Alpar, M. A. 2002, A&A, 393, 205

—. 2003, ApJL, 593, L93

Ertan, Ü., Alpar, M. A., & Çalışkan, Ş. 2013, in preparation

Ertan, Ü., & Çalışkan, Ş. 2006, ApJL, 649, L87

Ertan, Ü., & Cheng, K. S. 2004, ApJ, 605, 840

Ertan, Ü., Ekşi, K. Y., Erkut, M. H., & Alpar, M. A. 2009, ApJ, 702, 1309

Ertan, Ü., & Erkut, M. H. 2008, ApJ, 673, 1062

Ertan, U., Erkut, M. H., Ekşi, K. Y., & Alpar, M. A. 2006a, ArXiv Astrophysics e-prints

Ertan, Ü., Erkut, M. H., Ekşi, K. Y., & Alpar, M. A. 2007, ApJ, 657, 441

Ertan, Ü., Göğüş, E., & Alpar, M. A. 2006b, ApJ, 640, 435

Espinoza, C. M., Lyne, A. G., Kramer, M., Manchester, R. N., & Kaspi, V. M. 2011, ApJL, 741, L13

Esposito, P., Burgay, M., Possenti, A., et al. 2009a, MNRAS, 399, L44

Esposito, P., Tiengo, A., Mereghetti, S., et al. 2009b, ApJL, 690, L105

Esposito, P., Israel, G. L., Turolla, R., et al. 2010, MNRAS, 405, 1787

—. 2011, MNRAS, 416, 205

Faucher-Giguère, C.-A., & Kaspi, V. M. 2006, ApJ, 643, 332

Forman, W., Jones, C., Cominsky, L., et al. 1978, ApJS, 38, 357

Frank, J., King, A., & Raine, D. J. 2002, Accretion Power in Astrophysics: Third Edition

Gaensler, B. M., McClure-Griffiths, N. M., Oey, M. S., et al. 2005, ApJL, 620, L95

Gavriil, F. P., Dib, R., Kaspi, V. M., & Woods, P. M. 2007, The Astronomer's Telegram, 993, 1

Gavriil, F. P., & Kaspi, V. M. 2002, ApJ, 567, 1067

Gavriil, F. P., Kaspi, V. M., & Woods, P. M. 2002, Nature, 419, 142

Giacconi, R., Gursky, H., Kellogg, E., Schreier, E., & Tananbaum, H. 1971, ApJL, 167, L67

Gotthelf, E. V., & Halpern, J. P. 2007, Ap&SS, 308, 79

Gotthelf, E. V., Halpern, J. P., Buxton, M., & Bailyn, C. 2004, ApJ, 605, 368

Göğüş, E., Woods, P., & Kouveliotou, C. 2009, The Astronomer's Telegram, 2076, 1

Göğüş, E., Woods, P. M., Kouveliotou, C., et al. 2010, ApJ, 722, 899

Güver, T., Göğüş, E., & Özel, F. 2011, MNRAS, 418, 2773

Güver, T., Özel, F., & Göğüş, E. 2008, ApJ, 675, 1499

Güver, T., Özel, F., Göğüş, E., & Kouveliotou, C. 2007, ApJL, 667, L73

Halpern, J. 2008, GRB Coordinates Network, 8129, 1

Hulleman, F., Tennant, A. F., van Kerkwijk, M. H., et al. 2001, ApJL, 563, L49

Hulleman, F., van Kerkwijk, M. H., & Kulkarni, S. R. 2000, Nature, 408, 689

—. 2004, A&A, 416, 1037

Hulse, R. A., & Taylor, J. H. 1975, ApJL, 195, L51

Hurley, K. 2000, in American Institute of Physics Conference Series, Vol. 526, Gamma-ray Bursts, 5th Huntsville Symposium, ed. R. M. Kippen, R. S. Mallozzi, & G. J. Fishman, 763–770

Hurley, K., Cline, T., Mazets, E., et al. 1999, Nature, 397, 41

Ibrahim, A. I., Safi-Harb, S., Swank, J. H., et al. 2002, ApJL, 574, L51

Ibrahim, A. I., Markwardt, C. B., Swank, J. H., et al. 2004, ApJL, 609, L21

Illarionov, A. F., & Sunyaev, R. A. 1975, A&A, 39, 185

Inutsuka, S.-i., & Sano, T. 2005, ApJL, 628, L155

Israel, G. L., Campana, S., Dall'Osso, S., et al. 2007, ApJ, 664, 448

Israel, G. L., Covino, S., Stella, L., et al. 2002, ApJL, 580, L143

Israel, G. L., Covino, S., Perna, R., et al. 2003, ApJL, 589, L93

Israel, G. L., Rea, N., Mangano, V., et al. 2004, ApJL, 603, L97

Kaplan, D. L., Chakrabarty, D., Wang, Z., & Wachter, S. 2009, ApJ, 700, 149

Kargaltsev, O., Kouveliotou, C., Pavlov, G. G., et al. 2012, ApJ, 748, 26

Kaspi, V. M. 2010, Proceedings of the National Academy of Science, 107, 7147

Kaspi, V. M., Gavriil, F. P., Woods, P. M., et al. 2003, ApJL, 588, L93

Kaspi, V. M., & McLaughlin, M. A. 2005, ApJL, 618, L41

Keane, E. F., Kramer, M., Lyne, A. G., Stappers, B. W., & McLaughlin, M. A. 2011, MNRAS, 415, 3065

Kern, B., & Martin, C. 2002, Nature, 417, 527

King, A. R. 1999, Physics Reports, 311, 337

Klose, S., Henden, A. A., Geppert, U., et al. 2004, ApJL, 609, L13

Kothes, R., & Dougherty, S. M. 2007, A&A, 468, 993

Kothes, R., & Foster, T. 2012, ApJL, 746, L4

Kouveliotou, C., Dieters, S., Strohmayer, T., et al. 1998, Nature, 393, 235

Kouveliotou, C., Eichler, D., Woods, P. M., et al. 2003, ApJL, 596, L79

Krimm, H., Barthelmy, S., Campana, S., et al. 2006, The Astronomer's Telegram, 894, 1

Kuiper, L., & Hermsen, W. 2009, The Astronomer's Telegram, 2151, 1

Kumar, H. S., Ibrahim, A. I., & Safi-Harb, S. 2010, ApJ, 716, 97

Kumar, H. S., & Safi-Harb, S. 2010, ApJL, 725, L191

Landau, L. D. 1932, Phys. Z. Sowjetunion, 1, 285

Lasota, J.-P. 2001, New Astronomy Reviews, 45, 449

Lazaridis, K., Jessner, A., Kramer, M., et al. 2008, MNRAS, 390, 839

Leahy, D. A., & Tian, W. W. 2007, A&A, 461, 1013

—. 2008, AJ, 135, 167

Levin, L., Bailes, M., Bates, S., et al. 2010, ApJ, 721, L33

Lin, D. N. C., Woosley, S. E., & Bodenheimer, P. H. 1991, Nature, 353, 827

Mazets, E. P., Cline, T. L., Aptekar', R. L., et al. 1999, Astronomy Letters, 25, 635

Mazets, E. P., Golentskii, S. V., Ilinskii, V. N., Aptekar, R. L., & Guryan, I. A. 1979, Nature, 282, 587

McGarry, M. B., Gaensler, B. M., Ransom, S. M., Kaspi, V. M., & Veljkovik, S. 2005, ApJL, 627, L137

McLaughlin, M. 2009, in Astrophysics and Space Science Library, Vol. 357, Astrophysics and Space Science Library, ed. W. Becker, 41

McLaughlin, M. A., Lyne, A. G., Lorimer, D. R., et al. 2006, NAture, 439, 817

Menou, K., Perna, R., & Hernquist, L. 2001a, ApJL, 554, L63

—. 2001b, ApJ, 559, 1032

Mereghetti, S. 2008, A&ARv, 15, 225

Mereghetti, S., Chiarlone, L., Israel, G. L., & Stella, L. 2002, in Neutron Stars, Pulsars, and Supernova Remnants, ed. W. Becker, H. Lesch, & J. Trümper, 29

Mereghetti, S., Tiengo, A., Stella, L., et al. 2004, ApJ, 608, 427

Mereghetti, S., Esposito, P., Tiengo, A., et al. 2006a, ApJ, 653, 1423

—. 2006b, A&A, 450, 759

Mereghetti, S., Götz, D., Weidenspointner, G., et al. 2009a, ApJL, 696, L74

Mereghetti, S., Tiengo, A., Esposito, P., et al. 2009b, ArXiv e-prints

Michel, F. C. 1988, Nature, 333, 644

Minter, A. H., Camilo, F., Ransom, S. M., Halpern, J. P., & Zimmerman, N. 2008, ApJ, 676, 1189

Morii, M., Kawai, N., Kataoka, J., et al. 2005, Advances in Space Research, 35, 1177

Morii, M., Kobayashi, N., Kawai, N., et al. 2009, PASJ, 61, 51

Morii, M., Sato, R., Kataoka, J., & Kawai, N. 2003, PASJ, 55, L45

Muno, M. P., Gaensler, B. M., Clark, J. S., et al. 2007, MNRAS, 378, L44

Nakagawa, Y. E., Makishima, K., & Enoto, T. 2011, PASJ, 63, 813

Nakagawa, Y. E., Mihara, T., Yoshida, A., et al. 2009, PASJ, 61, 387

Olausen, S. A., Zhu, W. W., Vogel, J. K., et al. 2013, ApJ, 764, 1

Page, D. 2009, in Astrophysics and Space Science Library, Vol. 357, Astrophysics and Space Science Library, ed. W. Becker, 247

Page, D., Geppert, U., & Weber, F. 2006, Nuclear Physics A, 777, 497

Palmer, D., Esposito, P., Barthelmy, S., et al. 2008, The Astronomer's Telegram, 1548, 1

Palmer, D. M., Barthelmy, S., Gehrels, N., et al. 2005, Nature, 434, 1107

Patel, S. K., Kouveliotou, C., Woods, P. M., et al. 2003, ApJ, 587, 367

Perna, R., Hernquist, L., & Narayan, R. 2000, ApJ, 541, 344

Popov, S. B. 2008, Physics of Particles and Nuclei, 39, 1136

Predehl, P., & Schmitt, J. H. M. M. 1995, A&A, 293, 889

Pringle, J. E. 1974, PhD thesis, , Univ. Cambridge, (1974)

Rappaport, S. A., Fregeau, J. M., & Spruit, H. 2004, ApJ, 606, 436

Rea, N. 2012, private communication

Rea, N., Israel, G. L., Stella, L., et al. 2003, ApJL, 586, L65

Rea, N., Israel, G. L., Turolla, R., et al. 2009, MNRAS, 396, 2419

Rea, N., Esposito, P., Turolla, R., et al. 2010, Science, 330, 944

Rea, N., Israel, G. L., Esposito, P., et al. 2012, ApJ, 754, 27

Sato, T., Bamba, A., Nakamura, R., & Ishida, M. 2010, PASJ, 62, L33

Savchenko, V., Neronov, A., Beckmann, V., Produit, N., & Walter, R. 2010, A&A, 510, A77

Scholz, P., Ng, C.-Y., Livingstone, M. A., et al. 2012, ArXiv e-prints

Shakura, N. I., & Sunyaev, R. A. 1973, A&A, 24, 337

Tam, C. R., Gavriil, F. P., Dib, R., et al. 2008, ApJ, 677, 503

Tam, C. R., Kaspi, V. M., Gaensler, B. M., & Gotthelf, E. V. 2006, ApJ, 652, 548

Tam, C. R., Kaspi, V. M., van Kerkwijk, M. H., & Durant, M. 2004, ApJL, 617, L53

Testa, V., Rea, N., Mignani, R. P., et al. 2008, A&A, 482, 607

Thompson, C., & Duncan, R. C. 1995, MNRAS, 275, 255

—. 1996, ApJ, 473, 322

Tian, W. W., & Leahy, D. A. 2008, ApJ, 677, 292

—. 2012, MNRAS, 421, 2593

Tiengo, A., Esposito, P., & Mereghetti, S. 2008, ApJL, 680, L133

Tiengo, A., Esposito, P., Mereghetti, S., et al. 2009, MNRAS, 399, L74

Tiengo, A., Vianello, G., Esposito, P., et al. 2010, ApJ, 710, 227

Trümper, J. E., Zezas, A., Ertan, Ü., & Kylafis, N. D. 2010, A&A, 518, A46

Tuchman, Y., Mineshige, S., & Wheeler, J. C. 1990, ApJ, 359, 164

Turolla, R., Zane, S., Pons, J. A., Esposito, P., & Rea, N. 2011, ApJ, 740, 105

van der Horst, A. J., Connaughton, V., Kouveliotou, C., et al. 2010, ApJL, 711, L1

Wachter, S., Patel, S. K., Kouveliotou, C., et al. 2004, ApJ, 615, 887

Wang, Z., Bassa, C., Kaspi, V. M., Bryant, J. J., & Morrell, N. 2008, ApJ, 679, 1443

Wang, Z., & Chakrabarty, D. 2002, ApJ, 579, L33

Wang, Z., Chakrabarty, D., & Kaplan, D. L. 2006, Nature, 440, 772

Woods, P. M., Gogus, E., Kouveliotou, C., & et al. 2009, The Astronomer's Telegram, 2152, 1

Woods, P. M., Kaspi, V. M., Gavriil, F. P., & Airhart, C. 2011, ApJ, 726, 37

Woods, P. M., & Thompson, C. 2006, Soft gamma repeaters and anomalous X-ray pulsars: magnetar candidates, ed. W. H. G. Lewin & M. van der Klis, 547–586

Woods, P. M., Kaspi, V. M., Thompson, C., et al. 2004, ApJ, 605, 378

Woods, P. M., Kouveliotou, C., Gavriil, F. P., et al. 2005, ApJ, 629, 985

Yan, T., Perna, R., & Soria, R. 2012, MNRAS, 423, 2451